Dissertation

submitted to the

Combined Faculties for the Natural Sciences and for Mathematics

of the Ruperto-Carola University of Heidelberg, Germany

for the degree of

Doctor of Natural Sciences

Elucidation of regulatory micro-RNA/ messenger-RNA networks in B-cell chronic lymphocytic leukemia and mantle cell lymphoma

presented by

Diplom-Biologe Jan Meier

born in Berlin

Heidelberg, 2012

Submitted to the Combined Faculties for the Natural Sciences and for Mathematics of the Ruperto-Carola University of Heidelberg, Germany: May 29, 2012

Referees: PD Dr. Stefan Wiemann
Prof. Dr. Peter Lichter

Day of the oral examination:

The investigations of the following dissertation were performed from December 2007 till May 2012 under supervision of Prof. Dr. Peter Lichter, Dr. Martina Seiffert and Dr. Armin Pscherer in the division of molecular genetics at the German Cancer Research Center (DKFZ), Heidelberg, Germany.

Publications

Ernst A, Campos B, **Meier J**, Devens F, Liesenberg F, Wolter M, Reifenberger G, Herold-Mende C, Lichter P, Radlwimmer B; "De-repression of CTGF via the miR-17-92 cluster upon differentiation of human glioblastoma spheroid cultures"; Oncogne; 2010

Lössner C, **Meier J**, Warnken U, Rogers MA, Lichter P, Pscherer A, Schnölzer M; "Quantitative proteomics identify novel miR-155 target proteins"; PloS one; 2011

Meier J, Hovestadt V, Zapatka M, Pscherer A, Lichter P, Seiffert M; "Genome-wide identification of miR-155 target genes and disproportionally AGO2-associated miRNAs, including miR-155, using RIP-Seq"; manuscript in preparation

Declarations

I hereby declare that I have written the submitted dissertation "Elucidation of regulatory micro-RNA/ messenger-RNA networks in B-cell chronic lymphocytic leukemia and mantle cell lymphoma" myself and in this process have used no other sources or materials than those expressly indicated. I hereby declare that I have not applied to be examined at any other institution, nor have I used the dissertation in this or any other form at any other institution as an examination paper, nor submitted it to any other faculty as a dissertation.

Place, Date	Jan Meier

To Juliane

& my family

Table of Contents

Abbreviations

A	Adenosine
AGO	Argonaute protein
ALV	Avian leucosis virus
ARE	AU rich element
Array CGH	Array comparative hybridization
ATP	Adensone-tri-phosphate
B-CLL / CLL	B-cell Chronic lymphocytic leukemia
BIC	B-cell integration cluster
bp	Base pair
BSA	Bovine serum albumine
C	Cytidine
CCND1	Cyclin D1
cDNA	Complementary DNA
CNE	Conserved non-coding element
CpG	Cytosine-Guanosine di-nucletide
DNA	Desoxy-ribonucleic acid
EBV	Eppstein-Barr virus
ECM	Extracellular matrix
EMT	Epithelial-mesenchymal transition
esiRNA	Endogenous short interfering RNA
FACS	Fluorescence-activated cell sorting
FCS	Fetal cow serum
FDR	False discovery rate
G	Guanosine
GC	Germinal center
gDNA	Genomic DNA
HK	housekeeper
HL	Hodgkin's lymphoma
HRP	Horse radish peroxidase
IP	Immunoprecipitation
kb	kilobases
lincRNA	Large intergenic non-coding RNA
MCL	Mantle cell lymphoma
miRISC	miRNA indiced silencing complex
miRNA	MicroRNA

mRNA	Messenger RNA
ncRNA	Non-coding RNA
NGS	Next generation sequencing
NHL	Non-Hodgkin's lymphoma
nt	Nucleotides
PBS	Phosphate buffered saline
PCR	Polymerase chain reaction
piRNA	Piwi interacting RNA
PLB	Polysome lysis buffer
Pre-miRNA	Precursor miRNA (2nd biogenesis intermediate)
Pri-miRNA	Primary miRNA precursor (1st biogenesis intermediate)
qRT-PCR	Quantitative real-time reverse transcription PCR
RIP	RNA interacting protein immunoprecipitation
RISC	RNA induced silencing complex
RLC	RISC loading complex
RLU	Relative light units
RNA	Ribonucleic acid
rpm	Rotations per minute
rRNA	Ribosomal RNA
SAM	Significance analysis of microarrays
Seq	Sequencing
siRNA	Short interfering RNA
SN	Supernatant
T	Thymidine
TL	Total lysate
U	Uracil
UV	Ultraviolet
V	Volts
w/v	Weight per volume

Summary

B-cell chronic lymphocytic leukemia (CLL) is the most common type of leukemia in the Western world. CLL is not curable with currently available therapies. Another neoplastic entity that shares genotypic and phenotypic characteristics with CLL is mantle cell lymphoma (MCL), comprising approximately 6% of all Non-Hodgkin lymphomas (NHL).

MicroRNAs (miRNAs) are small single stranded RNA molecules with a length of ~21 nucleotides, which regulate the stability and translation of protein coding messenger RNAs (mRNAs). It is estimated that 30% of all protein coding genes of an organism are regulated by miRNAs. Within recent years, evidence arose that the deregulated expression of miRNAs plays a pivotal role in cancer. MicroRNA-155 and the miR-17-92 cluster are aberrantly expressed in various cancers including B-cell lymphomas. The present work aimed at the identification of transcripts regulated by these aberrantly expressed miRNAs. To this end, current standard techniques like quantitative real-time reverse transcription PCR, luciferase sensor assays and Western blot analyses were performed. As the results of these studies revealed only minor effects, an alternative screening method was established, which is based on the immunoprecipitation of RNA induced silencing complexes (RISC) with subsequent sequencing of precipitated mRNAs (RIP-Seq).

As a model system for RIP-Seq, HEK293T cells with stable, ectopic expression of miR-155 were generated. In comparison to the control cell line, these cells showed enhanced cell proliferation. RIP-Seq experiments using these cells revealed an enrichment of 67 mRNAs predicted as miR-155 targets, including transcripts of the transcription factor *CEBPB* and the RNA destabilizing protein *ZFP36*. Expression profiling further revealed significant changes in the transcriptome and miRNome as a consequence of ectopic miR-155 expression. For instance, the cell cycle gene *CCND1* and the cancer associated *ETS* transcription factor sub-family *PEA3* were severely up regulated. Using RIP-Seq, the targetomes of two B-cell lines representing CLL and MCL were identified. These targetomes comprise more than 1,000 target genes each, with more than 600 genes shared by both cell lines, including the putative tumor suppressor gene *BTG2* as one of the most prominent miRNA target genes. MicroRNA profiling of the immunoprecipitation as well as the corresponding total lysate fractions by RIP-Seq uncovered a recurrent

disproportional presence of several miRNAs, including miR-155 and members of the miR-17-92 cluster, within the AGO2 IPs. However, the underlying mechanisms, explaining the bias in miRNA binding to AGO2 remain so far elusive.

Zusammenfassung

Die chronische lymphatische Leukämie vom B-Zell Typ (CLL) ist die häufigste Leukämieform der westlichen Welt. CLL ist mit derzeit verfügbaren Therapien nicht heilbar. Eine weitere Neoplasie ist das Mantelzell-Lymphom (MCL), das einige der genotypischen und phänotypischen Charakteristika der CLL teilt und in etwa 6% aller Non-Hodgkin-Lymphome (NHL) ausmacht.

MikroRNAs (miRNAs) sind kleine, einzelsträngige RNA-Moleküle, mit einer Länge von ~21 Nukleotiden, die die Stabilität und Translation von Protein-kodierenden Boten-RNAs (mRNAs) beeinflussen. Es wird angenommen, dass 30% aller protein-kodierenden Gene eines Organismus durch miRNAs reguliert werden. Innerhalb der letzten Jahre mehrten sich die Hinweise, dass die abnormale Expression von miRNAs eine zentrale Rolle bei der Entstehung von Krebs spielt. MicroRNA-155 und das miR-17-92 Cluster sind in verschiedenen Krebsarten, unter anderem in B-Zell Lymphomen, abnormal exprimiert. Die vorliegende Arbeit hatte das Ziel Transkripte zu identifizieren, die durch diese abnormal exprimierten miRNAs reguliert werden. Zu diesem Zweck wurden zunächst Methoden wie quantitative real-time reverse transcription PCR, Luciferasesensor Assays und Western blot Analysen verwendet. Da die gemessenen Effekte jedoch relativ gering waren, wurde eine alternative Untersuchungsmethode etabliert. Diese basiert auf der Immunpräzipitation (IP) des „RNA induced silencing complex“ (RISC) und der anschließenden Sequenzierung der präzipitierten RNA (RIP-Seq).

Als Modellsystem für die Entwicklung der RIP-Seq Methode wurden HEK293T Zellen mit einer stabilen, ektopischen miR-155 Expression etabliert. Im Vergleich zur Kontrollzelllinie, zeigten diese Zellen eine erhöhte Zellproliferation. RIP-Seq Experimente ergaben eine signifikante Anreicherung von 67 mRNAs, wie zum Beispiel Transkripte des Transkriptionsfaktors *CEBPB* oder das RNA destabilisierende *ZFP36*, die als Zieltranskripte von miR-155 vorhergesagt wurden. Bei der Untersuchung der Expressionsprofile dieser Zellen zeigten sich signifikante Veränderungen im Transkriptom und MiRNom als Konsequenz der ektopischen miR-155 Expression. So waren zum Beispiel das Zellzyklusgen *CCND1* und die Krebsassoziierte *ETS* Transkriptionsfaktorfamilie *PEA3* stark hoch reguliert.

Unter Verwendung von RIP-Seq wurde das Targetom zweier B-Zelllinien identifiziert, die die Entitäten CLL und MCL repräsentieren. Diese Targetome umfassten jeweils mehr als

1000 Zielgene, von denen mehr als 600 in beiden Zelllinien identifiziert wurden. Ein herausragendes Transkript war das mögliche Tumorsuppressorgen *BTG2*. Die Messung von MikroRNAs in den IP- und zugehörigen total Lysat- (TL) Fraktionen, die durch RIP-Seq generiert wurden, zeigten eine wiederholte, disproportionale Anreicherung einiger miRNAs in AGO2-IPs. Zu diesen miRNAs gehören unter anderem miR-155 und einige miRNAs des miR-17-92 Clusters. Die Mechanismen, die diese Tendenz bei der miRNA - AGO2 Interaktion erklären könnten, sind jedoch noch nicht bekannt.

1 Introduction

1.1 Cancer

Cancer is the uncontrolled growth and spread of cells. It is the third most common disease leading to death worldwide. The International Agency for Research on Cancer (IARC) registered 12.4 million incidences of cancer and 7.6 million deaths from cancer in 2008. According to the growth and aging of the world's population, a constant increase in cancer burden worldwide is assumed. Calculations suggest an increase of cancer related deaths up to 17.0 million in the year of 2030 [1].

According to the World Health Organization (WHO), neoplastic lesions are classified by their origin. Solid tumors arising from the epithelium are termed carcinomas, those emerging from the mesenchyme and connective tissues are termed sarcomas and malignancies of the hematopoietic and lymphatic system are termed leukemia or lymphomas, respectively. Most tumors evolve from a locally restricted (benign) to an invasive (malignant) neoplasm, which is typically accompanied by a decreasing degree of cell differentiation. To date there are more than 100 different cancer types described. Virtually every tissue of an organism can give rise to a neoplastic tissue.

In order to prevent cancer, one of the first steps is the identification of carcinogens causing malignancies. For instance, chemicals like formaldehyde, aflatoxins from fungi, asbestos, ionizing radiation, viruses and tobacco smoke are classified as carcinogens. The WHO associates tobacco smoke, for instance, with the cause of 13 different cancers. Among these lung cancer is the most prominent one.

Although cancer research has made significant progress during the past decades, a more detailed understanding of the molecular characteristics of the individual entities is still needed in order to develop precise and effective treatments for the disease.

1.1.1 The Development of cancer

Tumorigenic cells have to achieve self-sufficient proliferation and insensitivity to growth control and thereby gain growth advantages that outperform the normal healthy cells of the affected tissue. According to current knowledge, tumorigenesis is a multi step

process, which seems to be fairly analogous to Darwinian evolution. Douglas Hanahan and Robert A. Weinberg in 2000 proposed a model, which is trying to structure the high diversity of cancer types coming along with a high complexity with regard to the underlying principles leading to cancer development [2]. They proposed six hallmarks typically acquired by human cancers.

Cancer cells sustain their proliferation by enhancing the release of mitogenic signals, stimulation of supporting cells and elevation of surface receptor levels accepting mitogenic signals. Somatic mutations of proteins like BRAF, involved in mitogenic signaling circuits, were shown to be involved in carcinogenesis by increasing the activity of the growth promoting MAPK signaling pathway [3]. More generally genes, which are promoting cancer development due to higher than normal activities, are termed oncogenes.

Cancer cells often show disrupted signaling pathways, which are supposed to attenuate proliferative signaling. For instance the phosphatase PTEN, which is negatively regulating the AKT/PI3K signaling is frequently mutated or aberrantly expressed due to promoter hyper methylation or microRNA mediated regulation [4,5,6]. Tumor suppressor genes like *TP53* or *RB*, which are central players in the regulation of the cell cycle, are often less or not active due to an inactivating mutation of the gene.

Cancer cells develop resistance to cell death. Triggering programmed cell death implies a shift in the balance of proteins driving apoptosis (e.g. BIM and BAX) and factors that block apoptosis induction (e.g. BCL-2, BCL-X_L and Mcl-1) [7]. Interestingly, microRNAs were shown to regulate pro-apoptotic factors like BCL-2, which is regulated by the miR-15a-16-1 cluster and anti-apoptotic factors like BIM, which are regulated by members of the miR-17-92 cluster. For instance, aberrant expression of these microRNAs is frequently observed in lymphomas [5,8].

A further hallmark of cancer cells is the acquisition of an unlimited replicative potential involving the telomeres as central players for this ability [9].

In addition, tumor cells are able to induce angiogenesis to ensure a constant supply of the tumor with nutrients and oxygen. The *VEGF* gene is one of the major factors involved in the orchestration of blood vessel formation [10].

Cancer cells acquire the ability to invade and metastasize into distant sites of the organism by following a regulatory program termed epithelial-mesenchymal transition

(EMT) [11]. As the EMT is a complex process, a large variety of factors seem to be involved. For instance, the adhesion molecule E-cadherin, which assembles cells of the epithelial layer, is frequently down-regulated in human carcinomas, enabling intravasation of tumor cells into the blood stream [12]. Metastatic cells, which enter the blood stream, have to leave the blood vessel into the tissue of a distant organ, termed extravasation, requiring matrix metalloproteinases, which are degrading the extracellular matrix (ECM) of the target organ. Finally, the metastasizing cells have to colonize the target organ by forming novel macroscopic tumors.

In 2011, eleven years after their remarkable publication "The Hallmarks of cancer", Hanahan and Weinberg published an update adding the topics "enabling characteristics" and "emerging hallmarks" according to the gained knowledge of the last eleven years [13]. They classified genomic instability of cancer cells as one of the enabling characteristics, since virtually every of the previously mentioned hallmarks emerge from genetic mutations and rearrangements of the genome. Accordingly clonal evolution of a certain tumor can be seen as an accumulation of enabling characteristics on the genomic level in single cells. Genomic instability typically manifests by the loss of DNA maintaining enzymes like DNA repair enzymes or enzymes detecting damaged DNA [14]. One example is the *BRCA1* gene, which is primarily associated with breast cancer and which was shown to be involved in DNA double strand break repair mechanism [15,16]. Many tumors also exhibit losses of telomeric DNA leading to chromosomal instability and therefore resulting in amplification, deletion or structural rearrangements of chromosomes [17]. Besides DNA mutations and chromosomal aberrations, epigenetic modifications like DNA methylation or histone modifications are contributing to these enabling characteristics.

Inflammation is considered to play an important role in cancer progression. There is increasing evidence that inflammatory cells, which are present in the near vicinity of lesions, supply the tumor with signaling molecules and thereby promote cancer progression [18,19,20]. Accordingly, the ability of cancer cells to evade from immune destruction is considered as an emerging hallmark of cancer. Finally, characteristic changes in the energy metabolism are frequently observed in cancer cells. Cancer cells are able to reset their glucose metabolism to glycolysis irrespective of the presence of oxygen. This effect was primarily observed by Otto Warburg [21]. Even though glycolysis

has much lower efficiency of ATP production compared to the aerobic glucose metabolism, glycolysis produces more byproducts like nucleosides and amino acids and thereby provides important reservoirs for the rapid division of tumor cells.

However, not all of the proposed characteristics have to be fulfilled in order to generate a neoplastic lesion. Thus globally, the establishment of a tumor is rather a serial process accumulating several of the aforementioned properties, e.g. by repeated exposure to carcinogens with increasing age. Pediatric malignancies represent an exception to this mechanistic view, as they are characteristic for an early disease progression.

With ongoing research the list of hallmarks will refine and increase. For instance the impact of non-coding RNAs and aberrant epigenetic DNA modifications on cancer development got into the focus of research.

1.2 B-cell neoplasms

Hematological malignancies affect the blood, bone marrow and lymph nodes. The World Health Organization (WHO) categorizes neoplasms according to the cell lineage they are originating from. Within these categories (e.g. myeloid, lymphoid, dendritic or mast cell neoplasms) the distinct diseases are further characterized with respect to their cell morphology, immunophenotype, genetic alterations and clinical syndrome.

In 1832 Thomas Hodgkin for the first time described abnormalities in the lymph system termed Hodgkin's lymphoma (HL). The histopathological characteristic are the multinucleated Reed-Sternberg cells [22]. In the 1970 Karl Lennert of Kiel proposed the Kiel classification system, based on morphologic changes of malignant cells in comparison to their normal counterparts [23]. Further research revealed different forms of lymphomas classified by Henry Rappaport leading to the "Working Formulation" in 1982 and introducing the term non-Hodgkin lymphoma (NHL), which excludes the classical Hodgkin's lymphoma. The Working Formulation classified the NHLs into the four groups low grade, intermediate grade, high grade and miscellaneous lymphomas according to size and shape of neoplastic cells [24]. This classification was replaced in 2001 and further updated in 2008 by the WHO based on the REAL-system applying immunophenotypic and genetic characteristics [25].

1.2.1 Human B-cell lymphomas

In the Western world about 20 new cases of lymphoma are diagnosed per 100,000 individuals and year. Of these, 95% refer to B-cell related malignancies. According to the WHO classification, there are 20 different B-cell lymphoma types varying in their genetic features and clinical behavior and therefore requiring different treatment strategies.

The B-cell development starts in the bone marrow. In this compartment the B-cell precursors arise from hematopoietic stem cells and evolve by rearranging the immunoglobulin (Ig) heavy- and light-chain (V)-region genes for the B-cell receptor (BCR). B-cells expressing a non-auto-reactive BCR are able to differentiate into mature naïve B-cells and leave the bone marrow. B-cells without BCR expression or with auto-reactive BCRs undergo apoptosis [26]. Antigen binding of the BCR and the interaction with T-helper-cells activates the naïve B-cells leading to clonal expansion in the germinal centers (GC) of lymphoid follicles (Figure 1-1). In the GCs the B-cells undergo somatic hypermutation rearranging the Ig variable (V)-region genes with the aim to improve antigen binding specificity of the BCR [27]. B-cells expressing BCRs with reduced affinity upon somatic hyper mutations undergo apoptosis. The selection process for B-cells, expressing high affinity BCRs, occurs in the light zone of the GC with close interactions to CD4+ T-cells and follicular dendritic cells (FDC). Finally, a subset of these B-cells undergo class-switch recombination, which changes the constant region of the heavy chain of immunoglobulin and leads to differentiation into memory B-cells or plasma B-cells [28].

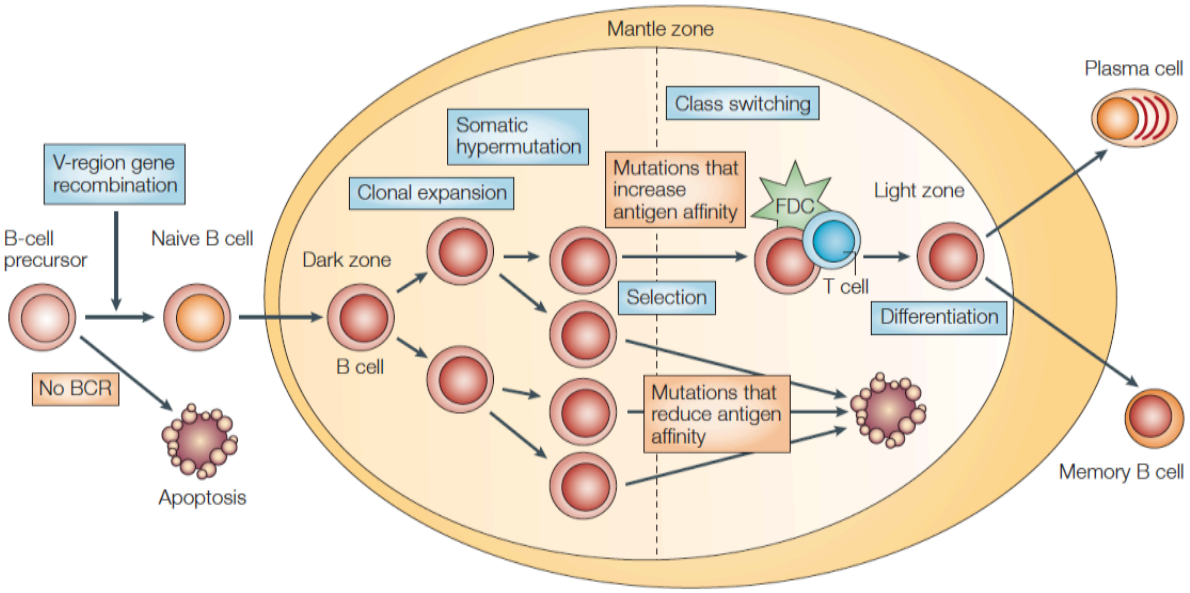

Figure 1-1: Scheme of B-cell maturation and activation in the germinal center. Source: [29]

The previously described developmental steps of B-cells seem to reflect the large variety of B-cell malignancies [30], (Figure 1-2). The different lymphoma types are also distinguishable by their gene-expression profile. Chromosomal rearrangements involving cancer-related genes are a typical feature of various types of B-cell lymphomas [31]. Many of these translocations involve the highly active Ig locus leading to activation of inactive proto-oncogenes, indicating that these chromosomal rearrangements most likely occur during V(D)J recombination, somatic hypermutation and class-switch recombination [32,33,34]. In addition to the rearrangements of BCR-related genes, genetic modifications like mutations of the tumor suppressor gene *TP53* or *ATM* are implicated in the pathogenesis of lymphomas as well [35,36,37,38]. Even though B-cell lymphomas acquire genetic lesions favoring their pathogenesis, the vast majority of B-cell lymphomas additionally benefit of BCR-promoted cell survival [39]. It is known for several lymphoma types that their BCRs bind auto-antigens supporting cell survival [40,41]. In addition, foreign antigens, often related to chronic infections, are also shown to promote lymphomagenesis [42]. Infection with the Epstein-Barr virus (EBV), which is known to be involved in the transformation of B-cells, is supposed to provide survival-promoting signals through the virus specific gene *LMP2A* [43,44]. Interestingly, it is shown that EBV drives the expression of a specific microRNA, miR-155, which plays a key role in B-cell immortalization [45,46,47]. Finally, there is strong evidence that the microenvironment

provides important survival signals for malignant B-cells. Several lymphoma types like follicular lymphoma, mucosa-associated lymphoid tissue (MALT) lymphomas or chronic lymphocytic leukemia (CLL) are highly dependent on accessory cells like tumor infiltrating $CD4^+$ T-cells or macrophages, providing survival-promoting signals [18,19,48].

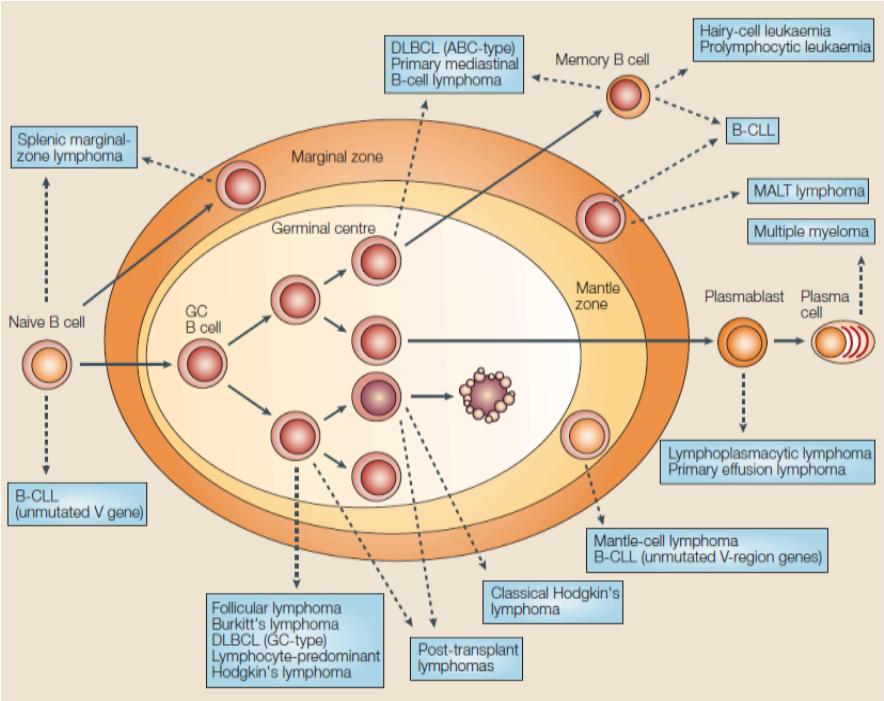

Figure 1-2: Cellular origins of B-cell lymphomas. Source: [29]

1.3 B-cell chronic lymphocytic leukemia (CLL)

B-cell chronic lymphocytic leukemia (CLL) is the most common type of leukemia in the western world representing up to 30% of all leukemias [49]. CLL predominantly occurs at advanced age with over 90% of CLL cases appearing in patients older than 50 years, and is more frequent in males. The clinical course of CLL is rather heterogeneous with survival times ranging from a few months to several years. The median survival time after diagnosis is 7.5 years. About 20% of CLL cases show a more aggressive clinical course [50]. Patients with CLL have an impaired immunologic activity with a high deficiency of immunoglobulins in approximately 50% of cases [51]. Autoimmunity is observed in 25% of patients [52]. For the diagnosis of CLL a persistent lymphocytosis greater than 5,000 cells/µl in the peripheral blood needs to be observed. Bone marrow aspirates typically exhibit lymphocytosis rates higher than 30%. Besides the bone marrow, lymph nodes are frequently and diffusely infiltrated by neoplastic lymphocytes. Furthermore, CLL cells can be found in the white pulp of the spleen, in the liver, tonsils, skin and pleura [53,54]. CLL

cells of the peripheral blood have a relatively well-differentiated morphology with a hyper condensed "soccer-ball"-appearing chromatin pattern [50], (Figure 1-3). From the pathological point of view, lymphocytosis and bone marrow infiltration are the most critical factors for predicting the clinical course [50]. CLL cells present a typical immunophenotype with low surface expression of immunoglobulins (Ig) and the presence of the antigens CD5, CD19, CD20, CD79a, CD22, CD23, CD43 and CD11c [50].

In order to classify the individual stages of the disease, clinicians use three major staging systems: (i) described by Rai *et al. [55]*, (ii) according to Binet *et al.* [56], or (iii) as determined by the international workshop on CLL systems [57]. Furthermore, the mutational status of *IgHV* genes appears to be of prognostic importance. The median survival time of patients with mutated *IgHV* genes is much higher than of patients with non-mutated *IgHV* genes [58]. It was believed that naïve B-cells with no antigen experience were the origin for CLL cells with unmutated *IgHV* genes (refer to 1.2.1), whereas B-cells after antigen stimulation in the GC were suggested as the normal counterpart of CLL cells with mutated *IgHV* genes (refer to Figure 1-2). However, gene expression profiling of CLL cells showed a similar pattern in cases with either mutated or unmutated *IgHV* genes, which was most similar to memory B-cells [59,60]. According to this, the expression status of the *ZAP-70* gene in CLL cells appeared to reliably discriminate between patients with or without *IgHV* mutation. The *ZAP-70* gene, which is a tyrosine kinase typically involved in T-cell receptor signaling, is therefore also a valuable prognostic marker for CLL [59].

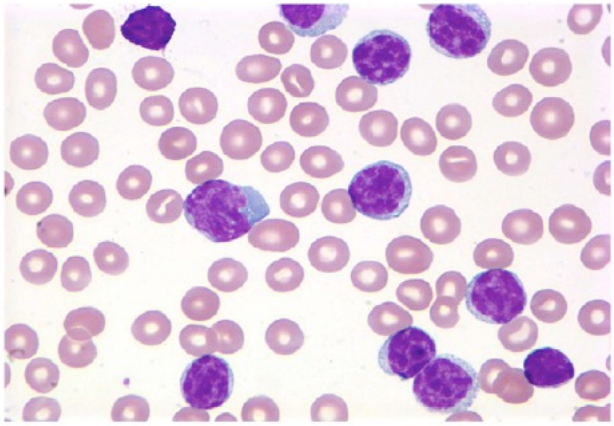

Figure 1-3: H & E stained blood smear of the peripheral blood of a CLL patient. The chromatin of the B-cells is stained in purple and shows a soccer ball like pattern. Source: [50]

Besides the pathological and immunological phenotypes, on the cellular level CLL cells frequently exhibit genomic aberrations. These aberrations are identified using fluorescence in-situ hybridization (FISH) [61]. A disease specific probe set detects chromosomal abnormalities like the deletion of regions on 13q, 11q, 17p, 6q and trisomy 12, which are frequently occurring in CLL [62]. Additionally, a genomic gain of chromosome 19 and the *MYCN* oncogene on 2p were identified using array comparative genomic hybridization (array CGH) [63]. Deletions of the chromosomal arm 17p were shown to have the worst prognosis (Figure 1-4). Contrary, patients with a sole 13q deletion exhibit the best prognostic value.

The heterozygous or homozygous deletion of 13q14 is the most frequent genomic aberration in CLL and occurs in other types of lymphoma as well [64]. The chromosomal region 13q14 carries the microRNAs miR-15a and miR-16-1, which are significantly down regulated upon loss of this fragment [8]. Ulf Klein and colleagues demonstrated an accelerated proliferation of human and mouse B-lymphocytes upon deletion of miR-15a and miR-16-1, which is associated with a modulation of cell cycle related genes [65].

Trisomy 12 is occurring in 10% to 20% of CLL cases. Patients with trisomy 12 show a higher overall survival, however the progression free survival is shorter in comparison to other genotypic subtypes [66], (Figure 1-4). The genes on chromosome 12, which could be involved in the pathomechanism of CLL are not identified.

About 20% of CLL patients, predominantly individuals with unmutated *IgHV* genes, carry a deletion of the chromosomal arm 11q [62,67]. Interestingly 11q contains the tumor suppressor gene *ATM*, which is mutated in 12% of CLL patients and associated with a poorer outcome of the disease [68].

In 30% of refractory CLL cases the deletion 17p13 is observed, which is known from other cancers [69], (Figure 1-4). Translocations in CLL are typically involving the chromosomal region 14q32, which carries the immunoglobulin genes (refer to 1.2.1). The most common translocations in CLL are t(14;18)(q32;q21) and t(14;19)(q32;q13) [70]. However, translocations in CLL are relatively rare in comparison to other lymphoma types.

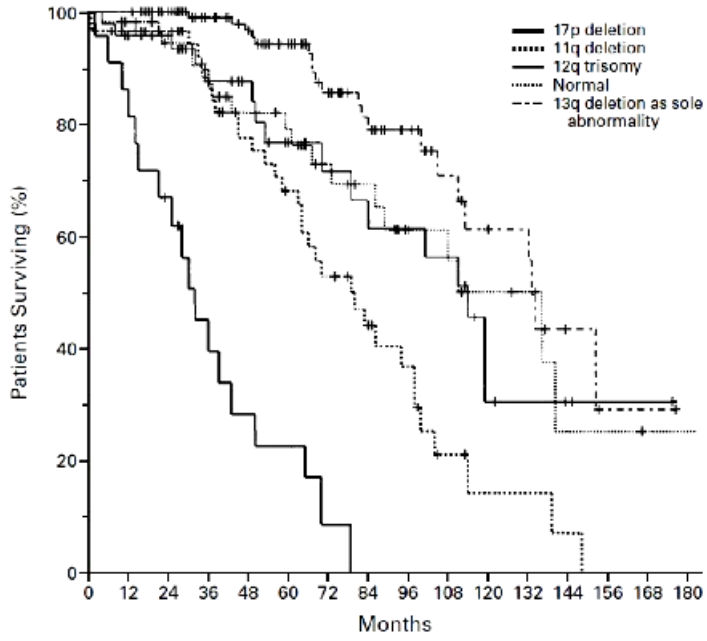

Figure 1-4: Kaplan-Meier analysis on overall survival of genetic subgroups of CLL patients including chromosomal deletions of 17p, 11q, and 13q, trisomy 12 as well as patients with normal karyotype. Source: [62]

With the establishment of next generation sequencing methods, previously unknown recurrent mutations in CLL were identified. In a cohort of 255 CLL patients *NOTCH1* was found muted in 12.2% of all cases. Furthermore, mutations in the gene *MYD88* were identified in 2.9% of CLL patients [71]. In a second study using exome sequencing, the *NOTCH1* mutation status was correlated to the overall survival of CLL patients. In these studies *NOTCH1* mutations were associated with 31% of Richter syndrome and 20.8% of chemorefractory CLL cases [72]. Richter syndrome (RS) describes the development of a high grade NHL like diffuse large B-cell lymphoma (DLBCL) from a primary CLL case. In comparison to the mutation rates of solid tumor types, the frequencies of mutations per CLL case were rather low.

The majority of CLL cells are non-proliferative cells, which are arrested in the G0/G1 phase of the cell cycle and which are relatively resistant to apoptosis [73]. However, proliferating CLL cells can be observed in certain foci termed pseudofollicles in the bone marrow and lymph nodes. In these pseudofollicles, CLL cells are able to interact with CD4+ T-cells and CD14+ myeloid cells, which are supposed to provide the CLL cells with survival and proliferation supportive signals [74]. Indeed, it was shown that CLL cells could be maintained *in vitro* only when accessory cells or their secreted factors are present. [75]. Recently, the survival promoting role of inflammatory signaling pathways

and cytokines has been demonstrated, which provides further indication for the importance of the microenvironment for the survival of CLL cells [19]. Cell survival associated signaling pathways like NFκB, NOTCH, MAPK/ERK, PI3K/AKT and WNT were shown to be active in CLL cells [76]. In addition, anti-apoptotic genes like *BCL2* and *MCL1* are up regulated in these cells [77,78].

A transformation to a more aggressive form of lymphoma is observed in some rare cases of CLL. One of the best characterized transformation events in CLL is the Richter syndrome (RS) (described above). After occurrence of the RS the disease is rapidly progressing and reduces the median survival to 5 months. The incidence for RS is approximately 3 to 10% of CLL cases [79].

1.4 Mantle cell lymphoma (MCL)

Mantle cell lymphoma (MCL) is a neoplasm of mature B-cells comprising approximately 6% of all Non-Hodgkin lymphomas. MCL is an incurable disease with a short median survival time of five to seven years predominantly occurring in males of advanced age. Current chemotherapeutic treatments usually have high rates of relapse [80]. Virtually all MCL cases carry the translocation t(11;14)(q13;q32), which is the defining genetic hallmark for this entity. The translocation involves the *CCND1* gene leading to its hyperactivation. In some rare cases the *CCND1* gene is not expressed, however these cases often show an aberrant expression of *CCND2* or *CCND3*. So far the proliferative behavior of the tumor is the best criterion for the prognosis of the disease [81]. MCL cells originate from mature B-lymphocytes with a typical gene expression pattern like in naïve B-cells. MCL cells colonize the mantle zone of lymphoid follicles (Figure 1-2) and can be morphologically subdivided into a blastoid or a non-blastoid type [82]. The blastoid variants have a higher proliferative activity and a more aggressive behavior than the non-blastoid cases [83], (Figure 1-5). Like in CLL, the *IgHV* genes appear to be either in the germ line status (unmutated) or somatically mutated, which is observed in 15-40% of cases. However, in contrast to CLL the mutational status of *IgHV* genes in MCL has no reliable prognostic value for the course of the disease [84].

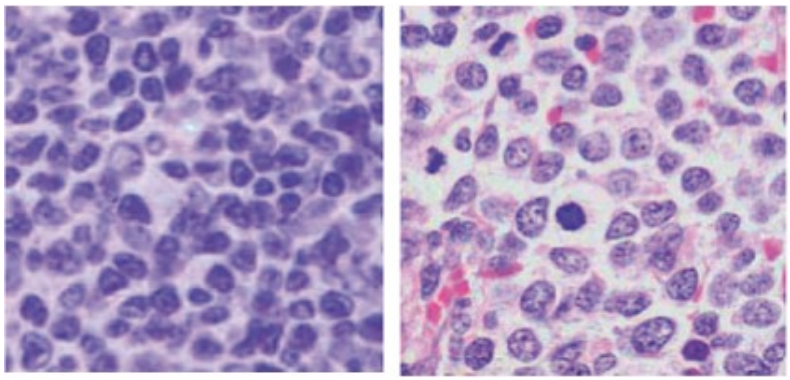

Figure 1-5: Lymph node sections of MCL patients with classical MCL (left) and blastoid MCL (right). The sections were H & E stained. Source: [85]

Besides the defining translocation t(11;14)(q13;q32) there are several other recurrent genetic lesions in MCL. Beà and colleagues identified chromosomal imbalances like gains on chromosome 3q, 7p, 8q and 18q or losses on chromosome 13, 6q, 1p and 11q by performing array CGH [86]. Another study screening 53 tumor samples with matrix-CGH showed that chromosomal deletions of 8p and 13q14 were associated with an inferior overall survival [87]. A more focused analysis of MCL cases by FISH revealed common gains on 3q26, 8q24, 15q23 and 7p15 and recurrent losses of 13q14, 11q22-q23, 9p21, 1p22, 17p13 6q27 and 8p22. Further, deletions of 8p, 9p and 13q14 were associated with a worse overall survival, supporting the findings of the matrix-CGH analysis [88]. The clinically aggressive variants generally show a more complex karyotype [86,89]. The observed chromosomal alterations suggest recurrent defects of the DNA damage pathways. For instance loss of the tumor suppressor gene *ATM* has been observed in up to 46% of MCL patients [38]. In up to 30% of the highly proliferative subtypes the CDKN2A locus encoding the two important cell cycle regulators *INK4a* and *ARF* is deleted [90]. The *CDK4* gene, which is an important factor of the G1-S phase transition in the cell cycle, is amplified in approximately 21% of the fast proliferating MCL cells [91]. Furthermore, activation of the *MYC* oncogene caused by a t(8;14)(q24;32) translocation is associated with rapid disease progression [92]. In addition, several factors of cell survival pathways are involved in the pathomechanism of the disease. The anti-apoptotic *BCL2* gene is frequently amplified and the pro-apoptotic gene *BIM* is frequently deleted in MCL cells [93]. Cancer associated signaling pathways like PI3K/AKT are highly active and the *PTEN* gene, a negative regulator of the PI3K/AKT signaling cascade, is frequently lost in MCL [94,95].

1.5 Non-coding RNAs

In the 1970s it was assumed that the number of human protein-coding genes lies somewhere between 35,000 to 100,000. By accomplishing the sequencing of the complete human genome in 2001 the hypothetical number of protein-coding genes was reduced considerably [96,97] and was estimated to approximately 21,000 representing only 1.5% of the human genome [98]. Historically, the highest proportion of the non-protein coding sequences was considered as "junk" DNA, which was supposed to be functionally silent and to a great extend derived from viruses. Today one knows that the human genome contains a large variety of highly conserved transcribed non-coding elements (CNEs), representing an enormous fraction of the human DNA sequence [99]. Recent results suggest a more important role for CNEs in the evolution of species, since in CNEs a more rapid change among the species in comparison to protein-coding genes is observed. Thus innovation in non-coding regulatory elements seems to be the major driving force in the evolution of new species [100].

With the development of massive parallel sequencing the variety of regulatory non-coding RNA species is constantly increasing. However, their mechanistic aspects of action and their regulatory role are poorly understood. So far diverse classes like piwi protein interacting RNAs (piRNAs), endoribonuclease-prepared siRNAs (esiRNAs), enhancer associated RNAs (eRNAs), large intergenic non-coding RNAs (lincRNAs) and activating non-coding RNAs (ncRNA-a) were identified.

Piwi-interacting RNAs are thought to silence transposable elements during germ line development. Experiments in mice have shown that piRNAs are involved in transcriptional silencing of target genes through DNA *de novo* methylation. PiRNAs are extremely abundant in spermatocytes and oocytes. According to their expression pattern two classes of piRNAs were identified in mammals. The first class is only expressed before pachytene stage during meiosis and therefore termed pre-pachytene-piRNAs. The second class becomes abundant after the pachytene stage [101,102].

Besides piRNAs numerous esiRNAs were detected in mouse oocytes, which are produced by a so far unknown mechanism since siRNAs typically are a product of RNA dependent RNA polymerases (RdRP). However, in mammals there are no RdRPs expressed. It was shown that the activity of esiRNAs, like microRNAs, depends on the enzymes DICER and

AGO2. *DICER* knock down experiments revealed a reduction of esiRNAs and an increase in mobile genetic elements complementary to the esiRNA sequences in mice [103,104].

Recently, a novel class of activating non-coding RNAs (ncRNA-a) has been identified. By next generation sequencing Orom and colleagues reported about 3,000 previously unknown non-coding RNAs. Functional analysis revealed an enhancing effect of ncRNA-a on the expression of specific genes. The authors could show that specific ncRNA-a enhance the expression of transcripts encoded in the near vicinity of the respective ncRNA-a [105].

In another study Kim and colleagues detected polymerase II (Pol II) recruitment to approximately 3,000 different activity-dependent enhancers in mouse cortical neurons. By performing high throughput sequencing they identified a novel class of non-coding RNAs with <2kb in length, which they termed eRNAs. The synthesis of eRNAs starts in the near vicinity of enhancers and furthermore seems to require a dynamic interaction between the enhancer and the nearest promoter. The functional role of eRNAs remains elusive [106].

Large intergenic non-coding RNAs (lincRNAs) represent another novel class of evolutionary conserved and therefore presumably functional RNAs [107]. The size of lincRNAs varies from 2.3 to 17.2 kilobases. Guttman and colleagues could show that specific lincRNAs are transcriptionally regulated by well-known transcription factors like TP53 and NF-κB [108]. Several non-coding RNAs of this class were functionally characterized. For instance *Xist* plays an important role in X-chromosome inactivation and *H19* and *Air* participate in genomic imprinting [109,110]. LincRNAs like *HOTAIR* are shown to be involved in gene regulation in *trans* by interacting with proteins of the polycomb family [111]. More generally lincRNAs are considered to function as scaffolding elements facilitating protein-protein interactions [100].

1.6 MicroRNAs

One of the most characterized non-coding RNA species is the class of microRNAs (miRNAs), which are organized in more than 100 miRNA families. MiRNAs are single stranded small non-coding RNAs (ncRNAs) of ~21 nucleotides (nt) in length derived from short hairpin precursors [112]. The first miRNA *lin-4* was discovered in 1993 in *C. elegans* and was shown to regulate the *lin-14* gene [113,114]. Initially, these novel ncRNAs were

named small temporarily RNAs (stRNAs). However, the term microRNA that defines a certain class of ncRNAs with common properties like length, biogenesis, expression pattern and mode of action has been introduced in 2001 [115,116,117,118]. From this point the number of identified miRNAs in plants and metazoans registered in the miRNA database "miRBASE" (http://www.mirbase.org) has constantly and rapidly increased.

1.6.1 MicroRNA biogenesis

MicroRNA sequences are encoded within introns and exons of non-coding and protein coding genes [8,119,120]. Roughly 50% of all miRNA sequences derive from precursor molecules that are shared by several miRNAs and are termed miRNA clusters (e.g. the miR-17-92 cluster) [121]. Furthermore, several miRNAs have paralogues on distant genomic regions [122].

As depicted in Figure 1-6, there are at least two different mechanisms for miRNA biogenesis known. In the canonical pathway the primary precursor sequences of miRNAs (pri-miRNAs) are typically polymerase II (Pol II) derived [123,124]. However, a minority of pri-miRNAs is transcribed by polymerase III (Pol III) [125]. The pri-miRNAs usually consist of several kilobases (kb) and contain secondary structures like hairpins. In the nucleus the pri-miRNAs are processed to ~70 nt secondary precursor miRNAs (pre-miRNAs) [121]. The pre-miRNA production is facilitated by the RNase III-type enzyme Drosha, which is connected to DiGeorge critical region gene 8 (DGCR8) forming the microprocessor complex [126,127,128]. During transcription of the primary precursor, DGCR8 binds to the double stranded RNA (dsRNA) part of a specific stem loop in the nascent pri-miRNA. The stem usually contains about 33 nt of dsRNA sequence. DGCR8 binds the single stranded portions (ssRNA) flanking the stem loop in addition. Finally, DGCR8 assists Drosha to cleave the bound stem loop approximately 11 nt distant from the ssRNA to dsRNA junction [129,130,131]. In addition, it has been shown that the biogenesis of several miRNAs requires accessory proteins (e.g. hnRNP A1 or KSRP) bound to the microprocessor complex during processing of the pri-miRNA. The protein hnRNP A1 has been reported to serve as an auxiliary factor binding to the loop of the pri-miR-18a (refer to 1.6.5), thereby relaxing the stem loop structure and supporting the cleavage by Drosha. Furthermore, approximately 14% of all pri-miRNAs contain conserved loops,

which could serve as interacting platforms for *trans*-acting factors like hnRNP A1 suggesting a more general regulation of this specific processing step [132,133,134,135].

The resulting pre-miRNA is exported from the nucleus to the cytoplasm mediated by exportin 5 (EXP5), a member of the nuclear transport receptor family [136,137,138], (Figure 1-6). The highly conserved RNase III enzyme Dicer further processes the pre-miRNA. The enzyme cleaves the pre-miRNA near the terminal loop, releasing a miRNA duplex with ~21 nt in length [139,140,141]. In addition, Dicer is connected to the two accessory proteins TRBP and PACT, which are facilitating the loading of the mature miRNA into the RNA induced silencing complex (RISC),[142,143]. During the formation of an intermediate RISC-loading complex (RLC), one strand of the miRNA duplex is incorporated into the RISC effector protein argonaute (AGO) whereas the passenger strand is degraded [144]. The thermodynamic stability of the two ends of the miRNA duplex usually determines the strand to be loaded to the complex [145]. In humans, four different members of the argonaute protein family (AGO1-4) are expressed. It is assumed that they possess similar functions, as all four members of this protein family seem to bind the same miRNA repertoire [146,147]. However, AGO2 is the only member of this family with a catalytically active RNase H domain enabling AGO2 to degrade the bound target transcript under specific circumstances [148].

Alternatively, miRNAs derive from a non-canonical biogenesis pathway. Here the miRNAs are exclusively encoded within small intronic sequences (Figure 1-6). During transcription of the host gene, the specific intron is spliced. The resulting lariat structure, which is also termed pre-mirtron, is enzymatically debranched leading to the formation of hairpin structures. The 5' or 3' overhangs of the hairpins are endonucleolytically cleaved by so far unknown enzymes, producing the pre-miRNA and thereby bypassing the Drosha dependent processing step. Like in the canonical pathway, the pre-miRNA is exported to the cytoplasm, further processed by Dicer and the mature miRNA is loaded to the RISC [149,150]. Once the mature miRNA is incorporated into the RISC (miRISC), the miRNA guides the protein complex via its seed sequence to target mRNAs, leading to their translational inhibition or degradation (refer to 1.6.2).

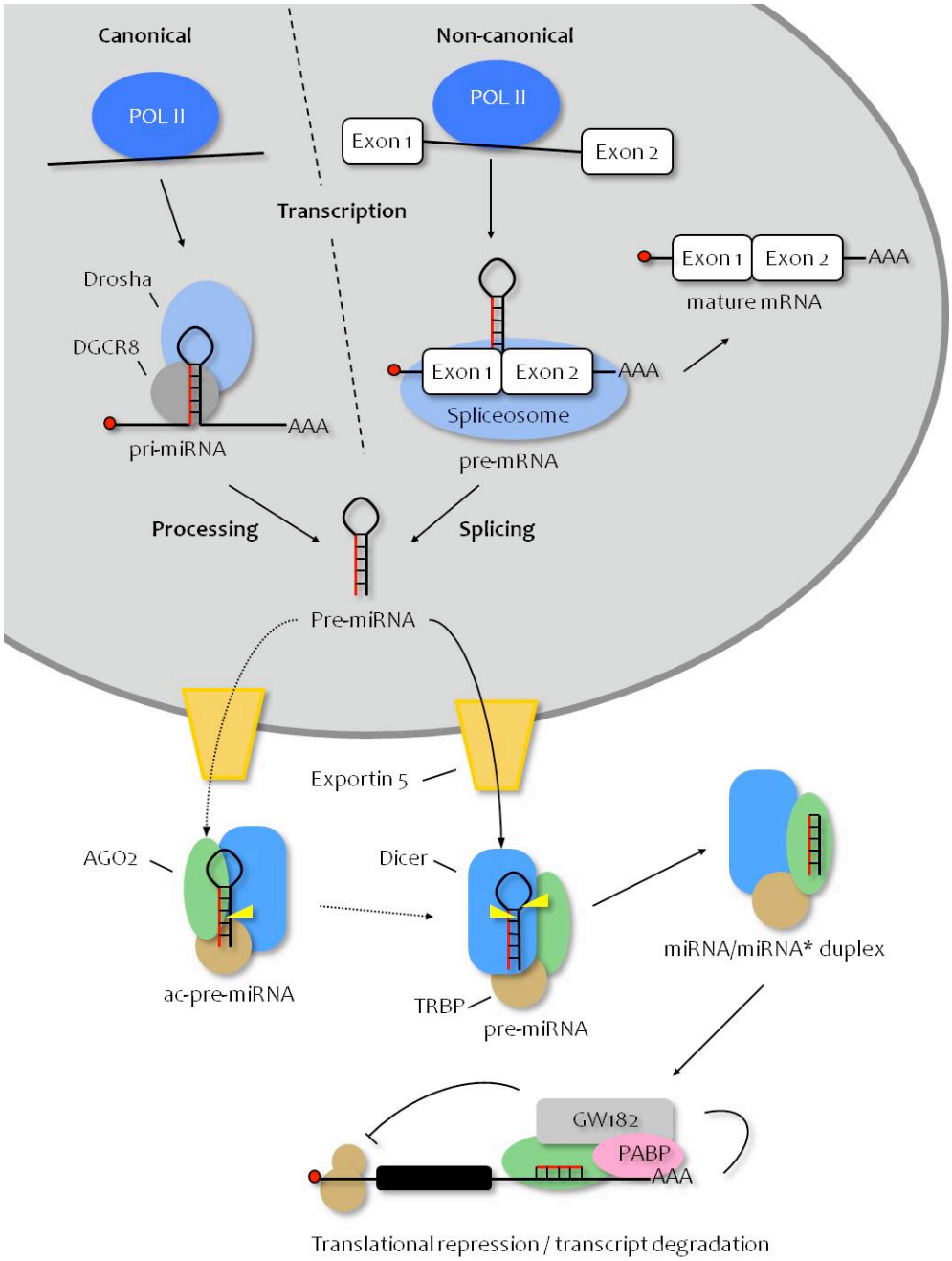

Figure 1-6: Schematic drawing of the miRNA biogenesis pathways.

In 2007, Landgraf and colleagues identified a small set of ubiquitously expressed miRNAs accounting for the majority of differences in miRNA profiles of various cell lines and tissues [151]. Additionally, they identified miRNAs exclusively expressed in certain tissues, raising the question how the expression and biogenesis of mature miRNAs is regulated. The production of functional miRNAs is modulated at various stages of the biogenesis pathway. The expression of the pri-miRNA can be driven or repressed by Pol II-associated transcription factors like the c-MYC oncogene [122]. Furthermore, Weber and colleagues

observed that 47% of 332 human miRNA genes tested are associated with CpG islands, suggesting an important role of DNA methylation in modifying the expression of pri-miRNA [152].

The processing step from pri- to pre-miRNA is regulated as well. As recently reported, some accessory proteins like hnRNP A1, KSHP and SMAD are playing important roles in Drosha dependent cleavage of certain pri-miRNAs [133,134,153]. It has been also observed that the main factors for miRNA biogenesis itself (e.g. Drosha, DGCR8 or Dicer) are tightly regulated. Typically, the expression or activity of these enzymes is modified by single negative feedback loops. Han and colleagues observed that DGCR8 is down regulated by its co-factor Drosha, degrading the *DGCR8* mRNA. Conversely, DGCR8 stabilizes the Drosha protein and thereby setting homeostatic levels of both enzymes for a constant miRNA biogenesis [154,155]. The activity of Dicer is controlled through negative feedback circuits as well, since several mature miRNAs, e.g. let-7 or miR-130a, have been reported to negatively regulate the expression of Dicer [156,157]. Additionally, a double-negative feedback circuit also controls Dicer activity. The major let-7 target gene *LIN28* has been shown to interfere with pre-let-7 processing by induction of a terminal uridylation of pre-let-7, thereby inhibiting further processing by Dicer [158,159,160].

The argonaute proteins affect the efficiency of miRNA production as well. In 2007, Diederichs and Haber reported that AGO2 is able to cleave cytosolic pre-miRNAs to a novel intermediate molecule termed ac-pre-miRNA (Figure 1-6) thereby enhancing the expression of mature miRNAs. Moreover, they generally observed a slight increase of miRNA production after ectopic expression of all human AGO proteins [161].

Pri-miRNAs serve as substrates for adenine deaminases (ADARs) changing specific adenines to inosines thereby modifying the affinity to the processing machinery. Additionally, hyper-edited dsRNAs are actively degraded by a RISC subunit [162]. Recent studies suggest that approximately 16% of pri-miRNAs are eventually modified by ADARs. Moreover, adenine deamination has been observed in the seed sequence of miR-379 and miR-411 resulting in the alteration of target recognition [163], (refer to 1.6.2).

Mature miRNAs are actively degraded. Even though the field of miRNA decay is poorly investigated, recent studies in *C. elegans* and plants suggest an active degradation of miRNAs by RNA specific nucleases [164,165]. Finally, major factors of the miRNA

biogenesis machinery are regulated by phosphorylation, hydroxylation or ubiquitination leading to alterations in their localization, activity and stability [166].

1.6.2 Operating principles of microRNAs

In 2005, Lewis and colleagues predicted that more than 30% of the human genes might be regulated by miRNAs binding to conserved sequence motifs raising the question of how microRNAs affect their targets [167]. MicroRNAs specifically identify target mRNAs by a 6-8 nt sequence located in the 5' part of the mature miRNA. Typically, the sequence stretch from nucleotide 2 to nucleotide 8 is termed the "seed" sequence, which has to generate a perfect RNA double-helix pairing to the target transcript [112,168]. It has been experimentally shown that target recognition is extremely sensitive to alterations of the seed sequence [169]. Besides the seed pairing, supplementary pairing of the 3' part of the miRNA is supportive and plays a minor role in target recognition. Furthermore, optimal location of this additional pairing was observed at nucleotides 13-16 with at least 3-4 coherent nucleotide pairings [168,170]. The vast majority of miRNA binding sites were identified in the 3' untranslated region (3'UTR) of messenger RNAs. In some rare cases also functional miRNA binding sites were identified in the 5'UTR and the open reading frame (ORF) of transcripts [171]. Grimson and colleagues could show that there are further factors influencing the efficacy of miRNA target recognition. First, miRNA binding sites in the vicinity of high AU content are more effectively recognized than those with low AU content. Second, effective target sites for miRNAs preferentially reside at both ends of the 3'UTR but not too close to the stop codon [170]. In addition, recent data indicate that proliferating cells specifically express mRNA splice variants with shortened 3'UTRs lacking miRNA binding sites and therefore circumventing their regulation by certain miRNAs [172].

The AGO proteins are the key component of the miRISC as they carry the mature miRNA, which is guiding the whole complex to a target mRNA. As previously reported, mammals express four argonaute proteins AGO1 to AGO4 [173]. Of these only AGO2 possesses an RNase H-like domain, which could eventually cleave the bound target mRNA [174]. Additionally, GW182 proteins are essential factors of the miRISC. In mammals three members (TNRC6A, -B and –C) of the GW182 protein family exist. GW182 proteins contain glycine tryptophan (GW) repeats enabling the direct interaction to the AGO proteins

[175], (Figure 1-6). GW182 proteins are the actual effectors of the miRISC since they mediate the translational repression and destabilization of mRNAs [176,177,178,179,180].
Once a specific mRNA is bound to a miRISC the translation of the mRNA is inhibited and/or the mRNA is degraded. To what extend mRNA targets are either cleaved or translationally inhibited is still a matter of debate [181]. Various experiments revealed that repression occurs at three different points of the mRNA translation process. The 7-methyl-guanosine cap (m^7G) of a mRNA seems to play a crucial role in translational inhibition [182]. Studies suggest that miRISCs bound to 3'UTR compete with elongation initiation factor eIF4E for the m^7G binding and therefore prevent the initiation of translation [183]. MiRISC binding interferes with the 40S and 80S ribosomal subunit recruitment and 80S initiation complex formation [184,185]. The deadenylation of mRNAs targeted by miRISCs promotes translational repression as well [186]. Furthermore experiments suggest mechanisms repressing the translation at the post-initiation step by recruiting proteases degrading the nascent amino acid chain [187,188].
Deadenylation and subsequent decapping initiate the mRNA decay. GW182 proteins facilitate deadenylation, as they recruit the deadenylase complex CCR4 - NOT1 [178]. Furthermore, experiments indicate that the poly(A)-binding protein (PABP) is required to interact with GW182 as well (Figure 1-6). The PABP connects the poly(A)-tail of the mRNA to the miRISC facilitating initiation of the deadenylation reaction [180,189]. Targeted mRNAs were observed to accumulate in specific cytosolic structures like P-bodies or stress granules (SGs). It appears that P-bodies act as sites for mRNA decay since they contain the CCR4-NOT1 deadenylase complex and the DCP1-DCP2 decapping enzyme complex [190,191]. Selbach and colleagues applied a novel technique termed pSILAC (pulse stable isotope labeling of amino acids in cell culture) to determine proteomic changes upon ectopic expression of certain miRNAs. They found that 32 hours post-transfection the alterations on the proteome presumably caused by the manipulated miRNA correlated with a mild reduction of the respective mRNA levels [192]. Hendrickson and colleagues performed immunoprecipitations (IP) with AGO-specific antibodies upon ectopic miR-124 expression in order to co-IP and test recruitment of mRNAs to the miRISCs. Thereby, they recognized that mRNA degradation accounted for approximately 75% of the changes they observed on protein level [193]. In a second study Guo and colleagues made similar observations. The reduction of proteins was mainly caused by a

decrease of mRNA steady state levels [194]. Besides the common negative regulation of miRNA targets, miRNAs were rarely observed to have the opposite effect. Recently, Eiring and colleagues could show that miR-328 is able to enhance the expression of certain targets. MicroRNA-328 binds the 5'UTR of the *CEBPA* mRNA thereby preventing hnRNP E2 from repressing the transcript. Thus, besides repression of numerous targets, miR-328 exhibits a second RISC independent function as an indirect translational activator [195].

The general discussion whether miRNA-targeted transcripts are rather destabilized or translationally blocked remains active and will be further addressed in the future, since the development of novel technologies to study this question is ongoing.

1.6.3 MicroRNAs and cancer

In 2004, Calin and colleagues performed expression profiling of miRNAs in B-cells of patients with chronic lymphocytic leukemia and identified at least two distinct subpopulations of CLL samples according to their miRNA expression pattern [196]. Furthermore, they suggested that approximately 50% of all human miRNAs are encoded on chromosomal regions known to be recurrent breakpoints in human cancers, indicating an important role for miRNAs in cancer development [197]. The miRNA cluster miR-15a-16-1 for instance is encoded in the chromosomal region 13q14, which is frequently deleted in CLL [8]. Interestingly, miR-15a and miR-16-1 were identified to directly regulate the expression of the anti-apoptotic factor *BCL2* [198]. In addition, single nucleotide polymorphisms (SNPs) in miRNAs or miRNA target regions of mRNAs are associated with different cancer types [199]. Although there is no direct evidence for a causative role of miRNAs in tumorigenesis, miRNAs might play an important role as tumor suppressors or oncogenes by regulating cancer associated genes. So far the expression of several miRNAs like let-7(a-i), miR-21, miR-26a, miR-34a, miR-17-92 and miR-155 were found to be altered in many cancer types [200]. Furthermore, miRNA signatures were shown to have predictive or prognostic value for certain cancer types. For instance high miR-21 levels in patients with colon adenocarcinoma were associated with poor survival and therapeutic outcome [201]. As body fluids are easily obtainable from cancer patients and miRNAs exhibit a high stability in these fluids, miRNA expression profiles of patient sera got into the focus of research as well. For instance, high miR-21 levels in the serum of patients

with DLBCL were shown to associate with relapse-free survival [202]. However, the mechanisms by which the miRNAs are transported to the body fluids are poorly characterized.

1.6.4 MicroRNA-155

The genomic sequence encoding miR-155 is located in the third exon of the B-cell integration cluster (*BIC*) gene on chromosome 21q21.3. The *BIC* gene was initially identified as a common integration site for the *avian leucosis virus* (ALV) [203]. Years later Tam and colleagues could show that the integration of the retroviral promoter of ALV activated the expression of the non-coding *BIC* gene, determining *BIC* as a proto-oncogene [204]. *BIC* was shown to be predominantly expressed in lymphatic organs like spleen and thymus [119]. In 2005, miR-155 was shown for the first time to be over-expressed in human B-cell lymphomas [205]. Thereafter, an elevated expression of miR-155 has been observed in DLBCL, Hodgkin lymphoma (HL) and Epstein-Barr virus transduced Burkitt's lymphoma (BL) [206,207]. MicroRNA-155 is 20 to 30-fold higher in expression in DLBCL than in normal B-cells [151]. Several transcription factors like NF-κB and AP1 or signaling molecules like TNF-α or INF-β were identified to regulate the expression of miR-155 [208,209,210]. Additionally, a regulatory role of miR-155 on several transcripts like *CEBPB*, *SMAD2*, *BACH1*, *ZIC3*, *PU.1*, *IKBKE*, *SHIP1*, *AID1* and *WEE1* has been experimentally shown [211,212,213,214,215,216,217]. Transgenic mice lacking miR-155 have impaired immune responses whereas mice over-expressing miR-155 exhibit perturbed peripheral blood cell populations with increased proliferation of pre-B cell populations [216,218,219]. Recently it has been shown, that miR-155 plays a key role during B-cell immortalization by EBV [45].

1.6.5 The microRNA cluster miR-17-92

The miR-17-92 cluster is located on chromosome 13, open reading frame 25 (c13orf25), a region frequently amplified in human cancers [122]. Ota and colleagues identified a close correlation of an enhanced expression level of the miR-17-92 cluster and a genomic amplification of the corresponding chromosomal region [220]. The pri-miRNA has a length of approximately 1.3 kb and carries the sequence of the miRNAs miR-17, miR-18a, miR-19a, miR-19b-1, miR-20a and miR-92a-1. Furthermore, there are homologous miRNAs in the miR-106a-92 cluster and the miR-106b-25 cluster. The miR-106a-92 cluster, located

on chromosome X, carries the three miRNAs 106b, 19b-2 and 92-2, homologues of miR-17, miR-19b-1 and miR-92-1, respectively. The miR-106b-25 cluster contains the miRNAs miR-106b, miR-93 and miR-25, homologues of miR-17, miR-20a and miR-92-1, respectively [120]. Aberrant expression of the miR-17-92 family has been observed in various tumors like DLBCL, CLL, multiple myeloma (MM), hepatocellular carcinomas, lung tumors and medulloblastomas [221,222,223,224,225,226]. It was shown that the proto-oncogene *c-MYC* is one of the transcription factors, which is driving miR-17-92 expression [227,228,229]. Manipulation of miR-17-92 in mice resulted in severe phenotypes. Ventura and colleagues observed that miR-17-92 deficient mice died directly after birth, showing hypoplastic lungs and reduced amounts of pre-B-cells [230]. Mice with enhanced expression of miR-17-92 in lymphocytes exhibited a lymphoproliferative phenotype coupled with autoimmunity and premature death [5]. Several transcripts regulated by miR-17-92 were experimentally identified. Among these were pro-apoptotic genes like *BIM* and *PTEN* as well as other cancer related genes like *CCND1*, *HIF-1a* or *CTGF* [5,231,232,233,234]. According to its oncogenic properties the miR-17-92 cluster got his secondary name "oncomiR-1".

1.7 Aim of the study

The microRNA miR-155 and the miR-17-92 cluster are aberrantly expressed in various cancers including B-cell lymphomas (refer to 1.6.4 and 1.6.5) potentially regulating up to several hundreds of transcripts. It was the aim of this study to identify transcripts regulated by these miRNAs in order to delineate their potential role in chronic lymphocytic leukemia and mantle cell lymphoma.

In a first approach, B-cell lines were screened for potential target genes using current standard techniques like expression arrays, qRT-PCR, luciferase sensor assays and Western blot analyses upon manipulation of miR-155 and miR-17-92 expression in cell lines. As these results were mild and novel findings suggested that miRNAs in general have limited regulatory effects on single target genes, I established a recently published screening method, which is based on immunoprecipitation of RNA induced silencing complexes and subsequent sequencing of co-precipitated RNA (RIP-Seq), to identify the targetome of miRNAs. Using cells with and without transgenic expression of miR-155, the targetome of this oncogenic miRNA should be characterized. A second aim was the analysis of the global miRNA targetome of leukemic B-cell lines to identify genes that

might act as tumor suppressors and to thereby uncover novel potential mechanisms of leukemogenesis.

2 Material and Methods

2.1 Material

2.1.1 Chemicals

Chemical	Producer
±-Thioglycerol	Merck, Darmstadt, Germany
2-Mercaptoethanol	Sigma-Aldrich, Munich, Germany
2-Propanol	Merck, Darmstadt, Germany
7-Aminoactinomycin D (7-AAD)	Sigma-Aldrich, Munich, Germany
Acetic acid	Roth, Karlsruhe, Germany
Agarose	Sigma-Aldrich, Munich, Germany
Ammonium acetate ($C_2H_3O_2NH_4$)	Sigma-Aldrich, Munich, Germany
Ammonium Persulfate (APS)	Sigma-Aldrich, Munich, Germany
Ampicillin	Roche, Mannheim, Germany
Annexin V	BD Biosciences, San Jose, USA
Bacto Agar	Sigma-Aldrich, Munich, Germany
Bacto Tryptone	Difco Laboratories Inc., Detroit, USA
Bacto yeast extract	Difco Laboratories Inc., Detroit, USA
Bicinchoninic acid (BCA)	Difco Laboratories Inc., Detroit, USA
Bis-Acrylamide (30% w/v)	Bio-Rad, Hercules, USA
Bovine serum albumine (BSA)	Sigma-Aldrich, Munich, Germany
Bromphenoleblue	AppliChem GmbH, Darmstadt, Germany
Chloroform	Merck, Darmstadt, Germany
Complete EDTA-free protease inhibitor cocktail	Roche, Mannheim, Germany
Copper (III)-sulfate	Sigma-Aldrich, Munich, Germany
Dimethylsulfoxide (DMSO)	Sigma-Aldrich, Munich, Germany
Dithiothreitol (DTT)	Merck, Darmstadt, Germany
Ethanol	Merck, Darmstadt, Germany
Ethylenediaminetetraacetic acid (EDTA)	Merck, Darmstadt, Germany
Etidium bromide	Sigma-Aldrich, Munich, Germany
Glycerine	Roth, Karlsruhe, Germany
Glycine	Roth, Karlsruhe, Germany
HEPES	Sigma-Aldrich, Munich, Germany
Hydrochloric acid (HCl)	Merck, Darmstadt, Germany
Hygromycin-B	Invitrogen, Carlsbad, USA
Isoamylalcohol	Merck, Darmstadt, Germany
Magnesium chloride	Merck, Darmstadt, Germany
Methanol	Sigma-Aldrich, Munich, Germany
Milk powder	Sigma-Aldrich, Munich, Germany
NP-40	Sigma-Aldrich, Munich, Germany
Nuclease free water	Ambion, Austin, USA
Phenol	Roth, Karlsruhe, Germany
Potassium chloride (KCl)	Sigma-Aldrich, Munich, Germany
Potassium dihydrogen phosphate (KH_2PO_4)	Sigma-Aldrich, Munich, Germany
RNase Out	Invitrogen, Karlsruhe, Germany
Sodium acetate (NaAc)	Merck, Darmstadt, Germany
Sodium chloride (NaCl)	Merck, Darmstadt, Germany
Sodium citrate	Merck, Darmstadt, Germany
Sodium dodecyl sulfate (SDS)	Merck, Darmstadt, Germany

Chemical	Producer
Sodium hydrogen phosphate (Na2HPO4)	Merck, Darmstadt, Germany
Sodium hydroxide (NaOH)	Merck, Darmstadt, Germany
Sodium azide (NaN3)	Sigma-Aldrich, Munich, Germany
TEMED	Sigma-Aldrich, Munich, Germany
TRIZMA-Base	Sigma-Aldrich, Munich, Germany
Trizol LS reagent	Invitrogen, Carlsbad, Germany
Trizol reagent	Invitrogen, Carlsbad, Germany
Tween-20	Sigma-Aldrich, Munich, Germany
Vanadyl ribonucleoside complex	New England Biolabs, Frankfurt aM, Germany

2.1.2 Enzymes

2.1.2.1 Restriction enzymes

Restriction enzyme	Supplier
Hind III	Roche, Mannheim, Germany
Nae I	New England Biolabs, Frankfurt aM, Germany
Not I	Roche, Mannheim, Germany
Pst I	New England Biolabs, Frankfurt aM, Germany
Sac I	Roche, Mannheim, Germany
Spe I	Roche, Mannheim, Germany
Xho I	Roche, Mannheim, Germany

2.1.2.2 Other enzymes

Enzyme	Supplier
Benzonase	Merck, Darmstadt, Germany
DNase I	Roche, Mannheim, Germany
FastStart Taq Polymerase	Roche, Mannheim, Germany
Proteinase K	Qiagen, Hilden, Germany
RNase A	Qiagen, Hilden, Germany
RNase H	New England Biolabs, Frankfurt aM, Germany
Superscript II reverse transcriptase (200U/µl)	Invitrogen, Carlsbad, USA
T4 DNA Ligase	Fermentas, St. Leon-Roth, Germany
T4 DNA Polymerase	New England Biolabs, Frankfurt aM, Germany

2.1.3 Kits

Kit	Supplier
Absolute™ qRT-PCR SYBR® Green Rox kit	ABgene, Epsome, UK
Agilent Bioanalyzer RNA Nano kit	Agilent Technologies, Palo Alto, USA
Agilent Bioanalyzer RNA Pico kit	Agilent Technologies, Palo Alto, USA
BCA protein quantification kit	Thermo Scientific, Rockford, USA
Big Dye Terminator sequencing kit	Applied Biosystems, Foster City, USA
Blood and Cell genomic DNA midiprep kit	Qiagen, Hilden, Germany

Kit	Supplier
ECL plex Western blot detection kit	GE Healthcare Europe GmbH, Freiburg, Germany
ECL Western blot detection kit	GE Healthcare Europe GmbH, Freiburg, Germany
ECL+ Western blot detection kit	GE Healthcare Europe GmbH, Freiburg, Germany
Endofree Plasmid Maxiprep kit	Qiagen, Hilden, Germany
Illumina mRNA-Seq kit	Illumina Inc., San Diego, USA
miRNA qRT-PCR Primer sets	Applied Biosystems, Foster City, USA
miRNA reverse Transcription kit	Applied Biosystems, Foster City, USA
miRNeasy microRNA preparation kit	Qiagen, Hilden, Germany
Plasmid minprep kit	Qiagen, Hilden, Germany
Qiaquick PCR purification kit	Qiagen, Hilden, Germany
Quiaquick DNA Gel extraction kit	Qiagen, Hilden, Germany
Absolute™ qRT-PCR SYBR® Green Rox kit	ABgene, Epsome, UK

2.1.4 Other consumables

Name	Supplier
ABI PRISM™ optical adhesive covers	Applied Biosystems, Foster City, USA
Adenosine 5'Triphosphate	Roche, Mannheim, Germany
Broad range multicolor protein mass standard	Fermentas, St. Leon-Roth, Germany
Deoxynucleotide (dNTP) mix	Roche, Mannheim, Germany
DNA mass standard (1kb DNA ladder)	Fermentas, St. Leon-Roth, Germany
ECL advance blocking agent	GE Healthcare Europe GmbH, Freiburg, Germany
Falcon 15ml Tubes	BD Biosciences, San Jose, USA
Falcon 50ml Tubes	BD Biosciences, San Jose, USA
Fluorescent dye protein mass standard	GE Healthcare Europe GmbH, Freiburg, Germany
Hybond LFP PVDF Western blot membrane	GE Healthcare Europe GmbH, Freiburg, Germany
Hyperfilm ECL	GE Healthcare Europe GmbH, Freiburg, Germany
Immobilon-P PVDF Western blot membrane	Millipore, Schwalbach, Germany
MicroAmp plates, optical 384-well reaction plates	Applied Biosystems, Foster City, USA
Microcentrifuge tubes 1.5 ml	Eppendorf, Hamburg, Germany
Microcentrifuge tubes 2.0 ml	Eppendorf, Hamburg, Germany
PCR tubes 8-stripes 0.2 ml	Sarstedt, Nümbrecht, Germany
Propidium iodide	Invitrogen, Carlsbad, USA
Protein G sepharose Beads	GE Healthcare Europe GmbH, Freiburg, Germany
Random hexamer primers	Invitrogen, Carlsbad, USA
RNase Zap	Ambion, Austin, USA
Safe lock tubes 1.5 ml	5 Prime, Gaitherburg, USA
Second strand buffer for SSII	Invitrogen, Carlsbad, USA
T4 gene 32 protein	New England Biolabs, Frankfurt aM, Germany
Universal human reference RNA	Stratagene, La Jolla, USA

2.1.5 Solutions

2.1.5.1 Standard Solutions

Standard solution	Composition
10x PBS	137 mM NaCl 27 mM KCl 100 mM NaH_2PO_4 17 mM KH_2PO_4 dissolve in ddH_2O
10x TBS	200 mM TRIZMA-Base 137 mM NaCl set pH 7.6 using HCl dissolve in H_2O
5x Loading buffer	100 mM EDTA 30% (v/v) Glycerine 0.25% (w/v) Bromophenolblue dissolve in H_2O
5x TBE	445 mM TRIS-Borat, pH 8.0 10 mM EDTA, pH 8.0
10% SDS	10% SDS (w/v) dissolve in H_2O

2.1.5.2 Medium and Antibiotics for bacteria

Medium	Composition
LB medium	1% (w/v) Bacto-Trypton 0.5% (w/v) Bacto-Yeast-Extract 1% (w/v) NaCl dissolve in H_2O adjust to pH 7.5
Ampicillin	Stock solution: 100 mg/ml Working solution 100 µg/ml diluted in H_2O Stored at -20°C

2.1.5.3 Bacteria

Bacteria	Supplier
OneShot™ Top10 Electrocomp™ e.coli	Invitrogen, Carlsbad, USA

2.1.5.4 Western blot Solutions

Western blot solution	Composition
10x SDS-running buffer	25 mM TRIS-HCl 192 mM Glycine 0.1% (v/v) SDS dissolve in 1L H_2O

Western blot solution	Composition
10x Transfer buffer	25 mM TRIS-HCl 192 mM Glycine dissolve in 1L H_2O
Blocking buffer (Milk)	PBS or TBS 0.1% (v/v) Tween-20 5% (w/v) Milk powder
Blocking buffer (BSA)	PBS or TBS 0.1% (v/v) Tween-20 5% (w/v) BSA
Stripping buffer (Sodium azide)	PBS or TBS 0.1% (v/v) Tween-20 5% (w/v) BSA or Milk 0.01% (v/v) Sodium azide
Stripping buffer (β-Mercaptoethanol)	100 mM β-Mercaptoethanol 2% (w/v) SDS 62.5 mM TRIS-HCL, pH 6.7
RIPA-buffer	50 mM TRIS 50mM 150 mM NaCl 0.1% (v/v) SDS 0.5% (v/v) Na-Deoxycholate 1% (v/v) NP40 Protease inhibitor cocktail (1 Tablet in 10ml)
Blocking buffer (advanced blocking agent)	PBS or TBS 0.1% (v/v) Tween-20 2% (w/v) Advanced blocking agent

2.1.5.5 Solutions for luciferase sensor assays

Solutions for luciferase sensor assays	Compositions
Passive lysis buffer	Promega, Fitchburg, USA
Firefly luciferase buffer	25 mM GlycylGlycine 1 M K_xPO_4 4 mM EGTA 2 mM ATP 1 mM DTT 15 mM $MgSO_4$ 0.1 mM CoA 100 µM luciferin dissolve in H_2O, set pH to 8.0
Renilla luciferase buffer	1.1 M NaCl 2.2 mM Na_2EDTA 220 mM K_xPO_4 0.44 mg/ml BSA 1.3 mM NaN_3 2.5 µM Coelenterazine dissolve in H_2O, set pH to 5.0

2.1.5.6 Solutions for RIP-Seq

Solutions for RIP-Seq	Composition
Bead elution buffer	1 M Glycine (pH 2.3)
Neutralization buffer	1 M TRIS-HCl (pH 8.0)
NT2 buffer (50 ml)	RNase free H_2O, 40 ml 50 mM TRIS (pH 7.4) 150 mM NaCl 1 mM $MgCl_2$ 0.05% NP-40
Polysome lysis buffer (5 ml)	RNase free H_2O 10 mM HEPES (pH 7.0) 100 mM KCl 5 mM $MgCl_2$l 0.5% NP-4 1 mM DTT RNase OUT, 12.5 µl 1x Protease inhibitor cocktail, 20 µl 0.4 mM Vanadyl ribonucleoside complex

2.1.6 Vectors

Vector	Supplier
pCMX_h-Cre	E. Greiner (DKFZ, Heidelberg) with approval of F. Steward (Dresden)
pMiRReport Luciferase Sensor	Ambion, Austin, USA
pREP4	Invitrogen, Carlsbad, USA
TK Renilla vector	Promega, Fitchburg, USA

2.1.7 Primer

2.1.7.1 Primer for sequencing, PCR and cloning

Primer name	Sequence (5' => 3')
ADNP_UTR_f	TTTACTAGTCTGGCGTTGGTGACATGC
ADNP_UTR_r	TTTGAGCTCACATTAAGCACAATACAGCAATTT
CCNT2_Seq_f1	TCAGGATTGGAGCTGCTTGT
CCNT2_Seq_r1	TGAAGTTATGCAAGACCAGAACA
CCNT2_UTR_f	TTTGAGCTCTTTGTTTAGGTCAATTTTTCCTTT
CCNT2_UTR_r	TTTAAGCTTACAACTGGCTGCCCTTTAAT
CDC2L6_UTR_f	TTTACTAGTCCAGAGCACAGGCTCCAG
CDC2L6_UTR_r	TTTGAGCTCAAAGCAGCTAAGAAAGAACTCAGC
CDC42_UTR_f	TTTGAGCTCTCTCTCCAGAGCCCTTTCTG
CDC42_UTR_r	TTTAAGCTTTGAGAAAGCATTGGTTCAACA
CKAP5_UTR_f1	TTTACTAGTAGAGCAGTCGCAAATGAAGC
CKAP5_UTR_r1	TTTAAGCTTATGGAGCATCTTGGGAGTCA
E2F8_UTR_f	TTTACTAGTTCAACAGATGTTGGCTTAGTTTAAT
E2F8_UTR_r	TTTGAGCTCAAATAATTTTTCCATAGACTTGATTGA
FBXW7_Seq_f1	TTGCCAATGTCAATCAATCA

Primer name	Sequence (5' => 3')
FBXW7_Seq_r1	CGTTCATCCATTCACCACAG
FBXW7_UTR_f	TTTACTAGTGCAGAAAAGATGAATTTGTCCA
FBXW7_UTR_r	TTTGAGCTCTTCAGTGGAAGAAACAGGCATA
IKKE_UTR_f2	TTTACTAGTGCACATGAGGCATCCTGAA
IKKE_UTR_r2	TTTGAGCTCAAGTCCTATAAACCAGAGGGAGTG
IRS2_Seq_f1	GTAGTAGCCCCTGCGCTGT
IRS2_Seq_r1	TGTTCAGGGCAGCCTCAC
IRS2_UTR_f	TTTACTAGTAGATCTGTCTGGCTTTATCACCA
IRS2_UTR_r	TTTGAGCTCATTTTATTGCATATGGCTATTAAGGA
KIF11_UTR_f	TTTACTAGTCGAGCCCAGATCAACCTTTA
KIF11_UTR_r	TTTGAGCTCTTGCCAGATAAGAAATTATGGAG
LAT2_UTR_f1	TTTACTAGTCAAGGCAAAGAGGGACCAC
LAT2_UTR_r	TTTGAGCTCAAATGGTTTTATTGAGATGTTTTGG
miR-155_f	TTTAAGCTTCTATATGCTGTCACTCCAGCTTT
miR-155_r	TTTCTCGAGTGGCAGATAGCTTCTGGAAT
miR-18af1	TTTAAGCTTACTTGTAGCATTATGGTGACAGC
miR-18ar	TTTCTCGAGGCAACTATGCAAAACTAACAGAGG
miR-19af1	TTTAAGCTTTGCAGATAGTGAAGTAGATTAGCATC
miR-19ar1	TTTCTCGAGTTTAGTGCTACAGAAGCTGTCACAT
miR-92af1	TTTAAGCTTTGTGGTAGTGAAAAGTCTGTAGAAAA
miR-92ar1	TTTCTCGAGATCCCCACCAAACTCAACAG
PEBP1_UTR_f1	TTTACTAGTTAGCTTGGGGACCTGAACTG
PEBP1_UTR_r1	TTTGAGCTCTTATTCAACTACAAGCAAACAGCA
RAB34_UTR_f	TTTACTAGTGGCTGAGGAGACTGTTCAGAG
RAB34_UTR_r	TTTGAGCTCAAGTGCTCGTAACAAAGAAATTTTA
RAB5C_UTR_f	TTTACTAGTCTCCTCCGCCTGAATGAC
RAB5C_UTR_r	TTTGAGCTCATTGACAAGATACTGATTGGTTACAT
RGL1_Seq_f	CACTTTGGAAAGGGTTTGGA
RGL1_Seq_r	CCAATCTCCTGGAAAGACCA
RGL1_UTR_f	TTTGAGCTCCCCCTTGTTTGCCAAAGG
RGL1_UTR_r	TTTAAGCTTTTTGGGTCTGGCAGCACAT

2.1.7.2 Primer for qRT-PCR

Primer name	Sequence (5' => 3')
ABR_qRT_f	CTTCCTGGTGGCTGTGAAG
ABR_qRT_r	CAAGAACCCCGAGAGAACC
ADNP_qRT_f	GACCCATCACTTACGAAAAACC
ADNP_qRT_r	TTTTGAGGAAAATGGACAAGC
BCL11A_qRT_f1	CCCCGCAGGGTATTTGTA
BCL11A_qRT_r1	TGCAAGAGAAACCATGCACT
CCNT2_qRT_f	GCGGATAAAGAGCTCTCGTG
CCNT2_qRT_r	GCAGTGTTTATTGTAAGCTGAGAGA
CDC42_qRT_f	TGGAGTGTTCTGCACTTACACA
CDC42_qRT_r	GGGCTCTGGAGAGATGTTCA
C-FOS_qRT_f	CTACCACTCACCCGCAGACT
C-FOS_qRT_r	AGGTCCGTGCAGAAGTCCT
CIC_qRT_f	ATGTATTCGGCCCACAGG
CIC_qRT_r	GGAAGGGGACTAAGGAGTGC
CSF1R_qRT_f	CATCATGGCCTTGCTGCT
CSF1R_qRT_r	TCCAGCGGACCTGGTACTT

Primer name	Sequence (5' => 3')
DOCK10_qRT_f	TCTGTCGAGGTCCGTGTTTA
DOCK10_qRT_r	GTCGTCCCTGCCCGTAAT
E2F2_qRT_f	AGCCCACAGCATCCTCAGT
E2F2_qRT_r	GCTGTCAGTAGCCTCCAAGG
E2F8_qRT_f	AATGACATCTGCCTTGACGA
E2F8_qRT_r	GTAAATGCGTCGACGTTCAA
ETV5_qRT_f	AACCAGTATCCATCAGAACAGAGA
ETV5_qRT_r	GGGCGATTATCTCCAGGAAC
FBXW7_qRT_f	CCTCCAGGAATGGCTAAAAA
FBXW7_qRT_r	AATGAGTTCATCTAAAGCAAGCAA
FOXP1_qRT_f	CATGTGAAGTCTACAGAACCCAAA
FOXP1_qRT_r	GCGGACTTGGAGAGAGTGAC
GIT2_qRT_f	CTTCCCCTCCACACTTTCCT
GIT2_qRT_r	CAGGTGTGCTGTTCTGCTTC
IRS2_qRT_f	TGACTTCTTGTCCCACCACTT
IRS2_qRT_r	CATCCTGGTGATAAAGCCAGA
LAT2_qRT_f	GAGGATCCAGCATCTTCCAG
LAT2_qRT_r	CCATGGCAATGGGGTCTAT
NDFIP2_qRT_f	CAGCAGCAGAAACATCTCAAAG
NDFIP2_qRT_r	AGCTGGTCTGCATCACTGAA
PIK3R1_qRT_f	AATGAACGACAGCCTGCAC
PIK3R1_qRT_r	CCGTTGTTGGCTACAGTAGTAGG
PTGER4_qRT_f	CTCCCTGGTGGTGCTCAT
PTGER4_qRT_r	GGCTGATATAACTGGTTGACGA
qRT_CCND1_f	ACGAAGGTCTGCGCGTGTT
qRT_CCND1_r	CCGCTGGCCATGAACTACCT
qRT_CEBPB_f	CTCTCTGCTTCTCCCTCTGC
qRT_CEBPB_r	GATTGCATCAACTTCGAAACC
qRT_DCTN2_f	ACTAGCGACCTACCTGAGGA
qRT_DCTN2_r	TCATAGGCAGCATTAGGATTGAC
qRT_GAPDH_f	GCTCTCTGCTCCTCCTGTTC
qRT_GAPDH_r	ACGACCAAATCCGTTGACTC
qRT_PEBP1_f1	CAGTCCTCTCCGATTATGTGG
qRT_PEBP1_r1	CTTTAGCGGCCTGTCCTG
qRT_PGK1_f	TGCAAAGGCCTTGGAGAG
qRT_PGK1_r	TGGATCTTGTCTGCAACTTTAGC
qRT_PHC2_f	CACCAAGTGGAATGTAGAAGACG
qRT_PHC2_r	GGAATTCCTCTGCTATCTCCTG
qRT_RAB5C_f1	CCAAGAACTGGGTGAAGGAG
qRT_RAB5C_r1	GCATAGGCTTGTGCTTCCTG
RAB34_qRT_f	TGATGTGGCATCTCTGGAAC
RAB34_qRT_r	TGAGCAGGGGTAAGGAAGAG
RAP1B_qRT_f	CGTGGCGCCTAGAGTAGC
RAP1B_qRT_r	GCCAAGAACGACTAGCTTATACTCA
RGL1_qRT_f	TCTGCAGAACCTGAACTCGAT
RGL1_qRT_r	CCACAGGTTTCACCTCCATC
SGK1_qRT_f	TTTCCAAAGAGGGGTTCTCC
SGK1_qRT_r	TGGCATGATTACATGGCTCT
SGK3_qRT_f	CAGCTGGGCTGACCTTGTA
SGK3_qRT_r	TGTCAAAGTTTCTGATATCATCTGG
SIRT1_qRT_f	TGAGCAGGGGTAAGGAAGAG
SIRT1_qRT_r	TGTACGACGAAGACGACGAC
SPI1_qRT_f	CCACTGGAGGTGTCTGACG
SPI1_qRT_r	CTGGTACAGGCGGATCTTCT

Primer name	Sequence (5' => 3')
TIA1_qRT_f	GGGATATGGCTTTGTCTCCTT
TIA1_qRT_r	GCCACCCATCTGTTGAATG
TNFAIP3_qRT_f	TGCACACTGTGTTTCATCGAG
TNFAIP3_qRT_r	ACGCTGTGGGACTGACTTTC
VAV3_qRT_f	CCTTAGATACAACTCTGCAGTTTCC
VAV3_qRT_r	GCCCAGCACTTTTGGACTTA

2.1.7.3 Primer for miRNA detection

miRNA	Target sequence (5' => 3')	Supplier
hsa-miR-155	UUAAUGCUAAUCGUGAUAGGGG	Ambion, Austin, USA
hsa-miR-17-3p	ACUGCAGUGAAGGCACUUGU	Ambion, Austin, USA
hsa-miR-17-5p	CAAAGUGCUUACAGUGCAGGUAGU	Ambion, Austin, USA
hsa-miR-18a	UAAGGUGCAUCUAGUGCAGAUA	Ambion, Austin, USA
hsa-miR-19a	UGUGCAAAUCUAUGCAAAACUGA	Ambion, Austin, USA
hsa-miR-19b	UGUGCAAAUCCAUGCAAAACUGA	Ambion, Austin, USA
hsa-miR-20a	UAAAGUGCUUAUAGUGCAGGUAG	Ambion, Austin, USA
hsa-miR-92a-1	AGGUUGGGAUCGGUUGCAAUGCU	Ambion, Austin, USA
RNU-66	GUAACUGUGGUGAUGGAAAUGUGUU AGCCUCAGACACUACUGAGGUGGUU CUUUCUAUCCUAGUACAGUC	Ambion, Austin, USA
RNU-6B	CGCAAGGAUGACACGCAAAUUCGUGA AGCGUUCCAUAUUUUU	Ambion, Austin, USA

2.1.8 Small RNAs

2.1.8.1 siRNAs

siRNA	Sequence (5' => 3')	Supplier
Silencer® select negative contr. #1	N.A.	Ambion, Austin, USA
Silencer® select negative contr. #2	N.A.	Ambion, Austin, USA
Silencer® select siCEBPB #1	CCGCCUGCCUUUAAAUCCATT	Ambion, Austin, USA

2.1.8.2 pre-miRs / anti-miRs

pre-miR / anti-miR	Sequence (5' => 3')	Supplier
hsa-anti-miR-155	N.A.	Ambion, Austin, USA
hsa-anti-miR-18a	N.A.	Ambion, Austin, USA
hsa-anti-miR-19a	N.A.	Ambion, Austin, USA
hsa-anti-miR-92a-1	N.A.	Ambion, Austin, USA
hsa-pre-miR-155	N.A.	Ambion, Austin, USA
hsa-pre-miR-18a	N.A.	Ambion, Austin, USA
hsa-pre-miR-19a	N.A.	Ambion, Austin, USA
hsa-pre-miR-92a-1	N.A.	Ambion, Austin, USA

2.1.9 Antibodies

2.1.9.1 Antibodies for Western blot

1st / 2nd	Name	Source	Blocking	Dilution	Supplier
1st	Anti-α-Tubulin	Mouse	PBS-T / 5% milk	1:5000	Sigma-Aldrich
1st	Anti-MAP3K14	Mouse	PBS-T/ 5% milk	1:2500	Abnova Corporation
1st	Anti-RAB5C	Rabbit	PBS-T / 5% milk	1:1000	Sigma-Aldrich
1st	Anti-TCF4	Rabbit	PBS-T/ 5% milk	1:1000	Aviva Systems Biology
1st	Anti-SOCS1	Rabbit	PBS.T/ 5% milk	1:1000	Abcam
1st	Anti-Lamin B	Mouse	PBS-T/ 5% milk	1:1000	Oncogene res. Prod.
2nd	Anti-Mouse IgG HRP-linked	Horse	PBS-T / 5% milk	1:5000	Cell Signaling Tec.
2nd	Anti-Rabbit IgG HRP-linked	Goat	PBS-T / 5% milk	1:5000	Cell Signaling Tec.
2nd	goat-α-mouse IgG-Cy5	Goat	PBS-T/ 5% advanced blocking agent		GE
2nd	goat-α-rabbit IgG-Cy5	Goat	PBS-T/ 5% advanced		GE

2.1.9.2 Antibodies for RIP-Seq

Name	Source	Isotype	Supplier
Anti-AGO2	Mouse	IgG1	Abnova
Anti-AGO2 (11A9)	RAT	IgG2a	G.Meister (MPI), Munich, Germany
Mouse serum Ig	Mouse	mixed	Santa Cruz
Rat Serum Ig	Rat	mixed	Jackson ImmunoResearch

2.1.10 Cell culture

2.1.10.1 Cell culture reagents

Reagent	Supplier
Dulbecco's Modified Eagle Medium (DMEM)	Gibco BRL, Invitrogen, Carlsbad, USA
Fetal bovine serum (FBS)	Biochrom, Berlin, Germany
Hygromycin B (50 mg/ml)	Invitrogen, Carlsbad, USA
TRAIL soluble ligand	Biochrom, Berlin, Germany
Nocodazole	Biomol GmbH, Hamburg, Germany
Penicillin-Streptomycin	Gibco BRL, Invitrogen, Carlsbad, USA
RPMI 1640	Gibco BRL, Invitrogen, Carlsbad, USA

2.1.10.2 Cell lines

Cell line	Accession No.	Supplier
GRANTA-519	ACC 83	DSMZ, Braunschweig, Germany
HEK-293T	CRL-1573	ATCC, Manassas, USA
JEKO-1	ACC 553	DSMZ, Braunschweig, Germany
MEC-1	ACC 497	DSMZ, Braunschweig, Germany

2.1.10.3 CLL and MCL patient samples on Illumina expression array

For detailed information about CLL and MCL patient samples analyzed by Dr. Alexandra Farfsing using Illumina expression arrays, please refer to [235].

2.1.10.4 Transfection reagents

Reagent	Supplier
Cell line nucleofector kit T	Lonza, Cologne, Germany
Cell line nucleofector kit V	Lonza, Cologne, Germany
Effectene	Qiagen, Hilden, Germany
HiPerfect	Qiagen, Hilden, Germany
TransIT LT1	Mirus Bio LLC, Madison, USA

2.1.11 Instruments

Instrument	Supplier
7900 HT FAST Real Time PCR Systems	Applied Biosystems, Forster City, USA
ABI Prism 3100 Genetic Analyzer, 16 Capillary DNA seqencer	Applied Biosystems, Forster City, USA
Automatic developing machine	Amersham, Freiburg, Germany
Axioplan microscope	Carl Zeiss, Jena, Germany
Balance BL 610 and BL150S	Sartorius AG, Göttingen, Germany
BD FACSCanto II workstation	BD Biosciences, San Jose, USA
Bioanalyzer 2100	Agilent Technologies, Palo Alto, USA
Biofuge freso refrigerated table top centrifuge	Heraeus/ Kendro, Hanau, Germany
Cell culture incubator	Thermo Scientific, Waltham, USA
Centrifuge 5810R	Eppendorf, Hamburg, Germany
Certomat T bacterial shaker	Sartorius AG, Göttingen, Germany
EAS Gel documentation assay	Herolab, Wiesloch, Germany
Gel elctrophoresis power supply	E-C apparatus corporation, USA
GS 6, GS 6KR, Centrifuge	Beckman, Wiesloch, Germany
GSA- and SS34 Rotor	DuPont, Boston, USA
Heating block QBT2	Grant Instruments, Emersacker, Germany
HiSeq 2000 sequencer	Illumina / Solexa, San Diego, USA
LB-940 Mithras Multilabel Reader	Berthold Technologies, Bad Wildbach, Germany
Mastercycler GradientS PCR-Machine	Eppendorf, Hamburg, Germany
Micro-centrifuge	NeoLab Laborbedarf, Heidelberg, Germany
Microwave oven	AEG, Frankfurt aM, Germany
Mini-Protean 3 gel and electrophoresis system	Bio-Rad, Hercules, USA
Multifuge 3 SR	Heraeus/ Kendro, Hanau, Germany
NanoDrop ND-1000	NanoDrop Technologies, San Diego, USA

Instrument	Supplier
Nucleofector device	Lonza, Cologne, USA
NuPAGE Gel running chamber	Invitrogen, Carlsbad, USA
Roller mixer RM-5 V30	Biocat GmbH, Heidelberg, Germany
Speedvac concentrator	Eppendorf, Hamburg, Germany
Thermomixer compact	Eppendorf, Hamburg, Germany
Typhoon Scanner 9000	Amersham, Freiburg, Germany
Unimax 1010 shaker	Heidolph Instruments, Schwalbach, Germany
Varifuge 3.0/ 3.0R	Heraeus/ Kendro, Hanau, Germany
Vi-cell XR Cell counter	Beckman Coulter, Brea, USA
Waterbath SW22	Julabo Labortechnik, Seelbach, Germany
Li-COR odyssey fc	Li-COR, Lincoln, USA

2.1.12 Software

Software	Supplier
BD FACS Diva	BD Biosciences, San Jose, USA
ImageJ	Open source
Linux	Open source
Microsoft office package	Microsoft, Redmond, USA
SDS 2.1	Applied Biosystems, Fortser City, USA
Sequence Scanner v1.0	Applied Biosystems, Fortser City, USA
RNAfold [236]	Open source
TFSEARCH (http://www.rwcp.or.jp/lab/pdappl/papia.html)	Open source

2.1.13 Web-based microRNA target prediction tools

Program	Version	Web address	Reference
DIANA-microT	3.0	http://diana.cslab.ece.ntua.gr/microT/	[237] [238]
miRWalk	03/29/2011	http://www.ma.uni-heidelberg.de/apps/zmf/mirwalk/	[239]
PITA	08.2008	http://genie.weizmann.ac.il/pubs/mir07/mir07_prediction.html	[240]
TargetScan	5.1	http://www.targetscan.org/	[167] [170]
miRanda	08.2010	http://www.microrna.org/microrna/home.do	[241]
PICTAR4	03.2007	http://pictar.mdc-berlin.de/	[242]
PICTAR5		http://pictar.mdc-berlin.de/	
RNA22	05.2008	http://cbcsrv.watson.ibm.com/rna22.html	[243]
miRDB	04.2009	http://mirdb.org/miRDB/	
RNAhybrid	2.1	http://bibiserv.techfak.uni-bielefeld.de/rnahybrid/	[244]

2.1.14 Tools and Algorithms for high throughput sequencing analysis

Program	Version	Web address	Reference
TopHat alignment	1.4.0	http://tophat.cbcb.umd.edu/	[245]
HTSeq-Count	0.5.3p3	http://www-huber.embl.de/users/anders/HTSeq/doc/count.html	
DESeq	2.9	http://www-huber.embl.de/users/anders/DESeq/	[246]
Human reference genome	19	http://www.genome.uscs.edu/cgi-bin/hgGateway	
R bioconductor	2.15.0	http://bioconductor.org	

2.2 Methods

2.2.1 Cell culture

2.2.1.1 Cultivation of cell lines

The cell lines MEC-1 (ACC 497), JEKO-1 (ACC 553) and GRANTA-519 (ACC 83) were obtained from the German Resource Centre for Biological Material (DSMZ). The cell line HEK293T (CRL-1573) was received from the American Type Culture Collection (ATCC). According to the suppliers instructions the cell lines MEC-1, Granta-519 and HEK293T were cultivated with Dulbecco's modified eagle medium (DMEM) containing 10% fetal bovine serum (FBS), 1000 mg/ml D-glucose and 500 u/ml penicillin/ 500 µg/ml streptomycin. The cell line JEKO-1 was cultivated in RPMI-1640 containing 20% FBS and 500 u/ml penicillin/ 500 µg/ml streptomycin. The cells were incubated at 37 °C, 95% humidity and 5% (for RPMI) or 10% (for DMEM) CO_2.

2.2.1.2 Generation and maintenance of stable cell lines

In order to generate cell lines, stably over-expressing miRNAs, $5x10^6$ cells were transfected with 2 µg of the episomal vector pREP4 containing the miRNA sequence of interest (Figure 2-1). As negative control the pREP4 vector backbone was transfected. Transfections were performed using TransIT-LT1 transfection reagent (Mirus bio LLC) (see 2.2.2.1) or by Amaxa nucleofection (Lonza) according to the protocol previously established by Dr. Alexandra Farfsing [247]. Transfected cells were cultured under

selective pressure for four weeks using a previously tested concentration of hygromycin B. The cells were passaged every second day. Non-transfected cells, which were used as positive control for selection, died after approximately two weeks under selective pressure. To confirm stable over-expression of the introduced miRNA, its expression was measured at various time points using qRT-PCR, (refer to 2.2.5).

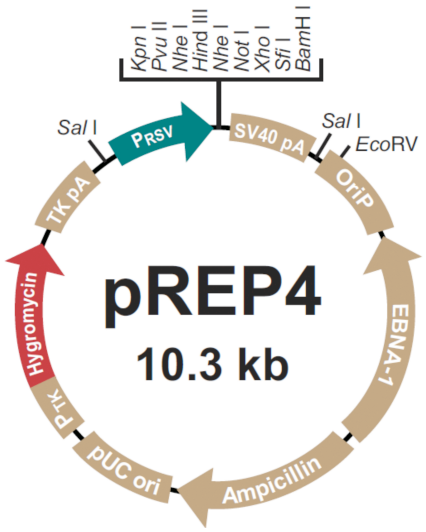

Figure 2-1: Schematic illustration of the episomal pREP4 vector backbone. The sequence to be expressed is introduced downstream of a rous sarcoma virus (RSV) promoter. Extrachromosomal replication in human cells is driven by the oriP and its binding protein *EBNA-1* (Epstein-Barr virus (EBV) nuclear antigen-1). The hygromycin resistance gene was included for stable selection of transfected cells. Source of the illustration: Invitrogen

2.2.2 Transfection methods

2.2.2.1 Chemical transfection

Transient transfection of expression vectors into HEK293T was performed using TransIT-LT1 transfection reagent (MIRUS bio LLC) according to the manufacturer's instructions. Transfection of siRNAs into HEK293T cells was achieved using HiPerfect transfection reagent (Qiagen) according to the manufacturer's instructions.

2.2.2.2 Nucleofection of cell lines

Transient transfection of the B-cell lines was performed using the nucleofection reagents and the nucleofector device from Lonza. For each transfection $5x10^6$ cells were harvested, washed once with PBS and suspended in 100 µl transfection reagent. After electroporation using the nucleofector device, the cells were directly suspended in 500 µl

cell culture medium and transferred to 6-well plates containing 2.5 ml of medium. The cell lines MEC-1 and GRANTA-519 were transfected using solution T (nucleofection reagent) and program O-17 on the nucleofector device [247].

2.2.3 General molecular biology techniques

2.2.3.1 Isolation of genomic DNA

For DNA isolation, up to $1x10^7$ cells were harvested and washed once with PBS by centrifugation for five minutes at 2000 rpm at room temperature. DNA was isolated using the Blood and Cell genomic DNA midiprep kit (Qiagen) according to the manufacturer's instructions.

2.2.3.2 Isolation of plasmid DNA

Plasmid DNA isolation from up to 5 ml bacteria cultures was performed by using the Plasmid Miniprep kit (Qiagen) according to the manufacturer's instructions. For larger volumes up to 300 ml of bacteria cultures the Endofree Plasmid Maxiprep kit (Qiagen) was used.

2.2.3.3 RNA isolation

For RNA isolation, up to $1x10^7$ cells were harvested and washed once with PBS as described above. Cell pellets were either stored at -80 °C or directly processed using the miRNeasy kit (Qiagen) according to the manufacturer's instructions, which allows the isolation of small non-coding RNAs in addition to larger RNA species.

2.2.3.4 Quantification by spectrometry

The quantity and quality of isolated genomic or plasmid DNA, and RNA was assessed using a NanoDrop ND-1000 instrument (NanoDrop Tec.). Nucleic acids are detected at their maximum absorbance wavelength of 260 nm. Contaminants like phenol or amino acids containing aromatic residues can be detected at 280 nm and residual ethanol can be detected at the 230 nm. Therefore, the optical densities of DNA and RNA preparations at these three wavelengths were acquired (OD_{230}, OD_{260} and OD_{280}) and ratios were calculated. An OD_{260}/OD_{280} ratio of 1.8 is considered as pure DNA and an OD_{260}/OD_{280} ratio of 2.0 as pure RNA. OD_{260}/OD_{230} ratios of 2.0 – 2.2 are considered as pure nucleic acids without any ethanol contamination.

2.2.3.5 Capillary gel electrophoresis

Capillary gel electrophoresis was performed using the RNA nano and RNA pico kits on a Bioanalyzer 2100 device (Agilent) according to the manufacturer's instructions to analyze the integrity of RNA samples. The basic principle is the separation of fluorescently labeled denatured RNA molecules in a capillary filled with a gel matrix according to their sizes. The RNA integrity number (RIN) is a measure of the ratio of the 18s and 28s ribosomal RNA species. A RIN higher than 8 (scale maximum: 10) was considered as RNA of good quality.

2.2.3.6 Design of PCR-primer

The web based tool "Primer3" [248] was used at default settings (http://frodo.wi.mit.edu/primer3/) in order to design standard PCR-primers. Briefly, the settings for the melting temperature (T_m) were between 57 °C and 63 °C. In order to avoid unspecific amplification products the primer length was set to 18-27 nucleotides.

To design primers for the amplification of DNA sequences that were ligated into vectors (see 2.2.4) the "Primer3" software tool was used as well. In order to generate restriction sites, the enzyme specific palindromic sequences were added 5' of the gene-specific primer sequence. Since some restriction enzymes require up to three additional nucleotides upstream of the restriction motif, the nucleotide sequence "TTT" was added 5' of the restriction site.

2.2.3.7 Polymerase chain reaction (PCR)

Polymerase chain reaction (PCR) was performed in order to amplify specific DNA fragments *in vitro* [249]. PCR is a cyclic reaction series of DNA denaturation, annealing of forward and reverse primer and DNA elongation with a thermo stable DNA polymerase. A typical reaction mix contains 50 ng of template DNA, 5 µl reaction buffer, 1.5 µl of forward and reverse primer (2 nM), 0.5 µl dNTP mix (10 mM), 0.3 µl FastStart ® Taq polymerase (Roche), filled up to 50 µl with ultra pure H_2O. The cycling conditions were 94 °C for 5 minutes; 35 cycles of 94 °C for 30 seconds, 58 to 65 °C for 1 minute, 72 °C for 1 minute, final elongation at 72 °C for 5 minutes and hold at 4 °C.

2.2.3.8 PCR product purification

The PCR products were cleaned using the Qiaquick PCR Purification kit (Qiagen) according to the manufacturer's instructions.

2.2.3.9 Agarose gel electrophoresis

Agarose gels were prepared by adding 1-3% (w/v) agarose to TBE-buffer. The mix was boiled in a microwave oven and mixed on a stirring device to create a homogeneous gel matrix. After casting the gel, DNA samples mixed with sample loading buffer (Fermentas) were loaded into the pockets of the gel. Typically, electrophoretic separation of DNA molecules was performed for 30 to 60 minutes and 100 V potential. Thereafter, the gel was stained with ethidium bromide for 5 minutes and stained DNA fragments were analyzed under 254 nm UV-light.

2.2.3.10 Gel extraction of DNA

To isolate PCR products, which have a defined length, the amplified DNA was separated by agarose gel electrophoresis as described above and the bands of interest were excised using a scalpel. The PCR products were further purified using the Qiaquick Gel extraction Kit (Qiagen) according to the manufacturer's instructions.

2.2.3.11 Sanger sequencing

Sanger sequencing was performed [250] in order to determine a DNA sequence of interest. This technique is a PCR-based method that relies on elongation termination after incorporation of derivates of all four dideoxynucleotides labeled with four different dyes respectively. The sequencing reaction was performed according to the manufacturer's advices of the PRISM BigDye Deoxy Terminator Cycle Sequencing kit (Applied Biosystems). Briefly, the denaturation step lasted 2 minutes at 96 °C, followed by 25 cycles of 5 seconds at 96 °C, 10 seconds at 55 °C and 4 minutes at 6 °C. After PCR, the DNA was precipitated using 100% ethanol and 1/10 volume of 3 M NaAc and washed with 70% ethanol. The dried DNA pellet was resolved in 11 µl of deionized formamide. DNA fragment separation and detection via laser-induced excitation of the fluorescently labeled dideoxynucleotides was performed on an ABI3100 capillary DNA sequencing device (Applied Biosystems).

2.2.4 Cloning

To achieve stable over-expression of various miRNAs in cell lines, the pre-miRNA sequences of the respective miRNAs were introduced into the episomal pREP4 vector backbone (Invitrogen). For cloning of luciferase sensor vectors, the full length 3'UTR of a candidate gene was inserted into the pMiRReport vector (Ambion) (see 2.2.7.4).

2.2.4.1 Amplification of the DNA insert

Amplification of the specific nucleotide sequence that should be integrated into a vector was performed by PCR (see 2.2.3.7) using genomic DNA isolated from peripheral blood cells of a healthy donor as the template sequence. Gene-specific primers were designed as described in 2.2.3.6. In order to generate sufficient insert DNA for the cloning procedure, 35 to 40 PCR cycles were run on a gradient PCR machine with annealing temperatures ranging from 58 °C to 63 °C. The PCR product was cleaned using the Qiaquick PCR Purification kit (Qiagen) according to the manufacturer's instructions (see 2.2.3.8). Approximately 5-10% of the amplified DNA was analyzed on a 1% agarose gel (see 2.2.3.9) to verify the expected size of the product.

2.2.4.2 Vector and insert DNA restriction by enzyme digestion

The vector backbone was linearized by digestion with two different restriction enzymes that cut within the multiple cloning site (MCS) of the plasmid. Thereby, vector re-ligation without insert DNA as well as the orientation of the insert was controlled. The PCR product, which was flanked by restriction sites for these same two enzymes was digested accordingly. Routinely, 2 µg of vector DNA or the total amount of the PCR product were digested in a 50 µl reaction mix over night at 37 °C. The restriction products were separated on a 2% agarose gel and the bands of the correct sizes were sliced out. The Qiaquick Gel Extraction kit (Qiagen) was used according to the manufacturer's instructions in order to elute the DNA sequences from the gel slices.

To insert the DNA of interest into a vector backbone, the T4-DNA ligase was used. A typical reaction mix contained 1 µl of the restricted vector backbone, 2 µl of the restricted insert, 5 units of T4-DNA ligase and the appropriate reaction buffer. Ligation was performed over night at 16 °C.

2.2.4.3 Transformation of competent bacteria

In order to amplify the newly generated vector, the ligation products were introduced into chemically competent TOP-10 *e. coli* bacteria (Invitrogen). Briefly, the competent bacteria were thawed on ice. Roughly 50% of the ligation reaction mix was added to the bacteria and incubated for 30 minutes on ice. After a brief heat shock at 42 °C for 30 seconds, the competent cells were incubated for additional two minutes on ice. Then, 700 µl of pre-warmed LB-medium was added and the cells were incubated for one hour at 37 °C and with gentle agitation on an Eppendorf shaker. Finally, the cells were plated on LB-agar medium containing 50 µg/ml ampicillin and incubated for 12 hours at 37 °C. Colonies growing on the selective medium were picked and transferred to 5 ml of LB-amp-medium. These liquid cultures were incubated over night at 37 °C gently shaking.
Glycerol-stocks containing 700 µl glycerol and 300 µl of the bacteria culture were prepared and stored at -80 °C. Plasmid DNA was isolated from the bacteria cultures using the Plasmid Miniprep kit (Qiagen) according to the manufacturer's instructions (see 2.2.3.2). The isolated plasmids were checked for correct insertion and potential mutations in the sequence of interest using Sanger sequencing (see 2.2.3.11).

2.2.5 Quantitative Real-Time Reverse Transcription PCR (qRT-PCR)

Quantitative real-time reverse transcription PCR (qRT-PCR) was used in order to determine the relative abundance of a certain RNA molecule in the sample of interest. Quantification is thereby achieved by monitoring the amount of amplified DNA during the PCR after every cycle. For the detection of DNA there are two common methods in use. The first strategy uses an unspecific dye, which intercalates into double stranded DNA (dsDNA) leading to a fluorescent signal when excited by a laser. The second strategy uses sequence specific probes labeled with a fluorescent dye and a quencher. After annealing of the probe to the target sequence, the quencher will by excised by the polymerase and the fluorescent dye gives a signal when excited by a laser.

2.2.5.1 Primer design for qRT-PCR

The primers for qRT-PCR were designed using the web-based tool "Universal Probe Library" from Roche Applied Sciences (https://www.roche-applied-sciences.com/sis/rtpcr/upl/index.jsp). In order to avoid amplification of genomic DNA as a

contaminant of the RNA sample, primers were selected which span at least one intron sequence.

2.2.5.2 Synthesis of cDNA

Single stranded DNA, which is complementary to its RNA template (cDNA), is generated by reverse transcription (RT). A total of 1 µg of the RNA sample was mixed with 2 µl of 5x reaction buffer, 1 µl of DNaseI and filled to 8 µl with H_2O. The mix was incubated for 15 minutes at 20 °C. Then, 1 µl of 25 mM EDTA, 1 µl of 300 ng/µl random hexamer primer and 1 µl of 10 mM dNTP mix were added, followed by 10 minutes of incubation at 65 °C and 10 minutes at 25 °C. Thereafter, 2 µl of 5x reaction buffer, 2 µl of 100 mM DTT and 1 µl H_2O were added to the mix and incubated for 2 minutes at 42 °C. Finally, 1 µl SuperScript II reverse transcriptase and 0.2 µl of T4p32 protein were added to the reaction mix. The mix with a final volume of 20.2 µl was incubated for 50 minutes at 42 °C for reverse transcription and 10 minutes at 94 °C to inactivate the reverse transcriptase.

2.2.5.3 qRT-PCR analysis

A typical quantitative real time PCR reaction contained 6 µl SYBR Green (Thermo Scientific), 100 nM forward and reverse primer, respectively and 2 µl of cDNA template. The reaction mix was amplified in a 7900 HT real-time PCR machine (Applied Biosystems) using the following settings: 30 minutes at 50 °C, 1 minute at 95 °C, 40 cycles of 15 seconds at 95 °C, 10 seconds at 60 °C and 1 minute at 72 °C. Finally a melting curve from 60 °C till 95 °C was produced to test the PCR product specificity. As SYBR Green labels any double stranded DNA like primer dimers or DNA contaminants, the melting curve is an important mean to evaluate the DNA content of the PCR reaction (see 2.2.5).

To calculate the efficiency of the PCR for each amplicon, a dilution row of human reference standard cDNA, which was reverse transcribed together with the specific RNA samples, was added on each plate. The relative abundance of the RNA of interest was normalized to at least two of three house keeping RNAs, *DCTN2*, *PGK1* or *GAPDH*, which were quantified in parallel. All samples were measured in triplicates and outliers were excluded from the analyses.

2.2.6 Protein analysis

2.2.6.1 Protein isolation

Typically, $1x10^7$ cells per sample were harvested, washed once using ice-cold PBS and lysed in 100 µl RIPA-buffer (see 2.1.5.4) containing 1 µl of the endonuclease Benzonase (Merck) to digest genomic DNA. To enhance cell lysis, the solution was pipetted up and down ten times followed by five minutes of incubation at 4 °C on a tumbler machine. Cell debris was removed by centrifugation at 13,000 rpm for 10 minutes at 4 °C. The supernatant containing the proteins was stored at -80 °C.

2.2.6.2 Protein quantification

The enzymatic biuret reaction was used to determine the protein concentrations in the lysates. This assay relies on the reduction of Cu^{2+} ions to monovalent Cu^{+} ions in alkaline medium. 200 µl of a copper-(III)-sulfate and bicinonic acid mix (ratio 1:50) was added to 10 µl of lysate and incubated for 30 minutes at 37 °C followed by analyzing the light absorbance at 550 nm with a plate reader. Calculation of protein concentrations was performed according to a standard curve of BSA samples ranging from 10 to 2,000 ng/µl, which were measured simultaneously.

2.2.6.3 Polyacrylamide gel electrophoresis (PAGE)

Dependent on the molecular weight of analyzed proteins, polyacrylamide gels ranging from 8% to 12% polyacrylamide were prepared. To induce the polymerization of the acrylamide and to stabilize the generated radicals, ammonium persulfate (APS) and N,N,N',N'-tetramethylethylendiamine (TEMED) was added to the reaction, respectively. Sodiumdodecylsulfate (SDS) was added to the mixture to apply a negative charge to the proteins and to keep them denatured during separation. The stacking gel, containing lower amounts of polyacrylamide, was cast on top of the separating gel. Alternatively, NuPAGE polyacrylamide gradient (4%-12%) precast gels were used (Invitrogen).

Protein samples were set to a desired concentration and denatured by adding sample loading buffer (see 2.1.5.4) and incubation at 95 °C for 10 minutes. Samples were then loaded into the gel pockets and electrophoresis was performed for approximately 45 minutes at a current of 180 V. A protein size marker (Spectra multicolor broad range

protein marker, Fermentas) was run in one of the lanes to allow size determination of the analyzed proteins.

2.2.6.4 Western blot

Proteins separated by SDS-PAGE were transferred to polyvinylidene fluoride (PVDF) membranes in a transfer tank (Biorad). PVDF membranes were activated in 100% methanol before protein transfer was carried out in transfer buffer (see 2.1.5.3) for 2 hours with 250 mA and a maximum of 100 V. The transfer reaction was cooled by ice. Membranes were then washed 3 times for 5 minutes in washing buffer (see 2.1.5.4) and stored in washing buffer at 4 °C until further processing.

To detect proteins of interest membranes were first blocked for one hour at room temperature using the indicated blocking buffers (see 2.1.5.4) followed by 3 washing steps. Antibodies targeting the proteins of interest were diluted as indicated (see 2.1.9.1) and incubated on the membrane over night at 4 °C on a rolling machine. After 3 washing steps with washing buffer, the secondary, HRP-conjugated antibody (see 2.1.9.1) was applied for one hour at room temperature on a rolling machine. Finally, the membrane was washed again 3 times and thereafter incubated with ECL or ECL+ solution (Amersham). Light emission was detected by using a hypersensitive film.

When using the ECL plex detection system, membranes were blocked with ECL advanced blocking agent (see 2.1.5.4) and incubated with two primary antibodies from two different species simultaneously. The incubation with the fluorophore-coupled secondary antibodies was under light protection. The detection of the fluorescence signals was performed on a Typhoon scanner (Amersham) or the Licor Odyssey Fc machine.

2.2.6.5 Tryptic digestion and mass spectrometry

For protein identification, the band containing the protein of interest was excised from a coomassie stained 1D gel and the protein was reduced with 10 mM DTT for 1 h at 56 °C followed by alkylation of the free sulfhydryl groups of cysteine residues with 55 mM iodoacetamide for 30 min at room temperature. Subsequently, the gel pieces were washed 3 times alternatively with H_2O and H_2O/acetonitrile (50:50 v/v). After drying with neat acetonitrile, trypsin (sequencing grade, Promega, Madison, USA) in 40 mM NH_4HCO_3 was added and digestion was carried out overnight at 37 °C. The resulting tryptic peptides were eluted from the gel by consecutive extraction steps using 0.1% TFA

in 50% acetonitrile, 100% acetonitrile and 0.1% TFA. The combined extraction solutions were dried in a speed-vac at 37 °C for 2 h. Peptides were redissolved in 5 µl 0.1% TFA by sonication for 15 min and were applied for separation on a nanoAcquity UPLC (Waters GmbH, Eschborn, Germany). Peptides were trapped on a nanoAcquity C18 column, 180 µm x 20 mm, particle size 5 µm (Waters GmbH, Eschborn, Germany). Separation was carried out at a flow rate of 400 nl/min on a BEH 130 C18 column, 100 µm x 100 mm, particle size 1.7 µm (Waters GmbH, Eschborn, Germany) using the following gradient of solvent A (98.9% water, 1% acetonitrile, 0.1% formic acid) and solvent B (99.9% acetonitrile and 0.1% µl formic acid): from 0 to 4% B in 1 min, from 4 to 40% B in 40 min, from 40 to 60% B in 5 min, from 60 to 85% B in 0.1 min, 6 min at 85% B, from 85 to 0% B in 0.1 min, and 9 min at 0% B. The nanoUPLC system was coupled online to an LTQ Orbitrap XL mass spectrometer (Thermo Fisher Scientific, Bremen, Germany). Data were acquired by scan cycles of one FTMS scan with a resolution of 60000 at 400 m/z and a range from 370 to 2000 m/z in parallel with six MS/MS scans in the ion trap of the most abundant precursor ions.

2.2.6.6 Protein identification

Database search was performed using the NCBInr database (release 2009_12_09) with the MASCOT search engine (Matrix Science, London, UK; version 2.2). Taxonomy was mammals. Peptide mass tolerance was set to 5 ppm and fragment mass tolerance to 0.6 Da. One missed tryptic cleavage site in case of incomplete hydrolysis was allowed. Carbamidomethylation of cysteine was set as fixed modification and oxidation of methionine as variable modification. Identification under the applied search parameters referred to a false discovery rate (FDR) < 2% and a match probability of $p<0.01$, where p is the probability that the observed match is a random event.

2.2.7 MicroRNA related analyses

2.2.7.1 Detection of miRNA expression using qRT-PCR

MicroRNA specific qRT-PCR was used to quantify the relative abundance of miRNAs. Since mature miRNAs typically have a length of 20-23 nucleotides it is critical to produce a detectable PCR product. In order to circumvent this problem, miRNA specific stem loop primers that artificially elongate the specific miRNA were used for reverse transcription

using TaqMan reverse transcription kit (Applied Biosystems). The resulting cDNAs were quantified in a HT7900 real-time PCR machine using specific primer sets consisting of a miRNA specific primer, a primer targeting the artificially elongated miRNA part and a specific probe labeled with fluorophore and quencher. Every PCR amplicon was tested in a dilution row of human reference standard cDNA, which was reverse transcribed simultaneously with the specific RNA samples to calculate the efficiency of the PCR. The relative abundance of the miRNA of interest was normalized to two house keeping small RNAs, RNU66 and RNU6B. All samples were measured in triplicates and outliers were excluded from the analyses.

2.2.7.2 Detection of miRNA expression using TaqMan arrays

To generate miRNA expression profiles, the TaqMan array system version 3 from Applied Biosystems was used. Sample preparation and measurements were performed according to the manufacturer's protocol. Twenty nanograms of RNA were used for reverse transcription. The resulting cDNA was pre-amplified using the pre-amplification primer pools and the pre-amplification master mix according to the manufacturer's instructions (Applied Biosystems). For these analyses, TaqMan array "A" cards and the ΔΔct method were used for quantification of miRNAs. Ct-values higher than 35 were considered as not expressed. The ct-values of expressed miRNAs were normalized to the median expression level of all expressed miRNAs of the respective sample.

2.2.7.3 Bioinformatic miRNA target prediction

In order to identify potential miRNA target genes, five different target prediction algorithms were used (see 2.1.13). All prediction algorithms have different criteria for predicting mRNA sequences as potential miRNA targets. For example, the RNAhybrid algorithm [244] predicts potential miRNA binding sites according to the minimum free energy hybridization of a long and a short RNA. In contrast TargetScanS [167,170] predicts potential miRNA targets by searching for the presence of conserved 8mer and 7mer sites matching the seed region of a certain miRNA.

2.2.7.4 Luciferase sensor assays

To verify the interaction of a miRNA with a potential mRNA target sequence, luciferase sensor assays were performed. For this purpose 3'UTR sequences of potential target

mRNAs containing the putative miRNA binding site were inserted (see 2.2.4) downstream of the *firefly* luciferase gene of the pMiRReport vector (see 2.1.6). The correct insertion of the sequence was confirmed by Sanger sequencing (see 2.2.3.11). The pMiRReport vector was transfected together with a TK *renilla* vector (Promega) into HEK293T cells (see 2.2.2.1). Simultaneously, the cells were transfected with either a miRNA over-expressing vector or the vector backbone as negative control. For these experiments, $4x10^4$ HEK293T cells were plated per well in 48-well plates 24 hours before simultaneous transfections with all three vectors. Cells were harvested 24 hours after transfection, washed once with ice-cold PBS and lysed by using passive lysis buffer (Promega). Luminescence signals were obtained by sequentially adding 10 µl of *firefly* buffer, containing the substrate for *firefly* luciferase, and 100 µl of *renilla* buffer, containing a quencher for the *firefly* luciferase signal and the substrate for the *renilla* luciferase, to 10 µl of cell lysate. The luminescence signals were quantified directly after the addition of each of the two buffers in a Mithras luminescence reader (Berthold technologies). The *firefly* luciferase signal was normalized to the *renilla* luciferase signal in each sample. All luciferase assays were performed in technical triplicates and at least in four independent biological replicates.

A reduction of the normalized *firefly* luciferase signal in the cells with miRNA over-expression compared to the control cells indicated a direct interaction of this miRNA with the introduced 3'UTR sequence and thus identifies the corresponding gene as a target of this miRNA.

2.2.8 Co-Immunoprecipitation of RNAs bound to AGO2

To isolate miRNAs and their targeted mRNAs incorporated into the RNA-induced silencing complex (RISC), immunoprecipitation (IP) of AGO2 protein was performed. For one IP reaction $2x\ 10^8$ – $4x\ 10^8$ cells were harvested, washed with ice-cold PBS and lysed in 400 µl polysome lysis buffer (PLB, see 2.1.5.6). The lysis was carried out for 5 minutes on ice, shaking the lysates periodically and gently. Thereafter, the lysates were frozen and stored at -80 °C.

The IPs were carried out in low binding tubes containing 50 µl protein G sepharose beads (GE healthcare) linked to 10 µg IgG isotype control antibody (see 2.1.9.2) or to 5 µg each of two different AGO2 antibodies (see 2.1.9.2). Antibodies were coupled to the protein G

sepharose beads in 500 µl NT2 buffer (refer to 2.1.5.6) for one hour at 4 °C on a tumbling machine followed by three washing steps with 1000 µl NT2 buffer. Cell lysates were thawed on ice and centrifuged at 13,000 rpm and 4 °C for 10 minutes to remove the debris. The supernatant was diluted 1:10 in NT2-buffer and 5 µl RNaseOUT (Invitrogen), 2 µl vanadyl ribinucleoside complex (New England Biolabs), 10 µl of 100 mM DTT (Invitrogen), 10 µl of 25 mM EDTA (Invitrogen) and 10 µl protease inhibitor cocktail (Roche) was added per ml of the mixture. Of this diluted lysate, 100 µl were removed and stored on ice representing the total lysate fraction (TL). The remaining lysate was then portioned to the prepared tubes containing sepharose beads either coupled to AGO2-specific antibodies or to control antibodies. Immunoprecipitation was performed for one hour at 4 °C on a tumbling machine. After centrifugation the supernatant was removed and stored at -80 °C representing the supernatant fraction (SN). The beads were further washed five times with 1000 µl of ice-cold NT2-buffer. To elute the bound proteins from the sepharose beads, they were incubated in 50 µl of 1 M glycine (pH 2.3) at room temperature for 10 minutes. The beads were spinned down and the supernatant was neutralized using 50 µl of 1 M Tris-HCl (pH 8). Thereafter, the proteins were degraded by adding 3 µl of proteinase K (Qiagen) to the neutralized supernatant and incubating the mixture for 10 minutes at 55 °C. In order to isolate the co-precipitated RNA, 350 µl TRIZOL LS reagent (Invitrogen) and 100 µl of chloroform was added to the IP-fraction as well as to the TL-fraction. Phase separation was performed on Phaselock tubes (3Prime) according to the manufacturer's instructions. The aqueous phase was mixed with 100% ethanol (1.5x of the initial volume) and loaded on RNeasy mini elute columns (Qiagen). Washing of the columns was performed according to the instructions of the miRNeasy kit (Qiagen). Finally, the RNA was eluted in 14 µl of RNase free water.

2.2.9 Next generation sequencing (Illumina)

Next generation sequencing (NGS) was used to identify and quantify transcripts, which were enriched in the AGO2-IP (refer to 2.2.8). NGS has several advantages compared to expression array analyses. Of importance, the sensitivity and the dynamic range for the detection of transcripts is superior by NGS compared to expression array analysis.

2.2.9.1 Sequencing library generation

The RNA fraction isolated by RIP was quantified by NanoDrop analysis and its quality was assessed by Agilent capillary electrophoresis using the RNA picoChips and the setting for total RNA analysis (refer to 2.2.3.5). The sequencing libraries were generated using 300 to 600 ng of RNA and the TruSeq mRNA sequencing Kit from Illumina according to the manufacturers instructions. Briefly, the RNA samples were poly-A purified using oligo-dT beads. The RNA was enzymatically degraded using endoribonucleases generating small fragments of approximately 200 bp in length. The cDNA synthesis was performed by first strand synthesis followed by second strand synthesis. After end repair and 3' end adenylation the sequencing adaptor oligo mix was ligated to the unstranded cDNA library. In order to perform a multiplexed sequencing run, six different barcoded sequencing adaptors were used. The cDNA library was amplified using 15 cycles of PCR according to the manufacturer's manual (Illumina). The enrichment and size distribution of the libraries were tested by Agilent capillary gel electrophoresis on a DNA1000 chip (refer to 2.2.3.5). The TruSeq libraries were generated from RIP-Seq samples of HEK293T pREP4-control and pREP4miR-155 cells as well as the RIP-Seq material from MEC-1 and JEKO-1 cells.

For sequencing, 6 samples were equimolar pooled per lane. 9 pmol of each sample library pool were hybridized per lane on an Illumina version 3 single read flow cell. The hybridization and cluster generation was performed on a cBot unit. The samples were single-end sequenced with a read length of 51 bp on an Illumina HiSeq 2000 sequencer. Raw data were sorted and analyzed according to barcoded library adaptors allowing one basepair mismatch within the barcode sequence.

2.2.9.2 Bioinformatic data analysis

Sequencing reads were mapped against the human reference genome version 19 using the TopHat algorithm version 1.4.0 (2.1.14) supplying Ensembl gene annotations version GRCh37.65 and default settings. RNA levels of 20318 proteincoding genes were calculated using the HTSeq-Count algorithm version 0.5.3p3 and default settings except defining unstranded sequencing libraries (2.1.14).

Further analysis was performed using the R statistical programming language version 2.15.0. Default settings were used unless otherwise noted. Testing for genes differentially

enriched between the IP and total lysate fractions was performed using the functions "estimateSizeFactors" and "nbinomTest" from the DESeq package version 1.8.2. (refer to 2.1.14) Log2-ratios of IP and total lysate fractions from the same biological sample were calculated for genes with an average normalized read count of at least 250 (10036 genes). The resulting ratios were normalized using the function "normalizeQuantiles" from the limma package version 1.32.0 and tested for differential enrichment between HEK-miR-155 and HEK-vector cells using the Significance Analysis of Microarrays (SAM) method from the siggenes package version 1.30.0.

2.2.10 Functional analyses

2.2.10.1 Cell proliferation assay (Click-iT)

Using flow cytometry, cellular properties like granularity (side scatter) or cell size (forward scatter) can be detected on a single cell level. Furthermore, this technique allows the detection of fluorescence intensities and thereby quantifying any fluorescently labeled component of the cell.

Cell proliferation can be directly quantified by monitoring the *de novo* synthesis of DNA during replication. This is used by the EdU click-iT assay (Invitrogen), which was performed to quantify cell proliferation by flow cytometry. After synchronization, cells were incubated with the thymidine analog EdU, which is actively incorporated into the *de novo* synthesized DNA in proliferating cells. The incorporated EdU was labeled with Alexa Fluor azide, which can be detected and quantified by flow cytometry. The percentage of EdU positive cells is therefore a measure for the proliferation rate of cells.

The cell lines HEK293T pREP4 control and HEK-miR-155 were synchronized by cultivation at complete confluency for 24 hours. Directly after reseeding the cells, 10µM of EdU was added to the medium. After six hours of incubation the cells were harvested, fixed, labeled with Alexa fluor azide and analyzed on a FACS Canto II device (BD Biosciences).

3 Results

3.1 Expression of miR-155 and miR-17-92 in primary CLL and MCL cells

MicroRNA-155 and the miR-17-92 cluster are aberrantly expressed in cell lines representing the entities CLL and MCL [251]. In order to quantify these miRNAs in primary CLL and MCL cells, malignant cells taken from the peripheral blood of ten CLL and ten MCL patients were isolated. Furthermore, CD19+ B-lymphocytes from the peripheral blood of three healthy donors were used as reference material. The expression of the mature miRNAs miR-155, miR-17-3p, miR-17-5p, miR-18a, miR-19a, miR-19b, miR-20a and miR-92a-1 was quantified by qRT-PCR using miRNA specific real-time PCR primer sets (refer to 2.1.7.3) and normalizing the data to the mean of the house keeping small RNAs RNU-66 and RNU-6B.

The obtained results revealed that almost all miRNAs of the miR-17-92 cluster showed a lower mean expression in CLL and MCL patients compared to healthy donors (Figure 3-1). MiR-92a-1 was the one exception, which was higher expressed in MCL patients in comparison to healthy donors and CLL cells. For the miRNAs miR-17-5p, miR-18a, miR-19a, miR-19b and miR-20a a lower mean expression was observed in MCL cells, and for miR-17-3p and miR-92a-1 a higher mean expression compared to CLL cells. Conversely, miR-155 was up to approximately eight-fold higher expressed in CLL and MCL patients in comparison to healthy donors. The mean expression value of miR-155 in MCL cells was lower than in CLL cells. Comparing relative expression levels of these miRNAs in cell lines [251] and patient material revealed that the miRNA expression in the cell lines in general was 1 to 2 magnitudes higher than in the primary cells.

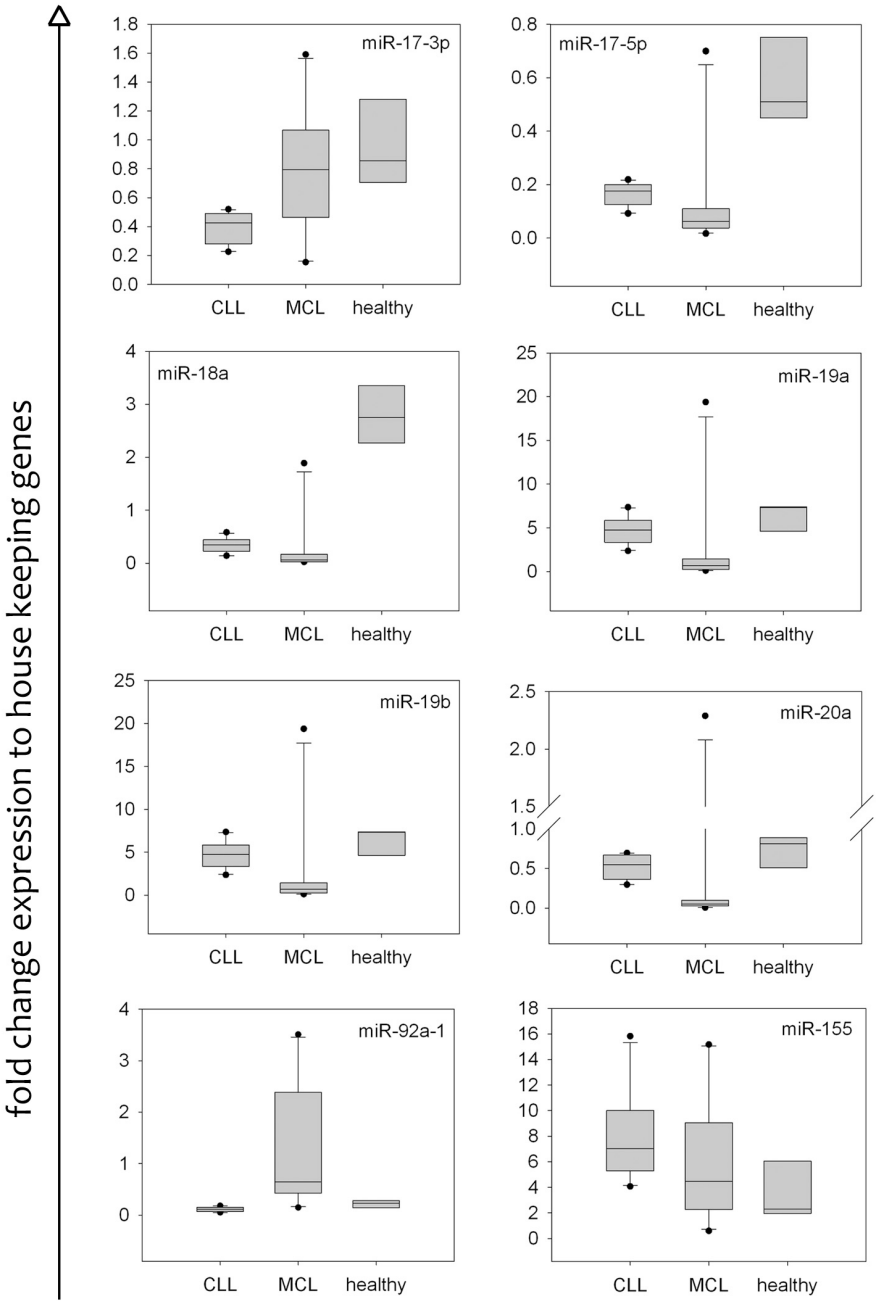

Figure 3-1: Box-whisker-plots of the qRT-PCR analysis of miR-155 and miR-17-92 expression in primary tumor cells of ten CLL patients, ten MCL patients and CD19+ sorted B-lymphocytes of three healthy donors. The expression values of all miRNAs were normalized to the mean of the two house keeping RNAs RNU-66 and RNU-6B.

3.2 Identification of miRNA target genes in CLL and MCL patients

Identification of miRNA targets has been achieved by various methods including the usage of bioinformatic target prediction algorithms, qRT-PCR and Western blot analyses to identify regulated genes, as well as luciferase sensor assays to evaluate direct interactions of miRNAs with sequences within the 3'UTR of genes.

In order to identify potential target genes of aberrantly expressed miRNAs in CLL and MCL patients, mRNA expression profiles of primary CLL and MCL cells were analyzed (refer to 3.1). For this purpose transcriptome data of 18 CLL and 6 MCL samples previously generated by Dr. Alexandra Farfsing by using Illumina Human Sentrix-6 BeadChip arrays (Illumina Inc., San Diego, USA) [247] were analyzed. Transcripts with a higher or lower differential expression value than the single standard deviation of the median in comparison to a pool of three healthy donors were considered for identification of potential miRNA target genes.

3.2.1 Bioinformatic prediction of potential miRNA target genes

Three computational prediction algorithms TargetScanS, PicTar and DIANA-microT, were used to identify potential miRNA targets among the deregulated transcripts of CLL and MCL patients (refer to 3.2, 2.1.13). Transcripts with higher expression in CLL and MCL cells in comparison to healthy donor B-cells, were evaluated for miR-19a target prediction, since this miRNA had "aberrantly" low levels in CLL and MCL (Figure 3-1). It therefore was expected that transcripts, which were repressed by miR-19a in normal B-cells, were more abundant in the absence of this control. Accordingly, potential targets of miR-155 were searched within the list of genes, which showed lower expression in CLL and MCL cells. In addition, miR-92a-1 target prediction was performed with genes that showed lower expression in MCL and/or a higher expression in CLL patients compared to healthy B-cells.

Potential miR-19a target gene ID	Up-regulated in CLL	Up-regulated in MCL	Prediction with TargetScanS	Prediction with PicTar	Prediction with DIANA-microT
SGK1	No	Yes	Yes	Yes	Yes
ETV5	No	Yes	Yes	No	Yes
RGL1	No	Yes	Yes	Yes	Yes
TIA2	Yes	Yes	Yes	Yes	Yes
FOXP1	Yes	No	Yes	Yes	Yes
CCNT2	Yes	Yes	No	Yes	Yes
DOCK10	Yes	No	Yes	No	Yes
E2F8	No	Yes	Yes	No	Yes
ADNP	Yes	Yes	Yes	Yes	Yes
ABR	Yes	No	No	Yes	Yes
NDFIP2	Yes	Yes	Yes	No	Yes
TNFAIP3	Yes	No	Yes	No	No

Table 3-1: Overview of potential miR-19a target genes aberrantly expressed in CLL or MCL and computationally predicted as miR-19a target.

Potential miR-92a-1 target gene symbol	Up-regulated in CLL	Down-regulated in MCL	Prediction with TargetScanS	Prediction with PicTar	Prediction with DIANA-microT
FBXW7	Yes	Yes	Yes	Yes	Yes
SGK3	No	Yes	Yes	No	Yes
CIC	Yes	No	Yes	Yes	Yes
IRS2	Yes	Yes	Yes	Yes	Yes
PTGER4	No	Yes	Yes	Yes	Yes
GIT2	Yes	No	Yes	Yes	Yes
CDC42	Yes	No	Yes	Yes	Yes
BCL11A	No	Yes	Yes	Yes	Yes

Table 3-2: Overview of potential miR-92a-1 target genes aberrantly expressed in CLL or MCL and computationally predicted as miR-92a-1 target.

Potential miR-155 target gene ID	Down-regulated in CLL	Down-regulated in MCL	Prediction with TargetScanS	Prediction with PicTar	Prediction with DIANA-microT
VAV3	Yes	Yes	Yes	No	Yes
SGK3	Yes	Yes	Yes	No	Yes
c-FOS	No	Yes	Yes	No	Yes
RAB5C	No	Yes	Yes	No	No
E2F2	Yes	No	Yes	No	Yes
CSF1R	Yes	Yes	Yes	Yes	No
Pu.1	Yes	Yes	Yes	No	Yes
LAT2	Yes	No	Yes	No	No
PIK3R1	No	Yes	Yes	No	No
RAB34	Yes	No	Yes	Yes	No
SIRT1	Yes	Yes	Yes	No	No
PEBP1	No	Yes	Yes	No	No
RAP1B	Yes	Yes	Yes	No	No

Table 3-3: Overview of potential miR-155 target genes aberrantly expressed in CLL or MCL and computationally predicted as miR-155 target.

For miR-19a twelve potential target mRNAs were found to be higher expressed in CLL and/or MCL cells and to be predicted as a target by at least one prediction algorithm (Table 3-1). Eight potential miR-92a-1 target mRNAs were identified in the list of aberrantly expressed transcripts (Table 3-2). Further, 13 potential target mRNAs were predicted for miR-155 by at least one prediction algorithm in the list of down-regulated transcripts in CLL and/or MCL patients (Table 3-3).

3.2.2 Experimental validation of potential target mRNAs

3.2.2.1 Manipulation of miRNA expression

Quantitative real-time reverse transcription PCR (qRT-PCR) is one of the current standard methods in order to verify the regulation of predicted target mRNAs after manipulating miRNA expression in cells. To modulate miRNA levels, commercially available miRNA precursor (pre-miR, 2.1.8.2) and miRNA blocking molecules (anti-miR, 2.1.8.2) for miR-19a, miR-92a-1 and miR-155 were transiently transfected into the B-cell line MEC-1 using the nucleofection system from Lonza (Lonza, Cologne, USA) according to the previously established protocol of Dr. Alexandra Farfsing [247] (refer to 2.2.2.2). Total RNA including the small RNA fraction was isolated 48 hours after transfection of pre-miRs and anti-miRs. QRT-PCR using miRNA specific primers was performed to validate increased miRNA

levels. The results were normalized to the mean expression of the two house keeping small RNAs RNU-6B and RNU-66.

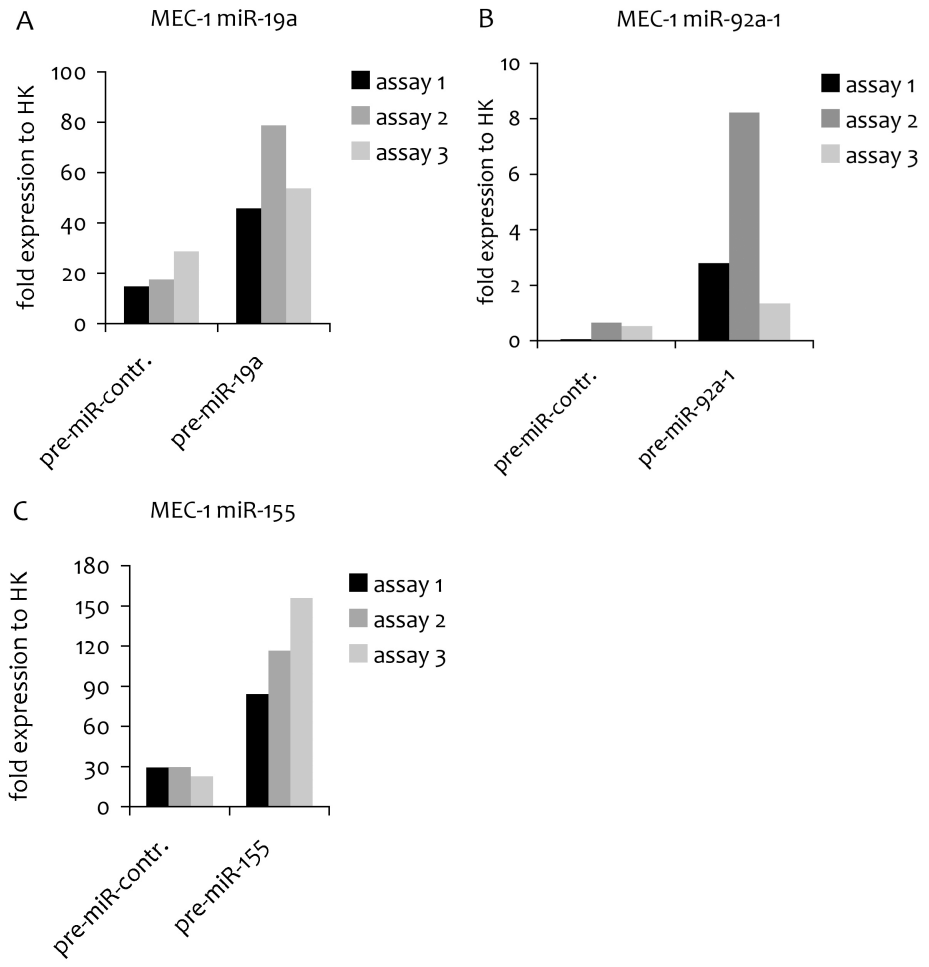

Figure 3-2: Quantification of miR-19a (A), miR-92a-1 (B) and miR-155 (C) by qRT-PCR after transient transfection of microRNA specific precursor molecules in three biological replicates. A scrambled miRNA precursor was used as negative control. All miRNA expression values were normalized to the mean of the two house keeping small RNAs RNU-6B and RNU-66.

Even though variations in the levels of manipulated miRNAs were detected in the transfected samples, an at least 1.8-fold increase was detectable for each miRNA of interest (Figure 3-2).

Since anti-miRs are binding and thereby blocking their target miRNAs, without necessarily degrading them, the activity of the anti-miRs could not be directly monitored by qRT-PCR.

3.2.2.2 Quantification of potential miRNA targets by qRT-PCR

The expression of potential miRNAs target genes was quantified by qRT-PCR (refer to 2.2.5) using RNA isolated from MEC-1 cells 48 hours after transfection. The potential target genes were measured separately in all biological replicates with pre-miR and anti-miR treatment. The expression levels were normalized to the mean value of the three house keeping genes *DCTN2*, *PGK1* and *GAPDH*. Statistical significance was calculated by performing the student's t-test. P-values lower than 0.05 were considered as significant. Twelve, eight and thirteen genes previously identified for being aberrantly expressed in CLL or MCL and predicted as putative miRNA targets were tested for differential expression after manipulation of miR-19a, miR-92a-1 and miR-155, respectively. Theoretically, transfection with pre-miRNAs was supposed to reduce the expression of their putative target mRNAs, whereas blocking the endogenous miRNA activity by anti-miRs should result in the opposite effect.

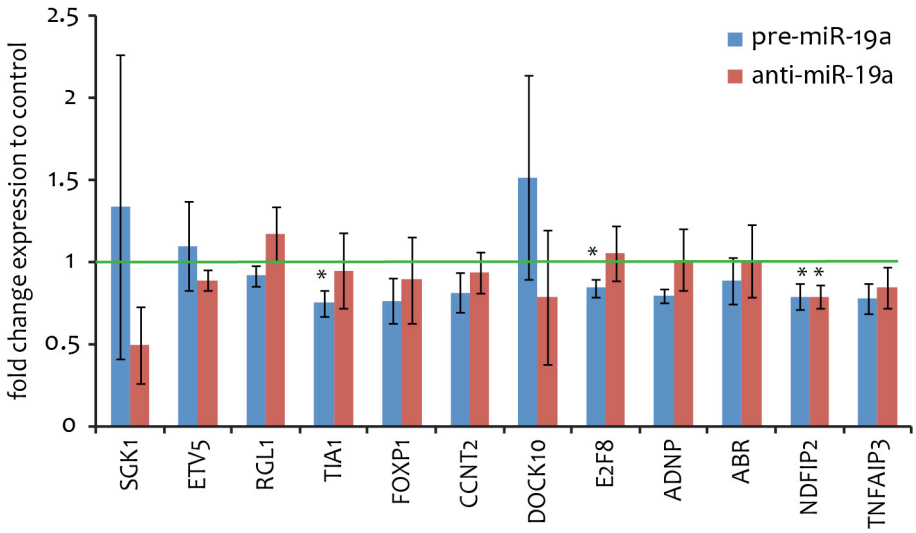

Figure 3-3: Quantification of potential target mRNAs of miR-19a, tested by SYBRGreen-based qRT-PCR. The expression values were normalized to the mean value of the three house keeping genes *DCTN2*, *PGK1* and *GAPDH*. The mean values of three biological replicates and the statistical significance (t-test) were calculated (*= p< 0.05). The control experiments were scaled to 1 (green line).

For most mRNAs tested as targets of miR-19a, the alterations were relatively mild, except for *SGK1* and *DOCK1* (Figure 3-3). In general the reduction or increase of transcript abundance was on average approximately 20% different compared to the control experiment. Among the twelve candidate genes, there were three genes significantly

deregulated upon pre-miR-19a or anti-miR-19a transfection. Nevertheless, except for *NDFIP2* no other transcript was significantly regulated by pre-miR and anti-miR treatment in parallel. However, *NDFIP2* was equally degraded upon pre-miR and anti-miR treatment. Unexpectedly, *SGK1* was down regulated after anti-miR instead of pre-miR transfection and *DOCK10* mRNA was increased upon pre-miRNA instead of anti-miR transfection.

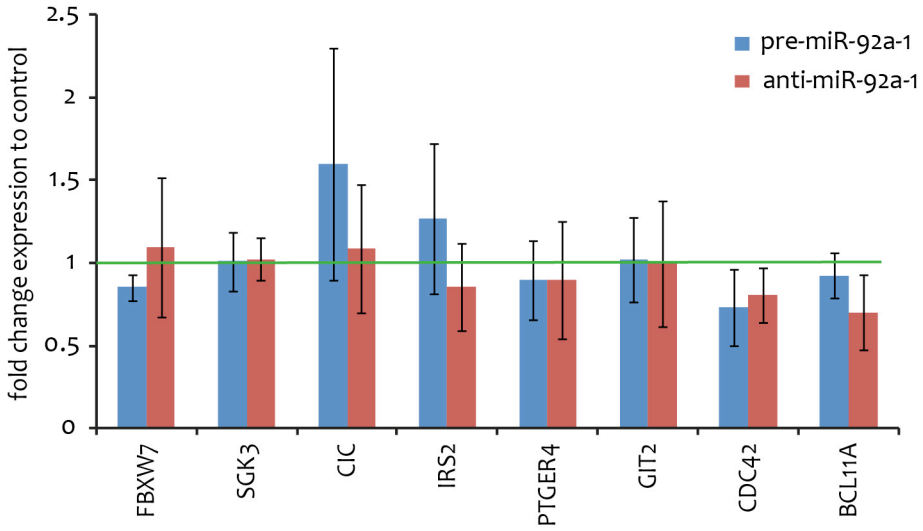

Figure 3-4: Quantification of potential target mRNAs of miR-92a-1, tested by SYBRGreen based qRT-PCR. The expression values were normalized to the mean value of the three house keeping genes *DCTN2*, *PGK1* and *GAPDH*. The mean values of three biological replicates and the statistical significance (t-test) were calculated (*= p< 0.05). The control experiments were scaled to 1 (green line).

Upon transfection with pre-miR-92a-1 or anti-miR-92a-1, none of the eight tested transcripts were significantly regulated (Figure 3-4). Again, the overall effects were relatively mild showing not more than approximately 20% differences for the majority of experiments in comparison to control. The only exceptions were *CIC* and *IRS2* transcript levels, which in contrast to the theoretical assumption, were up regulated and not down regulated upon pre-miR transfection. Nevertheless, the reduction of *FBXW7* after pre-miR-92a-1 transfection was a trend (p=0.084).

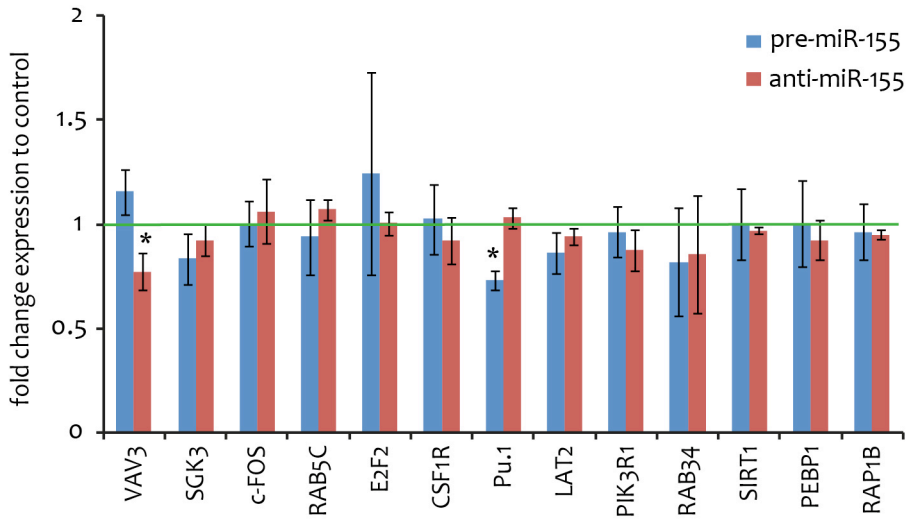

Figure 3-5: Quantification of potential target mRNAs of miR-155, tested by SYBRGreen based qRT-PCR. The expression values were normalized to the mean value of the three house keeping genes *DCTN2*, *PGK1* and *GAPDH*. The mean values of three biological replicates and the statistical significance (t-test) were calculated (*= $p < 0.05$). The control experiments were scaled to 1 (green line).

Similar results were obtained upon manipulation of miR-155, where only the mean values of *VAV3*, *E2F2* and *Pu.1* transcripts showed a higher than 20% difference in comparison to the control experiment (Figure 3-5). Of these, *Pu.1*, which is a previously published miR-155 target gene [216], was significantly lower expressed after pre-miR-155 transfection. However, the opposite effect after anti-miR-155 treatment was not significant. Notably, the reduction of gene expression did not directly correlate with the level of miRNA over-expression (Figure 3-2 A, B & C) in the three biological replicates (data not shown).

3.2.2.3 Identification of miRNA targets by luciferase sensor assays

Luciferase sensor constructs were created in order to detect reduced expression of predicted targets (refer to 3.2.1) on protein level. To this end the respective full length 3'UTRs of the potential miRNA target, containing the putative miRNA binding site, were cloned downstream of the open reading frame (orf) of a *firefly* luciferase gene into the pMIR-Report vector (Ambion, Austin, USA), (Figure 3-6). In some cases the length of the 3'UTR was critical for cloning and was therefore reduced to a minimal length of 1 kb, including the putative miRNA binding-site.

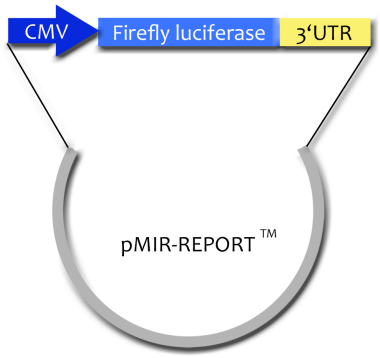

Figure 3-6: Schematic depiction of the luciferase sensor, which is commercially available from Ambion. The 3'UTR of the potential miRNA target gene, containing the putative miRNA binding site, is integrated downstream of the luciferase gene, which expression is driven by a CMV promoter. The vector backbone contains 6,470 bp excluding the 3'UTR.

The luciferase sensors were co-transfected with a *renilla* luciferase expression vector as well as the previously generated expression vectors pREP4miR-19a, pREP4miR-92a-1, pREP4miR-155 or pREP4-control (refer to 3.2.2.5) into HEK293T cells. The increase in miRNA levels upon transfection was confirmed by qRT-PCR (data not shown). The *renilla* luciferase expression vector was driven by a thymidine kinase (TK) promoter and not supposed to be affected by any miRNA. It therefore served as an internal control for transfection efficiency.

Cells were analyzed 24 hours after co-transfection. The luminescence signal of the *firefly* sensor was normalized to the respective signal from the *renilla* luciferase vector. Relative signal intensities of the samples with pREP4-control co-transfection scaled to one were calculated (Figure 3-7 - Figure 3-9, red lines). Every luciferase sensor was tested in four biological replicates, which were measured each in triplicates. Statistical significance was calculated using the student's t-test. P-values lower than 0.05 were considered as significant.

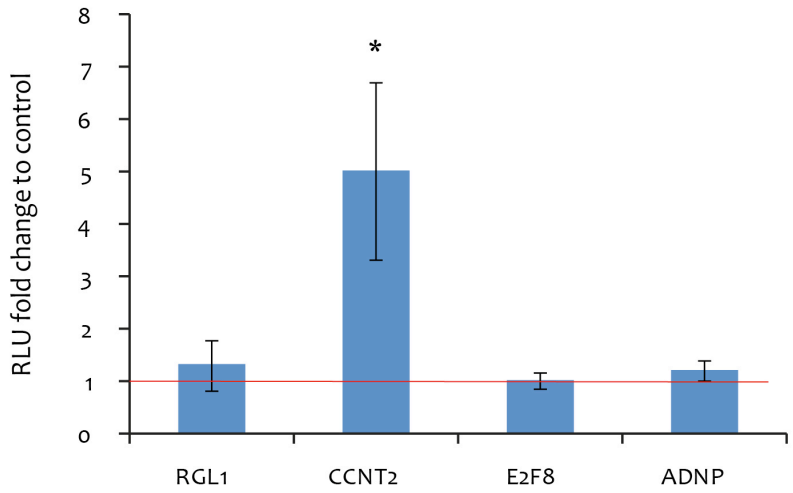

Figure 3-7: Results of the luciferase sensor assays of potential miR-19a targets depicted as relative light units (RLU). Firefly luciferase signals were normalized to *renilla* luciferase values and to the empty vector control results, which were scaled to 1 (red line). Every experiment was measured in triplicates and in four biological replicates. The calculated mean values and standard deviations are depicted. Statistical significance was calculated by the student's t-test (*=p<0.05).

For miR-19a four luciferase sensors were tested, but none of them showed reduced luciferase signals upon miR-19a transfection as expected (Figure 3-7). Instead, the results for CCNT2 showed a significant up-regulation and for RGL1, E2F8 and ADNP no significant changes were observed.

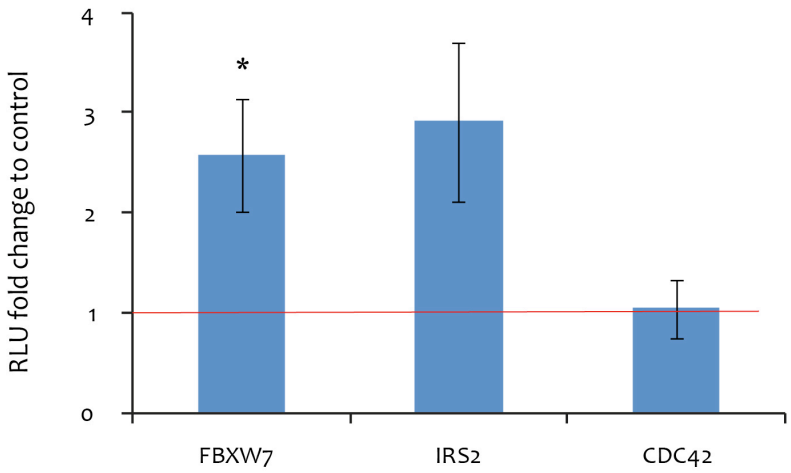

Figure 3-8: Results of the luciferase sensor assays of potential miR-92a-1 targets depicted as relative light units (RLU). Firefly luciferase signals were normalized to *renilla* luciferase values and to the empty vector control results, which were scaled to 1 (red line). Every experiment was measured in triplicates and in four biological replicates. The calculated mean values and standard deviations are depicted. Statistical significance was calculated by the student's t-test (*=p<0.05)

Three luciferase sensors were tested for responsiveness to miR-92a-1 (Figure 3-8). The luciferase signals for FBXW7 and IRS2 were enhanced. This effect was statistically robust for FBXW7. The luciferase activity of CDC42 was not altered upon ectopic miR-92a-1 expression.

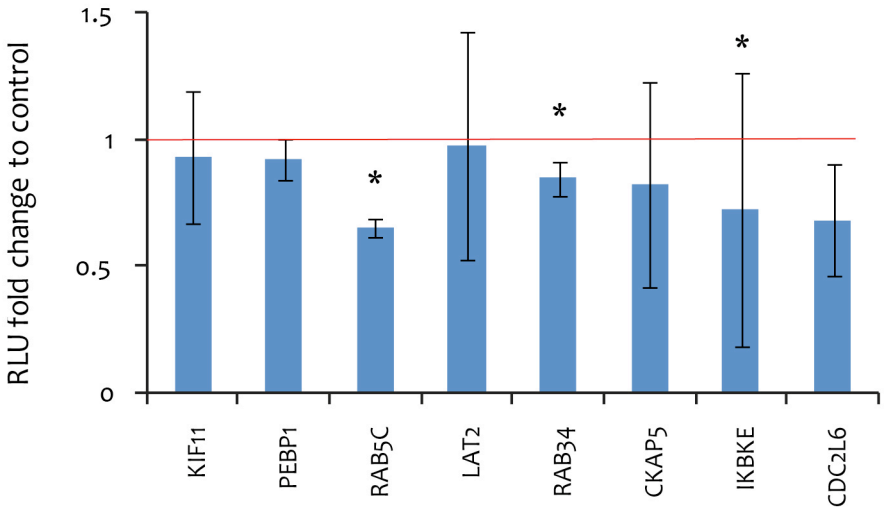

Figure 3-9: Results of the luciferase sensor assays of potential miR-155 targets depicted as relative light units (RLU). Firefly luciferase signals were normalized to *renilla* luciferase values and to the empty vector control results, which were scaled to 1 (red line). Every experiment was measured in triplicates and in four biological replicates. The calculated mean values and standard deviations are depicted. Statistical significance was calculated by the student's t-test (*=p<0.05).

In addition, seven luciferase sensors were tested upon miR-155 over-expression (Figure 3-9). The luciferase sensor for IKBKE was used as a positive control since IKBKE was previously published as a miR-155 target [213]. As expected, the signal of IKBKE was significantly reduced by approximately 30% upon miR-155 over-expression. The sensor for KIF11 was used as a negative control, since its 3'UTR contains no predicted miR-155 binding site (refer to 2.1.13) and the results showed no significant changes of the luciferase activity in comparison to the control. Of the remaining luciferase sensors RAB5C and RAB34 were significantly reduced by approximately 30% and 15%, respectively. Luciferase sensors for PEBP1, LAT2 and CDC2L6 were not significantly responsive to miR-155 co-transfection.

3.2.2.4 Identification of miRNA targets by Western blot

The results from qRT-PCR (refer to 3.2.2.2) and luciferase assays (refer to 3.2.2.3) suggested the gene *RAB5C* as a potential target of miR-155. Therefore, Western blot analyses were performed in order to confirm these results on protein level. To this end MEC-1 cells were transfected with pre-miR-155 or the corresponding pre-miR-control and protein was isolated 24, 48 and 72 hours after transfection (Figure 3-10 A). In a second approach MEC-1 cells were transfected with pre-miR-155 or anti-miR-155 in two biological replicates. Proteins from these cells were isolated 48h after treatment (Figure 3-10 B). Changes in RAB5C protein expression were analyzed by Western blot using the ECLplex system, scanning the membranes on a Typhoon fluorescence scanner 9000 and analyzing band intensities with ImageJ. RAB5C and α-tubulin expression were detected in parallel and the RAB5C-specific signals were normalized to the α-tubulin signals. Results of the pre-miR-control transfections were scaled to one (red line).

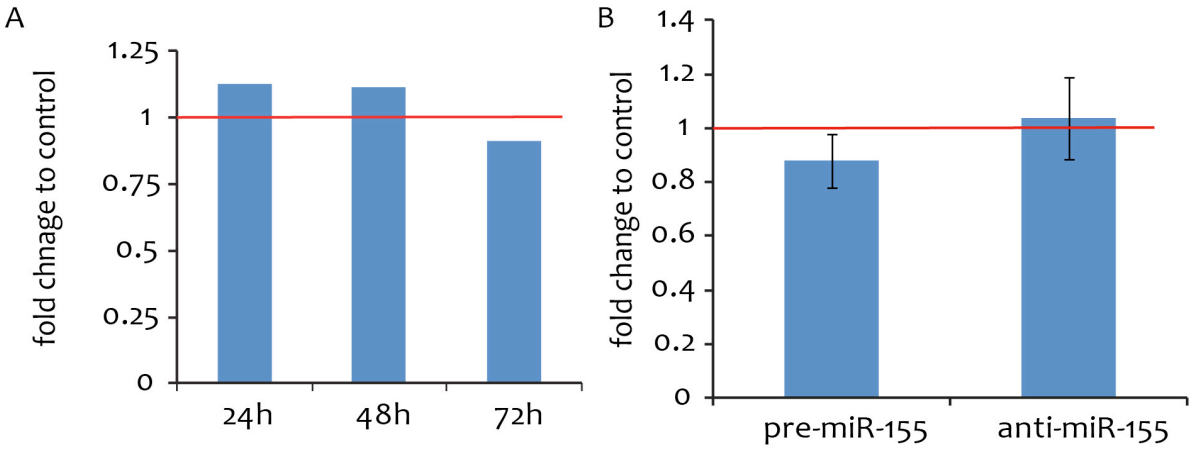

Figure 3-10: Western blot analysis of RAB5C 24, 48 and 72 hours after transfection with pre-miR-155 or pre-miR-control (A) and after 48h of pre-miR-155 or anti-miR-155 treatments (two replicates, B). The blots were scanned on a Typhoon 9000 scanner and the images were analyzed using the ImageJ software. The fluorescence signals of RAB5C were normalized to the α-tubulin expression of the respective sample. The normalized values of the pre-miR-control transfections were scaled to 1 (red line).

The transient over-expression of miR-155 in the B-cell line MEC-1 resulted in a approximately 15% increase of RAB5C protein 24 and 48 hours after transfection and a 10% decrease 72 hours after transfection in comparison to the pre-miR-control (Figure 3-10 A) Likewise, treatment with pre-miR-155 for 48 h resulted on average in approximately 15% RAB5C protein reduction whereas anti-miR-155 resulted in a on average slight increase of

RAB5C protein (Figure 3-10 B). In summary, the minor changes of RAB5C expression are not reflecting the results of the luciferase sensor assays (Figure 3-9).

3.2.2.5 Identification of miRNA targets in stable cell lines

To overcome uncertainties of experiments using transient miRNA over-expression, like transfection efficiency, secondary effects of the transfection itself, and timing of the read-out, cell lines with stable over-expression of the miRNAs of interest were generated. Using stable cell lines further creates more flexibility in performing functional assays to characterize phenotypes potentially induced by miRNA manipulation.

Genomic sequences coding for miR-19a, miR-92a-1 or miR-155 were cloned into the episomal pREP4 vector backbone (refer to 2.2.1.2). By using the RNAfold algorithm (refer to 2.1.12) these sequences were tested for potential RNA secondary structures of the respective transcripts, in order to ensure the generation of hairpins resembling the structure of the endogenously expressed pre-miRNA, which is necessary for proper miRNA biogenesis. In order to define the proper hygromycin B concentration for selection, the cell lines to be transfected were tested with a range of hygromycin B concentrations. Accordingly, 250 µg/ml and 100 µl/ml of hygromycin B were suitable to strongly reduce the cellular growth rates of MEC-1 and GRANTA-519 cells, respectively. The B-cell lines were transfected with the vectors pREP4miR-19a, pREP4miR-92a-1, pREP4miR-155 and pREP4-control using the Lonza nucleofection system. These cells as well as a mock transfection control were treated with indicated concentrations of hygromycin B to select for cells containing the pREP4 expression vector. After two weeks of selection the mock control cells were dead. The surviving B-cell lines containing the pREP4 vector were cultured under selective pressure for two additional weeks prior to preparing stocks of viable frozen cells. Finally, the cells were tested for miRNA expression using the miRNA specific qRT-PCR system (refer to 2.2.7.1). Expression values of the miRNAs were normalized to the mean of the house keeping small RNAs RNU-6B and RNU-66 (Figure 3-11 A & B).

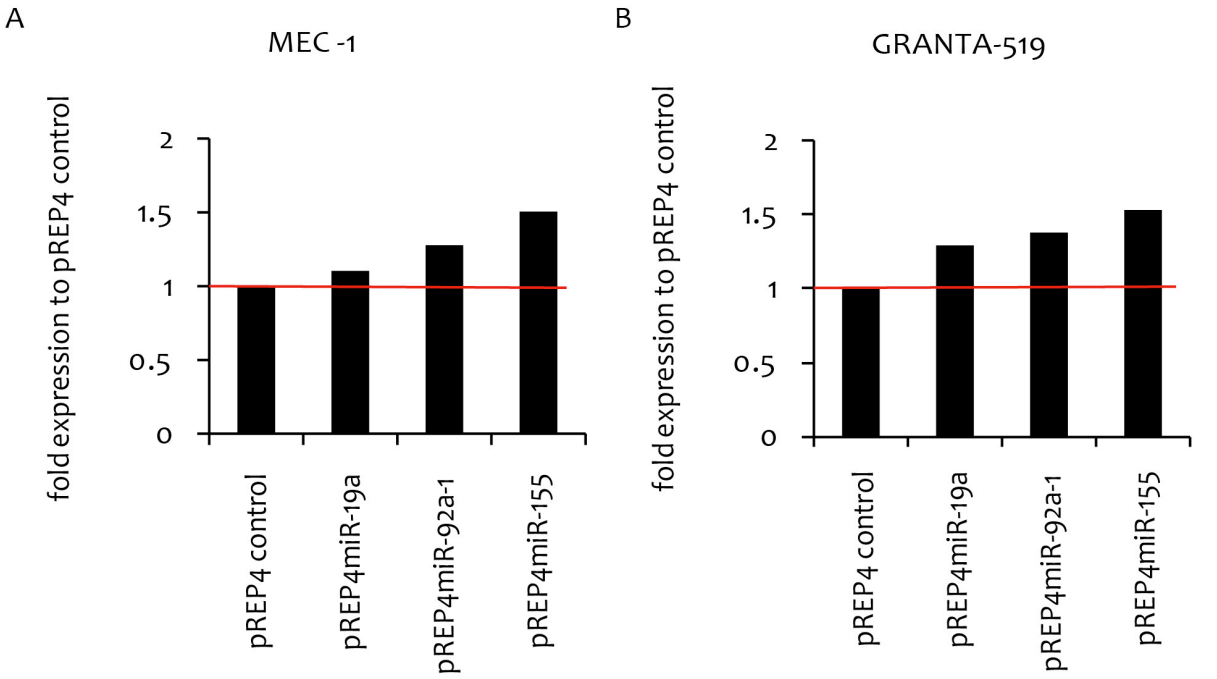

Figure 3-11: MicroRNA expression analyses of miR-19a, miR-92a-1 and miR-155 in the corresponding stable cell lines MEC-1 (A) and GRANTA-519 (B) using qRT-PCR. The miRNA expression values were normalized to the house keeping small RNAs RNU-6B and RNU-66 and the results of pREP4-control cells were scaled to one (first column, red line).

The results of the qRT-PCR analyses showed that miR-19a, miR-92a-1 and miR-155 were slightly higher expressed in the respective cell lines compared to the control cell line. In the stable MEC-1 cell lines the expression of miR-19a, miR-92a-1 and miR-155 were increased by approximately 10, 30 and 50%, respectively (Figure 3-11 A) and in GRANTA-519, the increase was approximately 30, 40, and 50%, respectively (Figure 3-11 B).

The stable cell lines were used to monitor the expression of potential miRNA targets by qRT-PCR to support the data of the transient manipulation of miRNAs (section 3.2.2). To this end putative miRNA targets were detected in the stable GRANTA-519 cell lines, which showed a superior miRNA over-expression compared to the stable MEC-1 cell lines (Figure 3-11). Similar to the effects after transient manipulation of the miRNAs (refer to 3.2.2.2), the changes in the stable cell lines were mild (data not shown).

Furthermore, the expression of the potential miR-155 target gene RAB5C was monitored on protein level in MEC-1 cells stably expressing miR-155 using the ECLplex based Western blot system as described above.

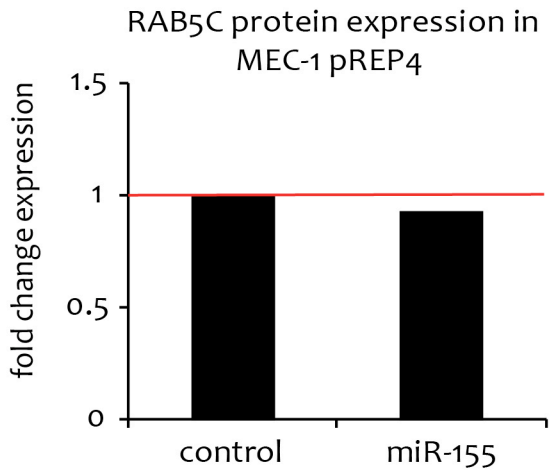

Figure 3-12: RAB5C protein expression in MEC-1 cell line with stable miR-155 overexpression tested in a single Western blot. The blot was scanned on a Typhoon 9000 scanner and the images were analyzed using the ImageJ software. The raw signal of RAB5C was normalized to the α-tubulin expression of the respective sample. The normalized value of the corresponding pREP4 control cell line was set to one.

The results of this single Western blot showed that RAB5C protein expression was reduced by approximately 5% in comparison to the control vector cell line (Figure 3-12). This observation was consistent with the data upon transient over-expression of miR-155 (Figure 3-10) suggesting a minor regulatory effect of miR-155 on RAB5C protein expression in MEC-1 cells.

3.3 Establishing RIP-Seq for targetome identification

As the above described screening for miRNA targets (refer to 3.2.2 and 3.2.2.5) did not deliver satisfactory results, an alternative method was needed. Therefore, the recently published RIP technique was established and refined [252,253]. The refined method combines the immunoprecipitation of RNA interacting protein (RIP) with subsequent 2nd generation sequencing of the co-immunoprecipitated mRNAs. For the RIP, antibodies binding AGO2, a central protein of the RNA induced silencing complex (RISC) were used (Figure 3-13). The aim of this method is to identify the miRNA "targetome", representing all mRNAs that are regulated by endogenously expressed miRNAs.

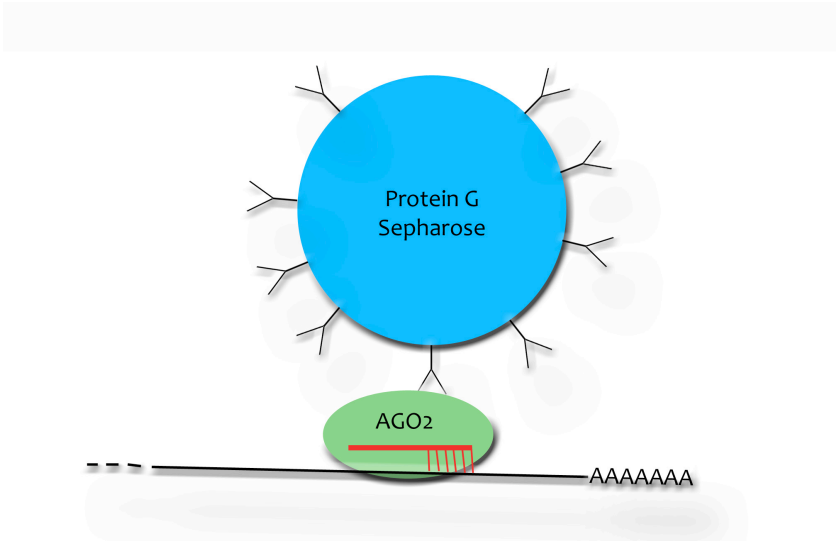

Figure 3-13: Schematic picture of the RIP method. Protein G sepharose beads were coated with antibodies specific for native AGO2 protein allowing its precipitation. MicroRNAs (red) that are incorporated into AGO2 protein specifically bind to target mRNAs (black). The binding of AGO2 protein by sepharose bead-coupled antibodies allows the co-immunoprecipitation and subsequent analysis of miRNAs and its target mRNAs.

3.3.1 Immunoprecipitation of AGO2 protein from cell lysates

An efficient precipitation of AGO2 protein was the major prerequisite of the RIP-Seq method. Protein G-coupled sepharose beads were coated with equal amounts of two different monoclonal AGO2-specific antibodies. Isotype control antibody-coupled beads were used as negative control. To verify AGO2-specific IP, the supernatants (SN) and IP fractions (IP) were analyzed by Western blotting (Figure 3-14).

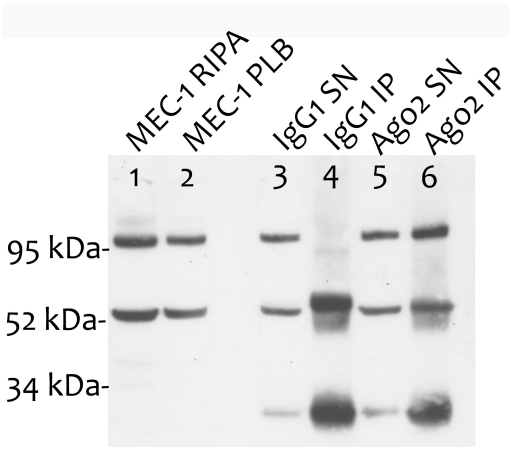

Figure 3-14: Western blot analysis of an AGO2 immunoprecipitation (IP) using MEC-1 cell lysates. Lanes 1 and 2 represent total cell lysates using RIPA-buffer or polysome-lysis buffer (PLB). Lanes 3 and 4 show the supernatant (SN) and IP fraction (IP) after immunoprecipitation with isotype control antibody (IgG1). Likewise lanes 5 and 6 represent the SN and IP fractions after AGO2 specific IP. AGO2 protein was detected as a band of approximately 96 kDa. The lower bands presumably represent the heavy and light chains of antibodies.

MEC-1 cells were either lysed in RIPA buffer (lane 1) or polysome lysis buffer (lane 2). The polysome lysis buffer was used for immunoprecipitation, as it is less denaturing leaving the cell nucleoli as well as protein-RNA interactions intact. Lanes 3 and 4 (Figure 3-14) represent the immunopurification of AGO2 using an unspecific isotype control antibody (IgG1). AGO2 is detectable as a band of approximately 96kDa in the supernatant (SN), (lane 3). However, the signal was absent in the IP fraction (lane 4). Contrary, a strong AGO2 band was detectable in the AGO2-specific IP (lane 6), which was stronger in comparison to the signal in the supernatant (lane 5) suggesting a successful enrichment of AGO2 by immunoprecipitation.

To validate AGO2 IP, the 96kDa band of lane 6 was excised from a Coomassie stained gel and was analyzed by matrix-assisted laser ionization (MALDI) time of flight (TOF) mass spectrometry. The analysis identified AGO2 by two different peptide fragments verifying successful enrichment of AGO2.

3.3.2 Generation of HEK293T cells stably over-expressing miR-155

The cell lines MEC-1 and GRANTA-519 stably over-expressing miR-19a, miR-92a-1 and miR-155 showed only a weak ectopic expression of miRNAs (Figure 3-11 A & B). In order to establish the RIP-Seq method, a cell line with a strong over-expression of miR-155 was

generated. For this purpose HEK293T cells, which show low endogenous miR-155 levels were used. The cells were transfected with the previously established pREP4miR-155 (hereafter HEK-miR-155) and pREP4empty (hereafter HEK-vector) vectors using TransIT-LT1 transfection reagent (refer to 3.2.2.5, 2.2.2.1). The transfected cells as well as a mock transfection control were treated with 250 µg/ml hygromycin B to select for vector containing cells. After two weeks of selection the mock control cells died in culture. The surviving pREP4 vector containing cells HEK-vector and HEK-miR-155 were cultured under selective pressure for two additional weeks prior to usage of the cells for experiments. Over-expression of miR-155 was confirmed by qRT-PCR relative to the mean of the house keeping small RNAs RNU-6B and RNU-66 (HK) (Figure 3-15).

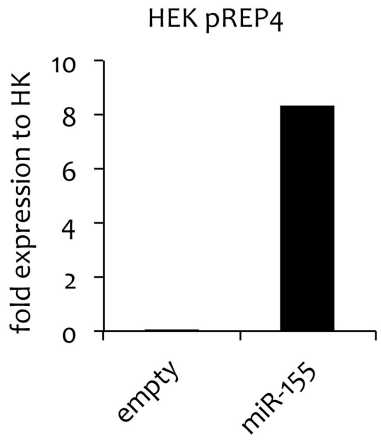

Figure 3-15: Quantification of miR-155 in stably transfected HEK293T cells using qRT-PCR. The expression of miR-155 was normalized to the mean expression of the two housekeeping small RNAs (HK) RNU-66 and RNU-6B.

QRT-PCR confirmed weak endogenous expression of miR-155 in HEK293T containing the pREP4 vector backbone (HEK-vector) (Figure 3-15). MiR-155 was eight-fold higher expressed in HEK-miR-155 cells in comparison to the mean expression of RNU-66 and RNU-6B and more than hundred-fold higher compared to the HEK-vector cell line.

3.3.3 Phenotypic characterization of HEK-miR-155

Since miR-155 was previously found to be associated with cell proliferation and growth by other groups [254,255], proliferation rates of HEK-miR-155 were analyzed.

3.3.3.1 Cell counter assays to analyze proliferation rates

Cell counts of HEK-vector and HEK-miR-155 cultures were assessed to identify potential differences in the proliferation rates of the cell lines. Briefly, equal amounts of cells were seeded and counted after 24, 48 and 72 hours of culture. In addition, cell viability was evaluated using trypan blue, which stains dead cells. The assay was repeated at least seven times disseminated over a period of at least three months. Furthermore, different batches of viably frozen cells were used. Statistical significance was calculated by performing the student's t-test. P-values lower than 0.05 were considered as significant.

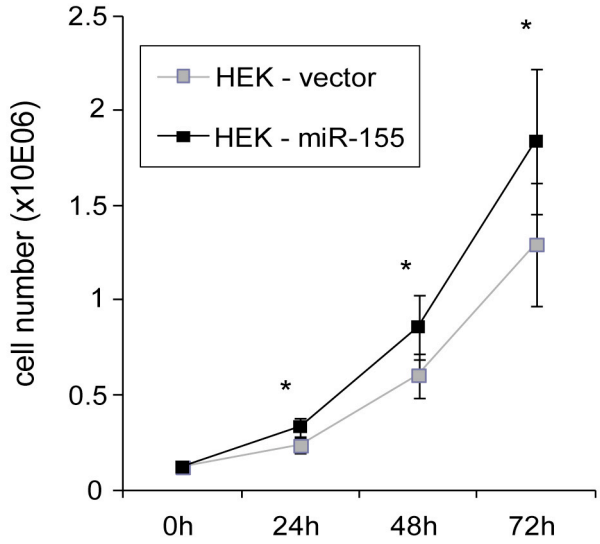

Figure 3-16: Cell counts of HEK-vector (grey) and HEK-miR-155 (black) (A). $3x10^5$ cells were seeded per well in 6-well plates. Cells were harvested 24 (n=7), 48 (n=9) and 72 (n=8) hours after seeding and counted by an automated cell counting device. Dead cells were excluded by trypan blue staining and the overall proportion of viable cells was calculated. Mean and standard deviations of independently performed experiments are depicted. Statistical significance was calculated by performing the student's t-test. Significant differences in cell numbers between both batch cell lines were observed at 24, 48 and 72 hours with $p< 0.0008$, 0.0002 and 0.0005, respectively. (*=$p<0.05$).

HEK-miR-155 cells showed significantly faster proliferation rates compared to the control cells (Figure 3-16). After 72 hours of incubation, a mean increase of 30% of HEK-miR-155 cells compared to the control was observed. Furthermore, no significant differences in cell viabilities were detected, indicating that the difference in viable cell numbers was not due to differences in cell death rates (data not shown).

3.3.3.2 FACS analyses of proliferation rates using the Click-iT assay

The incorporation rates of the thymidin analog EdU into DNA during replication were monitored in order to confirm accelerated proliferation of HEK-miR-155 (refer to Figure 3-16). To this end, cells were maintained in confluent cultures for 24 hours to synchronize the cells. After reseeding the cells, EdU was added to the medium for 6 hours. The cells were then harvested and the Click-iT reaction was performed, followed by flow cytometry analysis (Figure 3-17). The assay was performed in two biological replicates and technical triplicates. P-values lower 0.05 as calculated by student's t-test were considered as significant.

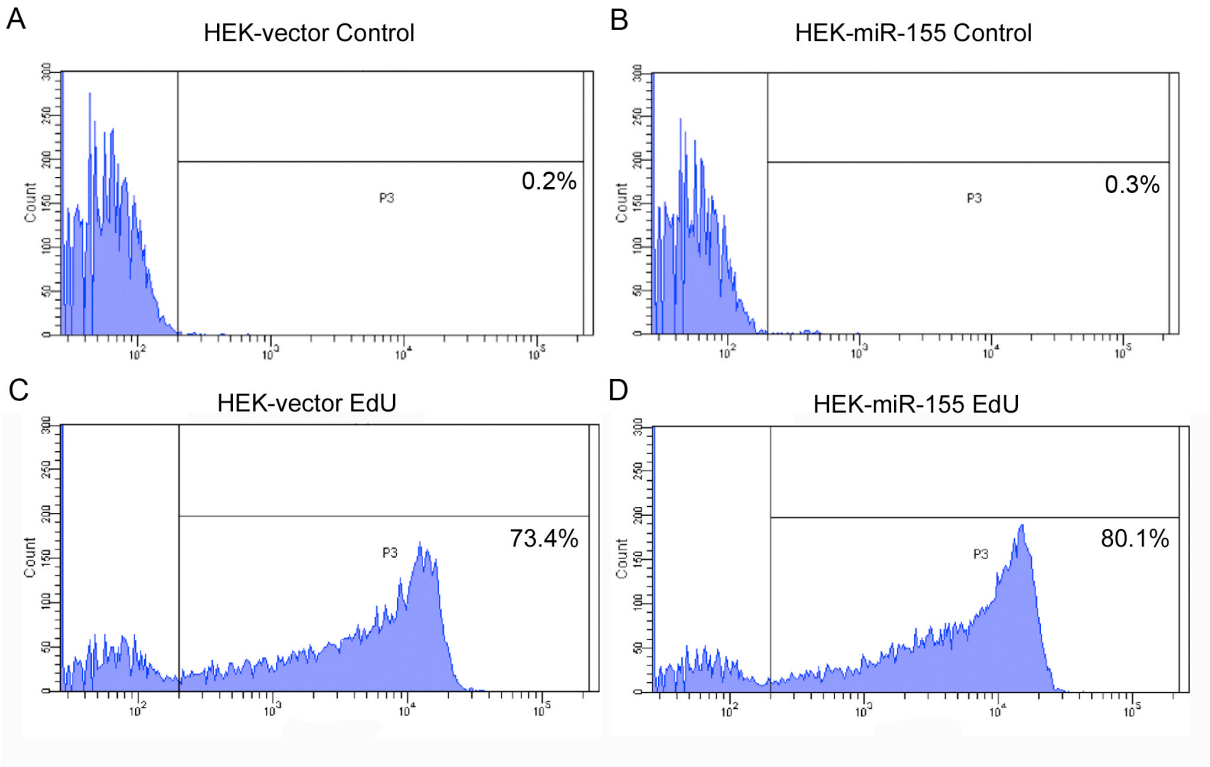

Figure 3-17: EdU incorporation in DNA during replication detected by flow cytometry (Click-iT assay). The stable cell lines HEK-vector and HEK-miR-155 were synchronized by 24 hours of culture under confluency. The cells were seeded in 6-well plates and incubated with 10 µM EdU (C & D) or equal amounts of DMSO (A & B) for six hours. Thereafter, the Click-iT reaction was performed and EdU incorporation was analyzed by flow cytometry. Histograms of one representative example are depicted and show the percentages of EdU positive cells.

Comparing the EdU incorporation rates of HEK-miR-155 and HEK-vector cells revealed a difference of 5-7% after six hours of incubation, indicating enhanced proliferation rates of HEK-miR-155 cells (Figure 3-17), which confirmed the findings of the cell counter assay

(refer to 3.3.3.1). Statistical analysis of the results using the student's t-test revealed a p-value of $p<0.021$.

3.3.4 Co-immunoprecipitation workflow

In order to proof the principle of the RIP-Seq method, it was aimed to identify putative miR-155 targets specifically enriched in the IP fraction of the HEK-miR-155 cell line compared to HEK-vector. RIP-Seq was performed as described (refer to 2.2.8 and 2.2.9) using a total of $2x10^8$ cells per IP reaction either with AGO2-specific or IgG1 isotype control antibodies. Three biological replicates of HEK-vector and HEK-miR-155 cells were performed.

3.3.5 Enrichment of miR-155 and putative miR-155 target mRNAs

Prior to next generation sequencing, the IP and TL fractions of HEK-vector and HEK-miR-155 cells were tested for the presence of miR-155 (Figure 3-18) and putative miR-155 target mRNAs using qRT-PCR (Figure 3-19).

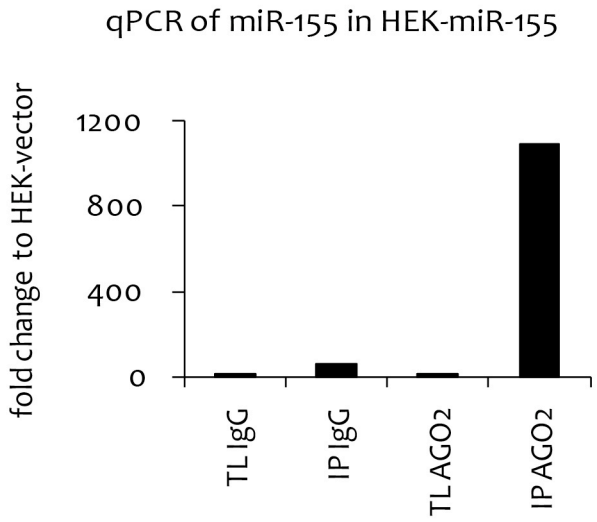

Figure 3-18: MicroRNA-155 abundance in IP and TL fractions of HEK-vector and pREP4miR-155. qRT-PCR was used for quantification and the abundance of miR-155 was normalized to RNU-6B. MiR-155 enrichment after AGO2 specific IP was compared to IgG IP (left). MiR-155 enrichment was compared between the IPs of HEK-miR-155 and HEK-vector cells (right).

The results of the miRNA quantification showed that miR-155 was almost absent in HEK-vector TL and IP fractions. However, miR-155 was approximately 14-fold enriched in the

AGO2 IP of the HEK-miR-155 cells compared to control IP (Figure 3-18) suggesting a successful and specific enrichment of miR-155.

To test whether miR-155 target mRNAs were enriched in the AGO-2 IPs, qRT-PCR analyses were performed using RNA of IP and TL fractions of HEK-miR-155 cells. The enrichment of *PHC2*, a published miR-155 target [192,256], was analyzed as a positive control. *GAPDH* served as a negative control, since miRNAs regulating this gene were supposed to be rarely expressed in HEK293T cells [151]. The results showed a consistent enrichment of *PHC2* (red columns) but not *GAPDH* (blue columns) in the IPs of HEK-miR-155 compared to control cells (Figure 3-19).

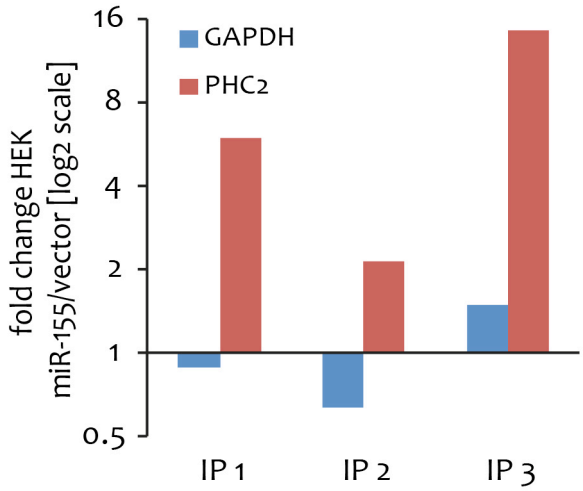

Figure 3-19: Quantification of *PHC2* and *GAPDH* mRNA levels in the IP of HEK-vector and HEK-miR-155 using qRT-PCR. Genes enriched in the IP of HEK-miR-155 were normalized to the enrichment values of HEK-vector IP.

3.3.6 MicroRNA expression profiling in total lysate and IP fractions

MicroRNA specific TaqMan arrays were used to test the miRNA profile in TL and IP fractions of HEK-miR-155 and HEK-vector cells. MicroRNAs with an average Δct value higher than 35 were considered as not expressed and were excluded from further analyses. In total 248 and 193 miRNAs were detected in HEK-miR-155 IP and TL, respectively. For HEK-vector cells, 197 miRNAs were detectable in the TL fraction and 249 in the IP fraction. Figure 3-20 displays the top 30 miRNAs enriched by AGO2 IP of both stable cells lines. The Δct values were normalized to the median of all expressed miRNAs in the respective sample. Values higher than zero indicate a relatively strong enrichment of the depicted miRNAs. According to this, miR-17 was the miRNA with the highest enrichment in HEK-miR-155 (black bars). Globally the miRNA enrichment profiles of the IPs

were similar in both cell lines. With the exception of miR-155 and miR-331, the 30 most highly enriched miRNAs were common to HEK-vector and HEK-miR-155. As expected, miR-155 was highly enriched in the IP of HEK-miR-155, but was underrepresented in the IP of the control cells (grey bars) again confirming the over-expression and successful enrichment of this miRNA in the HEK-miR-155 cell line. As miR-17, miR-222, miR-106a and miR-20a were present in levels higher than miR-155, the ectopic expression of miR-155 was in a physiological range in HEK-miR-155 cells.

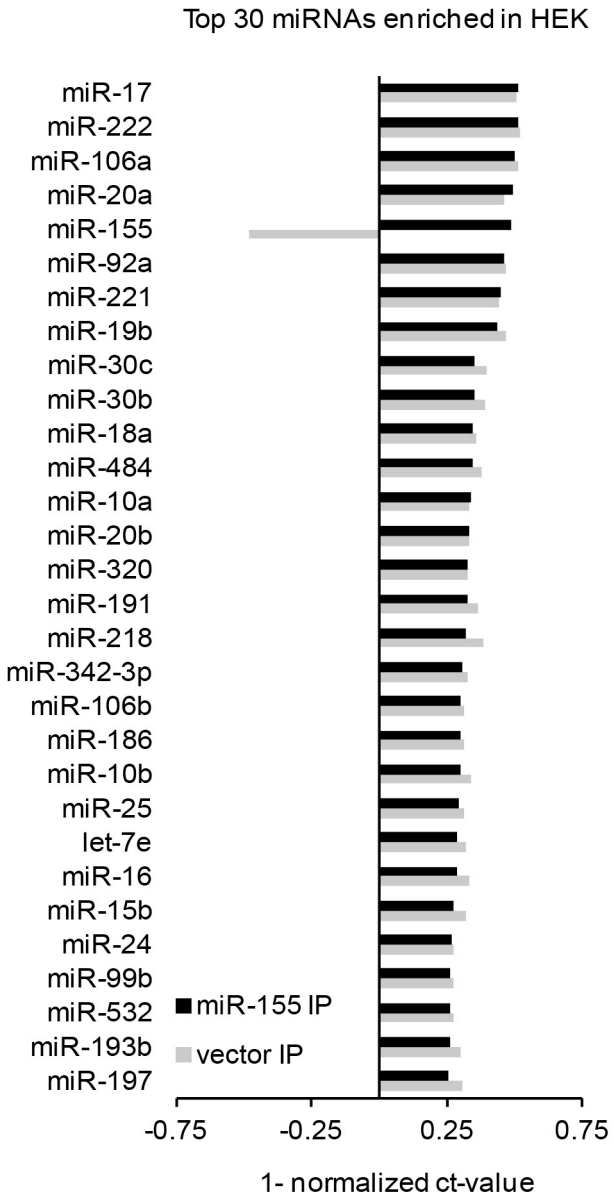

Figure 3-20: Summary of the top 30 miRNAs in HEK-vector (grey bars) and HEK-miR-155 (black bars) cells enriched by AGO2 IP. The miRNAs were quantified by TaqMan arrays (Applied Biosystems). The Δct values were normalized to the median of all expressed miRNAs in the respective sample. Values higher than zero were highly enriched in the IP of the respective sample.

Comparing the miRNA profiles of the TLs of both cell lines revealed a differential expression of 57 miRNAs with a fold change higher or lower than the single standard deviation. According to this, 25 miRNAs were higher and 32 miRNAs were lower in HEK-miR-155 compared to HEK-vector. Out of these, 11 were exclusively detectable in HEK-vector cells and 5 miRNAs were exclusively present in HEK-miR-155 cells including miR-155 itself. Comparing the IP fractions of HEK-miR-155 and HEK-vector revealed 24 miRNAs and 23 miRNAs over-proportionally enriched in the IP fraction of HEK-vector and HEK-mIr-155, respectively (Figure 3-21). Notably, miR-155, miR-98 and miR-34a were clearly differentially enriched between the IPs of HEK-miR-155 and HEK-vector.

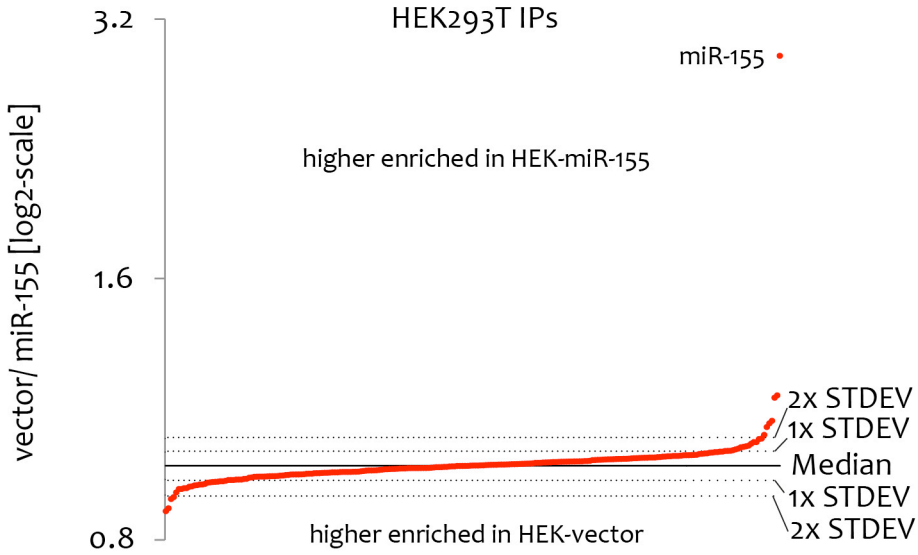

Figure 3-21: Comparison of the miRNA enrichment profiles in the IP fractions of HEK pREP4empty and pREP4miR-155. MiRNAs with enrichment ratios higher than the median are relatively more enriched in HEK-miR-155. Dashed lines indicate fold-changes higher or lower than the 1- fold or 2-fold standard deviation from the median.

Finally, the expression profiles of TL and respective IP fraction of the same sample were matched. In case the miRNA expression profile of TL and enrichment profile of the IP were equal, the ratios of all miRNAs between TL and IP should be relatively constant. Ratios that were higher or lower than the single standard deviation from the median were considered as disproportionally enriched or depleted in the IP fraction. As expected, there was a bias towards the global enrichment of miRNAs in the IP fractions compared to the total lysates. Interestingly, 28 and 19 miRNAs appeared to be over-proportionally enriched in the IP fractions of HEK-vector and HEK-miR-155, respectively (Table 3-4).

Furthermore, 17 of these miRNAs were commonly overrepresented in the IP fractions and of both cell lines.

HEK-vector	Relative miRNA level	HEK-miR-155	Relative miRNA level
hsa-miR-222	0.728	hsa-miR-155	0.739
hsa-miR-92a	0.732	hsa-miR-222	0.746
hsa-miR-221	0.762	hsa-miR-92a	0.753
hsa-miR-106a	0.777	hsa-miR-501-3p	0.755
hsa-miR-17	0.784	hsa-miR-221	0.774
hsa-miR-320	0.790	hsa-miR-320	0.775
hsa-miR-342-3p	0.792	hsa-miR-17	0.787
hsa-miR-197	0.799	hsa-miR-342-3p	0.797
hsa-miR-615-5p	0.804	hsa-miR-20a	0.807
hsa-miR-191	0.809	hsa-miR-10a	0.809
hsa-miR-20a	0.815	hsa-miR-615-5p	0.815
hsa-let-7e	0.818	hsa-miR-106a	0.828
hsa-miR-10b	0.818	hsa-miR-191	0.829
hsa-miR-30b	0.818	hsa-miR-125a-3p	0.832
hsa-miR-501	0.821	hsa-miR-125a-5p	0.835
hsa-miR-30c	0.826	hsa-miR-197	0.838
hsa-miR-99b	0.828	hsa-miR-425-5p	0.841
hsa-miR-346	0.830	hsa-miR-99b	0.841
hsa-miR-10a	0.830	hsa-miR-346	0.843
hsa-miR-125a-5p	0.830		
hsa-miR-193b	0.835		
hsa-let-7a	0.836		
hsa-miR-542-5p	0.836		
hsa-miR-454	0.837		
hsa-miR-186	0.838		
hsa-miR-484	0.838		
hsa-miR-125a-3p	0.840		
hsa-miR-425-5p	0.840		

Table 3-4: MicroRNAs overrepresented in AGO2 IPs versus TLs. (miRNA levels relative to the median are depicted, smaller numbers indicate a relatively higher enrichment of the respective miRNA)

3.3.7 High throughput identification of putative miR-155 targets

To identify target genes of miR-155, the mRNA content of the TL and IP fractions of three independently performed RIP experiments was analyzed by high throughput sequencing. The reads were mapped against the human reference genome version 19 using the TopHat algorithm. For the IP and TL fractions 35M and 68M reads were generated, respectively. RNA profiles of TL or IP fractions were generated using the HTSeq-Count algorithm.

3.3.7.1 Global changes on mRNA expression in TLs and IP enrichment profiles mediated by miR-155

To evaluate the effects of ectopic miR-155 expression on the global mRNA expression, mRNA profiles of TL fractions of HEK-vector and HEK-miR-155 cells were compared. The analysis revealed that 339 mRNAs were down regulated and 121 mRNAs were up regulated in HEK293T cells upon ectopic miR-155 expression ($p<0.05$) (Figure 3-22 A, Table S 4 and Table S 5). Notably, among the top 20 over-expressed genes in HEK-miR-155 we identified *CCND1* and all three members of the ETS transcription factor subfamily *PEA3*, which are *ETV1*, *ETV4* and *ETV5* (Table S 5). The IP fractions of both cell lines were compared to identify transcripts potentially enriched in the RISC due to the presence of miR-155. Here, 213 mRNAs with higher abundance and 409 mRNAs with lower abundance in the IP fraction of HEK-miR-155 cells were identified ($p<0.05$) (Figure 3-22B, **Table S 2** and Table S 3). Interestingly, CCND1 was also enriched in the IP of HEK-miR-155. Computational miRNA target prediction for the *CCND1* 3'UTR indicated the presence of several putative miRNA binding sites for miR-17, miR-19a, miR-15, miR-16-1, miR-20a and miR-106a suggesting that the enrichment of *CCND1* mRNA the IP fractions was likely a secondary effect and not due to miR-155 interaction. Indeed CCND1 was previously shown regulated by miR-15/16 and members of the miR-17-92 family [257,258].

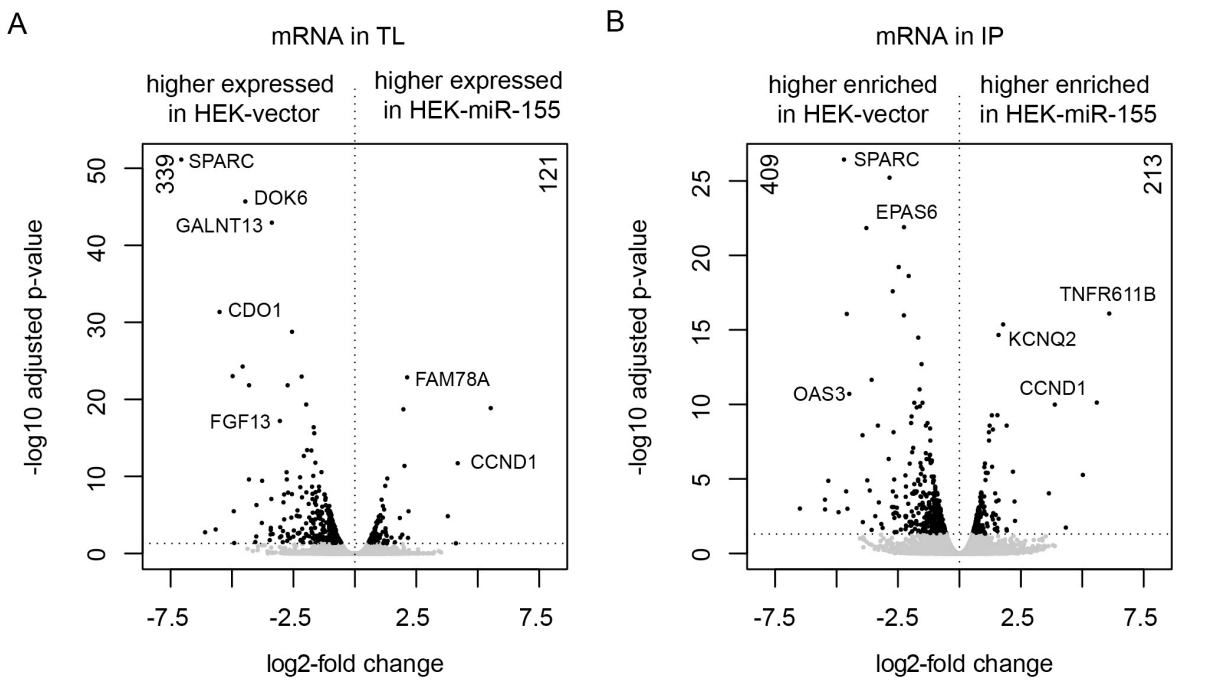

Figure 3-22: Volcano plots matching TL (A) and IP (B) fractions of HEK-vector and miR-155. In total 463 mRNAs were aberrantly expressed in TL fractions with 339 significantly down regulated and 121 significantly up-regulated transcripts in HEK-miR-155 (black, $p<0.05$) (A). Matching the IP fraction of both cell lines revealed 213 significantly higher enriched and 409 significantly lower enriched mRNAs in HEK-miR-155 (black, $p<0.05$) (B).

3.3.7.2 Identification of miR-155 targets in HEK293T

The mRNA levels detected in the IP fractions were normalized to their respective TL fractions in order to compensate for global changes in mRNA expression. In total, 100 transcripts were differentially ($p<0.01$, FDR 10%) enriched in the IPs of HEK-miR-155 cells in comparison to the HEK-vector cell line (Figure 3-23). Notably, there was no differentially enriched transcript identified in HEK-vector cells.

Target prediction algorithms were used in order to identify putative miR-155 targets within the lists of co-precipitated mRNAs for both cell lines. For this purpose, five target prediction tools TargetScan, MiRANDA, DianaMicro-T, MiRWALK and PITA were used [167,170,237,238,240,241]. Transcripts predicted by at least three of these five algorithms with a seed match of seven or eight nucleotides and a p-value lower than 0.05 were considered as putative miRNA targets. These analyses revealed that miR-155 was predicted to regulate 67 of the 100 enriched mRNAs. At least 20 of these are

experimentally identified miR-155 targets as suggested by MiRWalk database (Table 3-5; bold letters).

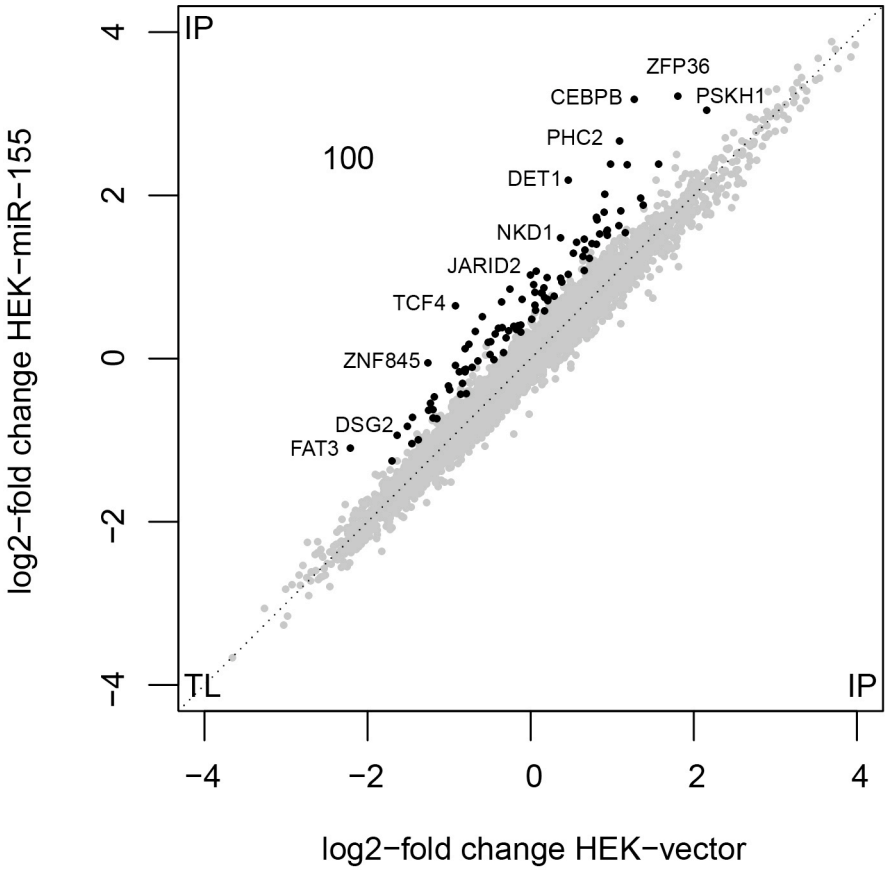

Figure 3-23: Starburst plot comparing the total lysates (TL) and immunopurifications (IP) of HEK-vector and miR-155. Significantly enriched transcripts are shown in black (n=100).

Gene	Difference in log2-FC	p-value		Gene	Difference in log2-FC	p-value
CEBPB*	1,91E+00	4,98E-05		NFIB*	6,21E-01	6,18E-04
DET1	1,73E+00	2,99E-05		RGL1	6,21E-01	1,26E-03
PHC2	1,58E+00	9,97E-06		PAK2	6,20E-01	3,89E-04
TCF4*	1,57E+00	8,97E-05		**BACH1**	6,18E-01	1,44E-03
ZFP36*	1,42E+00	1,50E-04		DUSP14	6,17E-01	6,88E-04
AGTRAP*	1,41E+00	3,99E-05		CARD10	6,13E-01	4,09E-04
MAP3K10	1,20E+00	1,59E-04		EID2	6,11E-01	9,17E-04
CSNK1G2	1,11E+00	3,19E-04		RNF166	5,93E-01	1,38E-03
JARID2*	1,03E+00	2,59E-04		FBXO9	5,82E-01	3,59E-04
RAPGEF2*	1,01E+00	1,69E-04		LDLRAP1	5,79E-01	7,58E-04
TRIM32	1,01E+00	1,30E-04		**TRIP13**	5,78E-01	9,07E-04
DHX40	9,32E-01	1,20E-04		MASTL	5,60E-01	5,68E-04
ZNF320	9,29E-01	2,39E-04		CDC42EP4	5,57E-01	8,27E-04
VAMP3	8,93E-01	2,49E-04		TMTC2	5,51E-01	1,63E-03
PSKH1	8,89E-01	6,98E-05		**FOS**	5,50E-01	1,27E-03
ATP6V1G1	8,85E-01	2,09E-04		BRWD1	5,40E-01	8,47E-04
IER5	8,73E-01	4,49E-04		**ARFIP1**	5,35E-01	9,27E-04
CNNM1	8,40E-01	1,89E-04		TAPT1	5,33E-01	1,72E-03
TSHZ3	8,34E-01	4,78E-04		TUSC1	5,12E-01	6,38E-04
C3orf18	8,17E-01	7,48E-04		**RCN2**	5,05E-01	1,96E-03
EN2	8,11E-01	2,19E-04		**RAB34**	5,04E-01	9,37E-04
DCK*	7,92E-01	1,79E-04		TSPAN14	4,69E-01	1,18E-03
ARRDC2	7,70E-01	5,28E-04		C2orf18	4,47E-01	1,70E-03
ZNF652	7,35E-01	3,09E-04		**CHAF1A**	4,36E-01	1,28E-03
BBS7	7,19E-01	5,98E-04		EIF5A2	4,25E-01	1,81E-03
EYA2	7,11E-01	5,18E-04		**ANKFY1**	4,22E-01	1,52E-03
ZNF468	6,99E-01	9,77E-04		MPP5	4,21E-01	1,83E-03
CTNND1*	6,80E-01	5,38E-04		**SMAD5**	4,17E-01	1,53E-03
ARVCF	6,79E-01	1,13E-03		STK38	4,17E-01	1,50E-03
ATP6V1C1	6,73E-01	3,49E-04		LRP12	4,10E-01	1,60E-03
GALT	6,70E-01	1,19E-03		GNE*	3,90E-01	1,97E-03
TBC1D14	6,70E-01	1,09E-03		AHRR	3,90E-01	1,10E-03
DPY19L1	6,46E-01	5,78E-04		PDK1	3,65E-01	1,54E-03
MAP3K14	6,32E-01	9,67E-04				

Table 3-5: Predicted miR-155 target mRNAs, which were significantly (p<0.01, FDR 10%) enriched by AGO2 IP of HEK-miR-155 in comparison to the control cell line HEK-vector starting with the strongest enriched mRNA. Known targets (according to MiRWalk database) are marked with bold letters. Genes negatively related to proliferation (according to Ingenuity) are marked with asterisks (*).

3.3.7.3 MiR-155 targets related to proliferation

According to cell counter and EdU incorporation assays, HEK-miR-155 had a significant higher proliferation rate in comparison to HEK-vector (refer to 3.3.3). To identify functionally relevant transcripts regulated by miR-155, the Ingenuity database was searched for genes related to proliferation. In total 17 out of 67 potential miR-155 target

genes were associated to cell proliferation, of which 10 were characterized as negative regulators of proliferation (Table 3-5; *).

3.3.7.4 The miR-155 mediated repression of *CEBPB* causes increased *CCND1* gene expression

The miR-155 target gene *CEBPB* was described to repress the expression of CCND1 in macrophages [259]. Furthermore, screening of the *CCND1* promoter region for protein interaction sites using the TFSERACH algorithm revealed several putative CEBPB binding sites. Therefore, knockdown experiments were performed using *CEBPB*-specific siRNAs to test its functional association to *CCND1* expression. Quantitative RT-PCR analysis revealed a knockdown of *CEBPB* transcript of approximately 40% 24h and 48h after transfection. Associated with that, a slight increase of up to 1.8-fold of *CCND1* expression was observed (Figure 3-23). Of note, knockdown of *CEBPB* in HEK293T cells had no effect on the proliferation rate of the cells (data not shown).

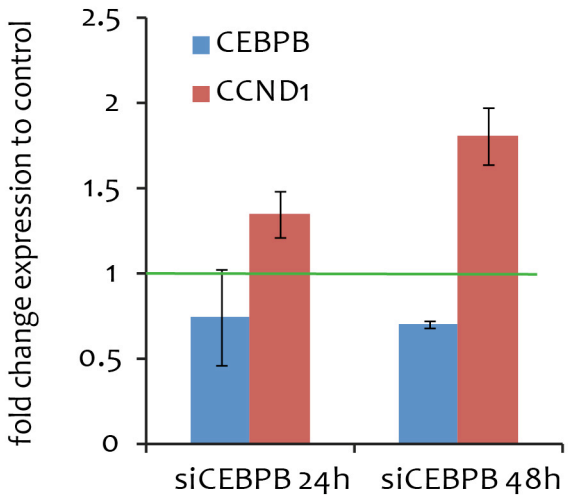

Figure 3-24: Transient knockdown of CEBPB in 2 biological replicates tested by qRT-PCR. The expression of CEBPB was blocked by siRNA. The knockdown was tested after 24h and 48h of transfection. Expression values were normalized against the mean of two housekeeping genes (HK) DCTN2 and GAPDH. CEBPB mRNA levels were up to 40% reduced compared to scrambled control treatments (blue columns). Simultaneously CCND1 expressions were on average increased by 1.8-fold (red columns)

3.3.8 Verification of miR-155 targets by luciferase sensor assays

Luciferase sensors were generated in order to confirm potential miR-155 targets in HEK293T cells identified by RIP-Seq. Luciferase sensors were cloned for *DUSP14*, *MAP3K14* *PHC2* and *CEBPB* and were either co-transfected with empty or miR-155 containing

vectors. The *firefly* luciferase signals were normalized to corresponding *renilla* luciferase signals. The analyses were performed in three separate replicates. The luciferase signals for all putative miR-155 targets tested were decreased upon miR-155 co-transfection (Figure 3-25). The luciferase sensor for *CEBPB* showed the strongest effect with an approximately 40% decrease of the luciferase signal upon miR-155 expression. The sensors for *PHC2* and *MAP3K14* were significantly reduced by 10 to 15%. Even though the response for *DUSP14* was not significant the luciferase signal was on average reduced by ~10%.

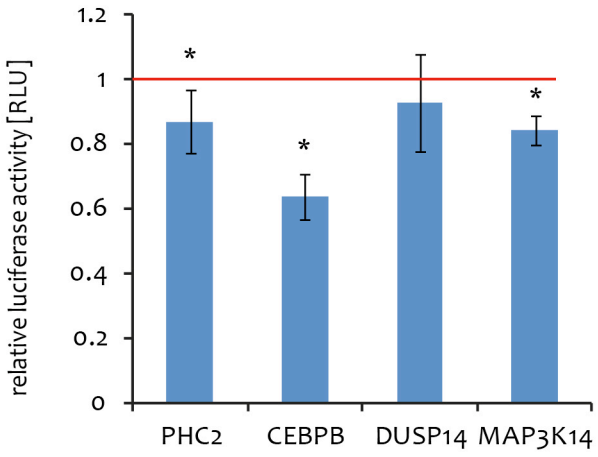

Figure 3-25: Luciferase sensor assays of potential miR-155 target genes in HEK293T as identified by RIP-Seq. Reference experiments co-transfecting the empty vector were set to 1 (red line). The relative levels of luciferase signals after co-transfection of miR-155 are shown (* $p<0.05$).

3.3.9 Verification of miR-155 targets by Western blot

Western blot analyses were performed to test changes on proteins identified as putative miR-155 in HEK293T cells by RIP-Seq. Briefly, HEK293T were transiently transfected with the miR-155 containing vector or the corresponding empty vector. 48 hours post-transfection the cells were harvested and proteins were isolated from three cellular sub fractions (cytoplasm, membranes/ organelles and nucleus). The protein fractions were tested for the putative miR-155 targets TCF4 and MAP3K14. Furthermore, SOCS1 was tested, since SOCS1 was previously published as miR-155 target in breast cancer [255]. Actin and LaminB were used as reference standard (Figure 3-26).

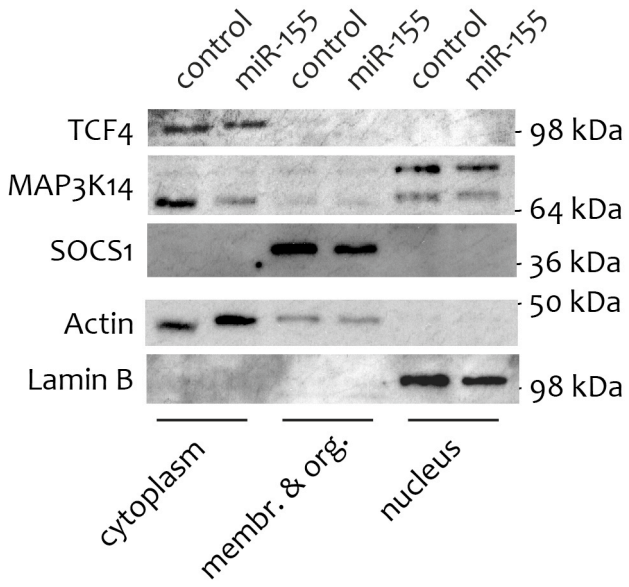

Figure 3-26: Western blot analysis of putative miR-155 targets in HEK293T identified by RIP-Seq. The proteins were separately isolated from cellular sub-fractions.

According to the results of the Western blots MAP3K14 protein levels were clearly reduced upon enforced miR-155 expression, reflecting the results of the luciferase sensors (Figure 3-25). The reduction of TCF4 and SOCS1 were less pronounced.

3.4 Identifying the microRNA targetome of MEC-1 and JEKO-1

It was the aim of the study to identify targets of aberrantly expressed miRNAs in CLL or MCL with potential pathomechanistic relevance. To this end RIP-Seq studies of the cell lines MEC-1 and JEKO-1 were performed, which represent CLL and MCL, respectively. A total of $4x10^8$ cells were used for the immunoprecipitation with either AGO2 specific or IgG1 isotype control antibodies in three biological replicates each. For RNA sequencing of the TL and IP fractions, Illumina TruSeq mRNA-Seq libraries were generated according to the manufacturer's instructions (refer to 2.2.8 and 2.2.9). Library generation of one of the three biological replicates of JEKO-1 was not successful and thus was not further processed. The 50bp reads were mapped against the human reference genome version 19 using the TopHat algorithm. RNA expression profiles of the total lysates or the enriched mRNAs in the IP fractions were calculated using the HTSeq-Count algorithm (refer to 2.1.14). The numbers of reads per sample are summarized in supplementary Table S 6. To test statistical significance, p-values were calculated among the replicates

using the DESeq algorithm (refer to 2.1.14). Figure 3-27 and Figure 3-28 display the significantly enriched transcripts of MEC-1 and JEKO-1.

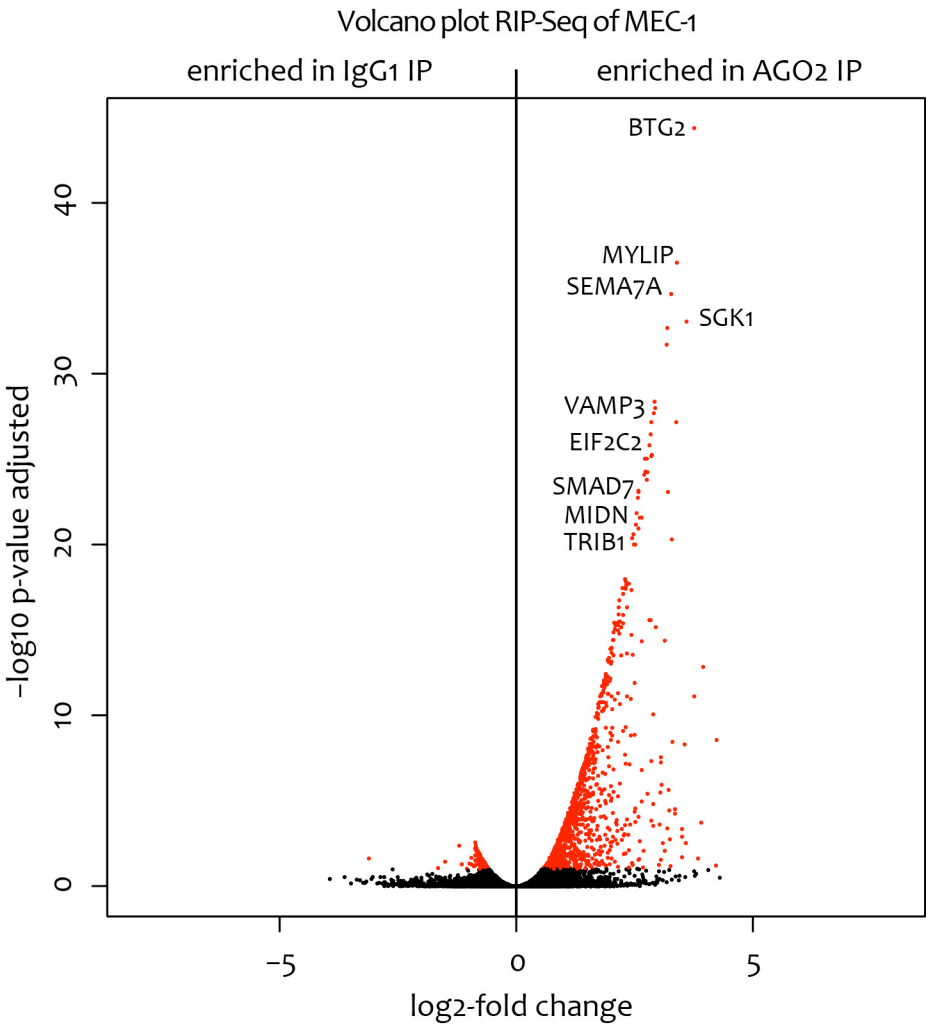

Figure 3-27: Volcano plot comparing the AGO2 IP fractions of MEC-1 against the IP using the IgG1 isotype control antibody. The red points indicate significantly enriched transcripts ($p<0.01$).

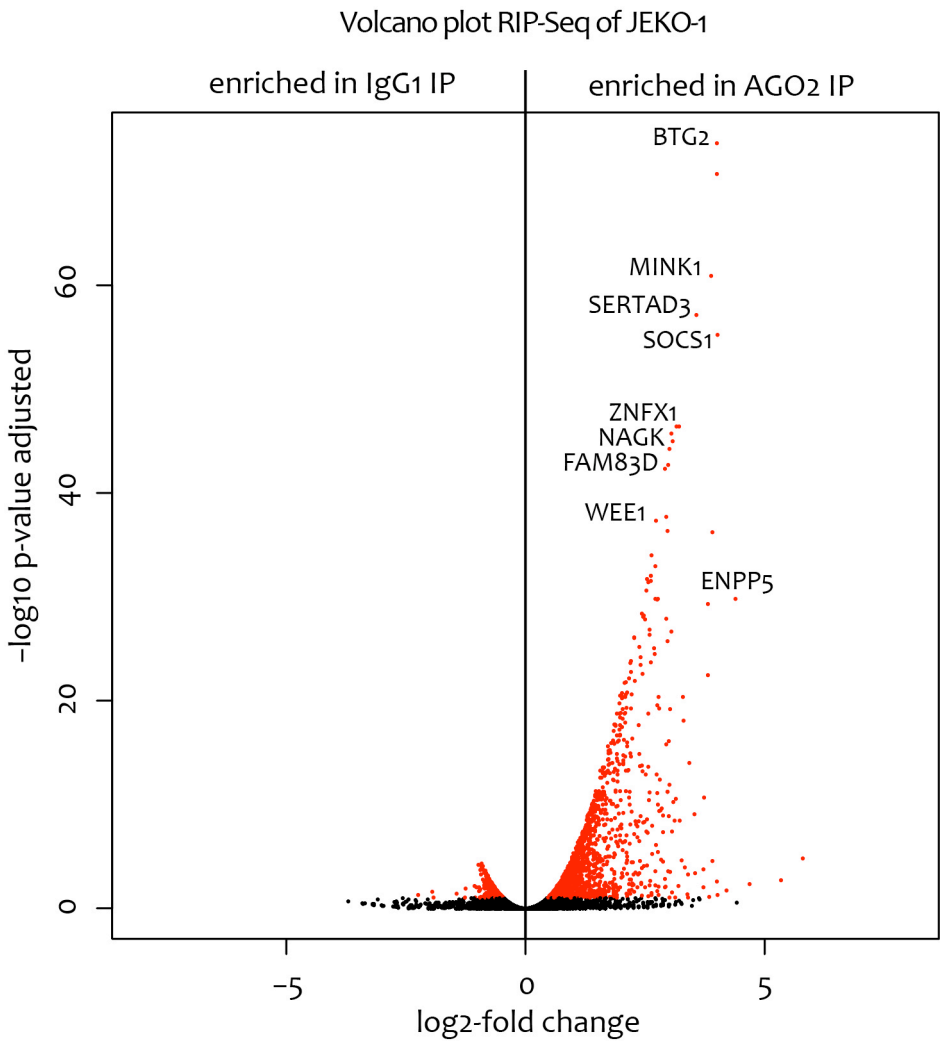

Figure 3-28: Volcano plot comparing the AGO2 IP fractions of JEKO-1 against the IP using the IgG1 isotype control antibody. The red dots indicate significantly enriched transcripts (p<0.01).

Log2-fold changes of AGO2 IP versus control IP were calculated and transcripts with a log2-fold change of at least 0.6 and a p-value of p<0.05 were considered as significantly over-represented in the AGO2 IP. In total, 1,096 and 1,379 mRNAs were significantly enriched in the AGO2 IP of MEC-1 and JEKO-1, respectively. Moreover, there was an overlap of 688 mRNAs in both cell lines, indicating a common set of miRNA-regulated transcripts. Among these, *BTG2* was detected as the most significantly enriched transcript in both IPs. Table 3-6 and Table 3-7 are summarizing the top ten enriched mRNAs of MEC-1 and JEKO-1.

Gene ID	Log2-fold change (AGO2 IP vs. IgG1 IP)	p-value
BTG2	3.757	4.38E-45
MYLIP	3.392	3.13E-37
SEMA7A	3.277	2.17E-35
SGK1	3.605	9.13E-34
ATG16L1	3.188	2.14E-33
EXD3	3.180	2.00E-32
SIAH1	2.926	4.31E-29
VAMP3	2.937	1.08E-28
GIGYF1	2.913	2.17E-28
C7orf43	3.382	6.98E-28

Table 3-6: Summary of the top 10 AGO2 associated mRNAs of MEC-1.

Gene ID	Log2-fold change (AGO2 IP vs. IgG1 IP)	p-value
BTG2	4.004	2.04E-74
S100A11	4.000	1.85E-71
MINK1	3.876	1.16E-61
SERTAD3	3.572	7.46E-58
SOCS1	4.019	5.68E-56
C7orf43	3.208	4.14E-47
ZNFX1	3.158	4.14E-47
MARCH9	3.052	1.89E-46
NAGK	3.074	1.04E-45
TBC1D20	3.012	5.37E-45

Table 3-7: Summary of the top 10 AGO2 associated mRNAs of JEKO-1.

Furthermore, putative miRNA targets in MEC-1 and JEKO-1 identified by RIP-Seq were screened for potential miRNA targets previously tested by qRT-PCR, luciferase sensor assays and Western blot analyses (refer to 3.2.2). Several of these, including *SGK1*, *SGK3*, *FBXW7*, *CCNT2*, *DOCK10*, *E2F2* and *RAB5C*, were tested as potential miRNA targets of miR-155, miR-19a and miR-92a-1. Notably, RAB5C was confirmed as miR-155 target by luciferase assays and Western blot analyses (refer to 3.2.2.3, 3.2.2.4 and 3.2.2.5).

3.5 Integration of targetome and miRNA data of MEC-1 and JEKO-1

MicroRNA expression and AGO2 IP enrichment profiles of JEKO-1 and MEC-1 were generated using the TaqMan array system from Applied Biosystems as described above.

In MEC-1, 203 and 159 miRNAs were detected in the IP and the TL fraction, respectively. In JEKO-1, 223 miRNAs were detected in the IP fraction and 157 miRNAs in the total lysate. The top 30 enriched miRNAs in the IPs of MEC-1 and JEKO-1 are summarized in Table 3-8 and Table 3-9. According to this 23 miRNAs including miR-155, miR-17, miR-18a, miR-19b, miR-20a and miR-92a-1 were common to the top 30 ranked microRNAs of both cell lines.

miRNA	Relative Δct–value to median	Number of prediction hits	miRNA	Relative Δct–value to median	Number of prediction hits
miR-106a	0.492	510	miR-21	0.660	167
miR-155	0.498	144	let-7e	0.667	237
miR-17	0.508	211	miR-142-3p	0.668	211
miR-20a	0.524	39	miR-106b	0.673	424
miR-92a-1	0.532	242	miR-16	0.675	323
miR-19b	0.534	304	miR-484	0.681	289
miR-146a	0.536	209	miR-365	0.682	198
miR-191	0.585	61	miR-15b	0.683	317
miR-222	0.615	192	miR-25	0.692	290
miR-342	0.621	273	miR-24	0.694	277
miR-30b	0.622	282	miR-18a	0.702	132
miR-193b	0.624	226	miR-320	0.715	364
miR-30c	0.624	282	let-7d	0.721	263
miR-20b	0.650	499	miR-29a	0.732	263
miR-150	0.652	356	miR-223	0.736	192

Table 3-8: Summary of the top 30 miRNAs enriched in the IP fraction of MEC-1. The relative Δct-value indicates the abundance of the respective miRNA relative to the median of all expressed miRNAs of the sample. The lower the value the higher is the abundance of the miRNA. The count of prediction hits indicates the total number mRNAs that were enriched in the respective IP and contain a predicted binding site for this miRNA.

Out of the 1,096 mRNAs that were enriched by AGO2 IP of MEC-1 cells (refer to 3.4), 928 were predicted to bind to at least one of the top 30 enriched miRNAs. On average approximately 7 miRNAs were predicted to be associated per enriched mRNA. Furthermore, every miRNA of the top 30 candidates had an average prediction hit count of 266.5 mRNAs.

miRNA	Relative Δct-value to median	Number of prediction hits	miRNA	Relative Δct-value to median	Number of prediction hits
miR-106a	0.433	592	miR-106b	0.652	499
miR-20a	0.440	44	miR-25	0.653	337
miR-17	0.440	259	let-7e	0.656	256
miR-92a-1	0.441	289	miR-342-3p	0.666	307
miR-19b	0.458	349	miR-15b	0.674	393
miR-20b	0.598	578	miR-142-3p	0.691	177
miR-484	0.605	362	miR-26a	0.699	313
miR-146a	0.609	241	miR-24	0.712	322
miR-193b	0.611	278	miR-19a	0.713	328
miR-155	0.611	118	miR-345	0.714	236
miR-30c	0.615	285	miR-339-5p	0.717	282
miR-18a	0.623	152	let-7a	0.718	241
miR-30b	0.625	285	miR-365	0.719	178
miR-191	0.634	63	let-7d	0.721	276
miR-16	0.642	395	let-7b	0.728	242

Table 3-9: Summary of the top 30 miRNAs enriched in the IP fraction of JEKO-1. The relative Δct-value indicates the abundance of the respective miRNA relative to the median of all expressed miRNAs of the sample. The lower the value the higher is the abundance of the miRNA. The count of prediction hits indicates the total number mRNAs that were enriched in the respective IP and contain a predicted binding site for this miRNA

Out of the 1,379 mRNAs identified by RIP-Seq of JEKO-1 cells (refer to 3.4), 1,134 were predicted to bind to at least one of the top 30 expressed miRNAs. On average more than 6 miRNAs were predicted to be associated per enriched mRNA. The *TSC1* mRNA was present in the IP fractions of both cell lines and was predicted to be a target of 25 of the top 30 expressed miRNAs. As previously mentioned, *BTG2* was the most significantly enriched mRNA in both cell lines. The integration of miRNA and mRNA data revealed that among the top 30 miRNAs of MEC-1 and JEKO-1, 18 were predicted to bind to *BTG2* mRNA. These findings suggest a cooperative mode of action of miRNAs, where mRNAs are simultaneously regulated by numerous miRNAs.

3.6 Recurrent disproportional association of miRNAs with AGO2

MicroRNA profiles of IP and TL fractions of both cell lines were compared pairwise in order to identify potential discrepancies between the miRNA expression and its enrichment in the AGO2 IP, as previously identified in HEK293T cells. Therefore, ratios of

miRNA levels in the IP versus the TL fractions of each sample were calculated and a median value of these ratios was determined. MicroRNAs with ratios higher or lower than the single standard deviation of the median value were considered as disproportionally enriched or depleted in the IP fraction. In general, an enrichment of miRNAs in the IP fractions of MEC-1 and JEKO-1 was observed. Interestingly, the IP of JEKO-1 showed a disproportional enrichment of 16 miRNAs in the IP fraction. Moreover, 16 miRNAs were underrepresented in the IP compared to the TL fraction. For MEC-1, 18 miRNAs were over-proportionally enriched in the IP fraction and 17 miRNAs were underrepresented.

The miRNA profiles of the HEK293T RIP experiments (refer to 3.3.6) were compared with the data of the B-cell lines in order to identify recurrent disproportionally enriched miRNAs (Figure 3-29). Values higher than zero indicate an over-proportional residence of miRNAs in the IP fractions of the indicated cell lines and values lower than zero indicate miRNAs, which were relatively more present in the total lysates. Notably, three members of the miR-17-92 cluster and miR-155 were recurrently over-represented in the IPs. Since miR-155 was barely expressed in HEK-vector cells, the ratio between the IP and TL fraction could not be calculated in this case.

The majority of disproportionally enriched miRNAs in the IP fractions were among the most strongly expressed miRNAs, but there were also miRNAs with a below average expression level enriched in the IP, suggesting a miRNA-specific loading into RISC (data not shown).

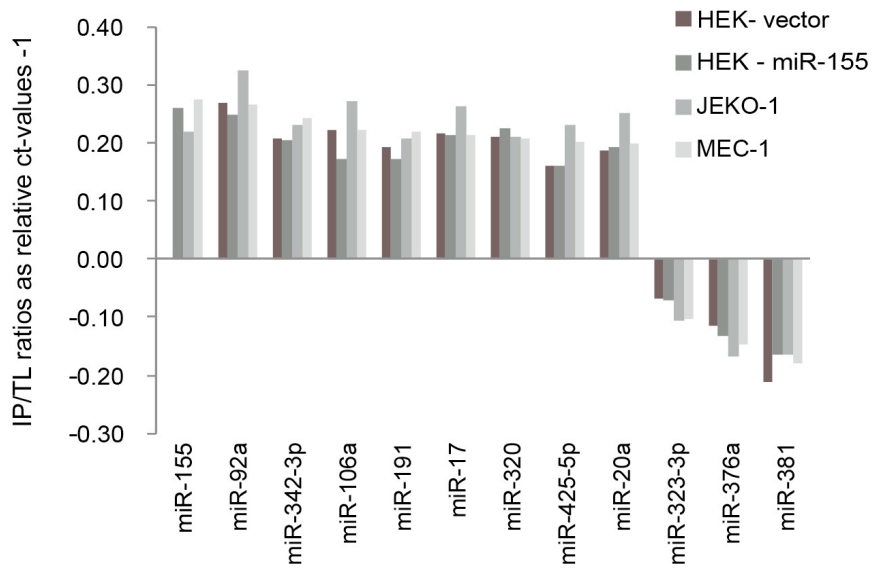

Figure 3-29: Summary of recurrent disproportionally detected miRNAs in the IP and TL fractions of HEK-vector, HEK-miR-155, JEKO-1 and MEC-1 cells. Values higher than zero indicate the over-proportional presence of the indicated miRNAs in the respective IP fractions. MicroRNAs that were underrepresented in the IPs are indicated by values lower than zero.

4 Discussion

4.1 RIP-Seq as an alternative tool for miRNA target identification

In 1993 the first microRNA *lin-4,* regulating the expression of the *lin-14* gene, was discovered in *C. elegans* [113,114]. From this point the class of single stranded small non-coding RNAs with a length of ~21 nt and a typical biogenesis patterns [112] was constantly increasing. Since miRNAs were predicted to regulate more than 30% of the human protein coding genes [167], one of the main focuses of research was the identification of target mRNAs. For this purpose methods like *in silico* target prediction, Northern blot analyses, qRT-PCR, luciferase sensor assays and Western blot analysis have been frequently used. However, all of these methods have their specific caveats including labor intensity and detection sensitivity.

4.1.1 Manipulation of intracellular miRNA levels

The artificial modification of miRNA levels is the pre-requisite for the observation of miRNA specific effects on gene expression. Specifically designed and commercially available miRNA precursor (pre-miRNAs) or miRNA blocking molecules (anti-miRNAs) are commonly used. Alternatively, expression constructs for over-expression or so called miRNA-sponges for their inhibition are options for miRNA manipulation [260]. In 2008, Sven Diederichs and colleagues could show that co-expression of AGO2 during siRNA-mediated silencing of genes enhanced the knockdown effect [261]. According to this, AGO proteins as the central part of the RISC might be one of the limiting factors for miRNA mediated gene regulation, as miRNAs and siRNAs are using the same machinery. Thus, the artificial alteration of miRNA expression, especially the over-expression by miRNA mimics or expression vectors, might alter the residence of endogenously expressed miRNA in the effector complexes, which probably leads to undesired secondary effects. Furthermore, the transfection of miRNA mimics or miRNA expression vectors might lead to an extremely high overexpression not resembling physiologic miRNA levels.

In the present study, miRNA mimics and anti-miRs for transient manipulation and custom-made miRNA expression vectors for stable over-expression of miRNAs were used. Global changes in miRNA expression and AGO2 association directly or indirectly caused by stable ectopic expression of miR-155 in HEK293T cells were monitored by miRNA specific TaqMan arrays. The results indicated that approximately 20% of all detected miRNAs were altered higher than the single standard deviation from the over all median upon ectopic miR-155 expression (refer to 3.3.6). Profiling of miRNAs associated to AGO2 revealed only minor differences within the group of the top 30 enriched miRNAs. 28 of the top 30 enriched miRNAs in HEK-miR-155 were shared by HEK-vector. As expected, miR-155 itself was one of the two differentially enriched miRNAs. Furthermore, four endogenously expressed miRNAs still showed a higher presence in AGO2 precipitates suggesting that the stable, artificial expression of miR-155 in HEK293T cells was at physiologic relevant level and that there was no depletion of endogenously expressed miRNAs from RISC complexes. However, the global miRNA expression was partly modified presumably as a secondary event.

4.1.2 Transcriptome-wide screening of potential miRNA targets

Expression arrays are commonly used to screen for miRNA target genes upon manipulation of miRNA levels. Potential target candidates are then usually confirmed by qRT-PCR. However, this approach is based on the assumption that all miRNA targets are degraded upon miRNA target binding of the RISC. Recent publications indicate, that indeed the majority of miRNAs targets are subsequently degraded [192,194,262]. However, there are exceptions. Willimott and Wagner for instance could show that miR-155 regulates the protein expression of BCL2 which contributes to an enhanced cell proliferation without affecting levels of the corresponding mRNA and thus cannot be detected by transcriptome analysis [254]. In general, miRNAs are thought to act as fine-tuning molecules causing mild changes on target mRNA expression [263]. It is thus feasible, that most target genes may not be identified by expression arrays, as the expected changes might be masked by the background noise of the arrays. In the first part of my study I tried to confirm putative miRNA targets by qRT-PCR (refer to 3.2.2.2). For the 33 potential target genes tested for miR-92a, miR-19a or miR-155 regulation, only mild, statistically not significant changes could be confirmed after miRNA overexpression

and knockdown simultaneously. This might be due in part to high variations in the transfection efficiencies of the B-cell line used for these experiments. However, analyzing these genes in the B-cell lines stably over-expressing the miRNAs of interest likewise resulted in mild effects without significance.

A second caveat of mRNA expression profiling for miRNA target identification is the lack of distinction between direct miRNA targets and secondary effects (later discussed in 4.1.4).

4.1.3 Identifying miRNA targets via protein analysis

Luciferase sensor assays are state of the art experiments to confirm miRNA-induced effects on protein level. These assays are labor intensive and not feasible for broad miRNA target screens, since they require the generation of individual luciferase sensor constructs for every putative miRNA target of interest. Additionally, luciferase signals showed strong fluctuations within replicates and therefore required many repetitions. Finally, putative miRNA binding sites need to be mutated to proof the functionality of this binding site.

In the present study luciferase sensors were generated for 19 genes to analyze their potential regulation by miR-19a, miR-92a or miR-155. Of these, eight showed a statistically robust reduction of the *firefly* luciferase signal after enforced expression of the respective miRNA. According to these analyses *RAB5C* and *RAB34* were identified as novel potential miR-155 targets. Control experiments with mutated miR-155 binding sites are planed. Subsequent Western blot analyses in B-cell lines with transient and stable expression of miR-155 revealed an approximately 5 to 10% reduction of RAB5C protein levels indicating that miR-155 acts as a fine-tuner for this protein. Indeed it was previously established, that miRNA mediated protein regulation generally results in a less than 2-fold protein reduction [264].

Stable isotope labeling of amino acids in cell culture (SILAC) is an alternative method to screen for miRNA targets on proteomic level using mass spectrometry [192,265,266]. However, like expression arrays, the SILAC approach does not distinguish primary targets from proteins altered as an indirect consequence of miRNA manipulation (later discussed in 4.1.4).

4.1.4 Identification of miR-155 targets in HEK293T cells using RIP-Seq

PAR-CLIP (photo-activatable-ribonucleoside-enhanced crosslinking and immunoprecipitation), HITS-CLIP (High-throughput sequencing of RNA isolated by crosslinking immunoprecipitation), RIP-Chip and RIP-Seq are recently described strategies to identify RNA-protein interactions. In contrast to the RIP technique, HITS-CLIP and PAR-CLIP rely on crosslinking of protein-RNA complexes using UV-light prior to RNA interacting protein immunoprecipitation [147,267,268,269]. By performing AGO 1-4 PAR-CLIP experiments, several thousand AGO-associated miRNA target genes were identified in HEK293T cells [147].

In the present study, the RIP-Seq method was established according to the protocol published by Keene and colleagues [269]. AGO2 protein was successfully immunoprecipitated and co-precipitated miRNAs and their target mRNAs were subsequently analyzed by 2nd generation sequencing. In order to proof the concept of this technique, HEK293T cells showing a poor endogenous miR-155 expression were stably transfected with either miR-155 (HEK-miR-155) or the corresponding empty vector (HEK-vector) to identify the miR-155 targetome. Comparing the mRNA profiles of the TL fractions revealed that the over-expression of miR-155 resulted in a deregulated expression of hundreds of genes. It is likely that several down-regulated mRNAs in the TL of HEK-miR-155 are predicted as miR-155 targets but might not be direct target genes of miR-155 (false positives). On the other hand genes that were increased upon over-expression of miR-155 might be co-precipitated by AGO2 IP due to binding of endogenous miRNAs as a secondary event. These could also be predicted as miR-155 targets and thus might be false positives as well. For instance, *CCND1* was highly enriched by AGO2 IP of HEK-miR-155. *In silico* analysis of the *CCND1* 3'UTR showed the presence of several putative miRNA-binding sites, including one for miR-155 suggesting that *CCND1* is a miR-155 target in these cells. Contradictory to that, the *CCND1* expression was also 18-fold increased in the TL fraction of HEK-miR-155. Thus, upon enforced miR-155 expression, *CCND1* might be stabilized by miR-155 explaining the enhanced presence and enrichment in TL and IP fractions of HEK-miR-155. However, stabilizing properties of miRNAs on target genes is a rarely described effect. Alternatively, the increased expression of *CCND1* could be an indirect event after miR-155 over-expression and the enrichment of *CCND1* mRNA in the IP of HEK-miR-155 cells was due to binding to endogenously expressed

miRNAs like miR-16, miR-106a and miR-92a. Indeed, *CCND1* was previously shown regulated by miRNAs like miR-15/16 and members of the miR-17-92 cluster, which are highly expressed in HEK293T cells [257,258]. In addition, *CCND1* was described being negatively regulated by *CEBPB,* a well-established miR-155 target [211,259] that was identified by RIP-Seq in this work as well. Knockdown experiments using *CEBPB*-specific siRNAs revealed increased *CCND1* levels, supporting this hypothesis. A recent study that screened for miR-155 targets by correlation of miRNA and mRNA expression profiles identified *CCND1* as a direct miR-155 target [270].

In order to compensate for secondary changes in RNA expression profiles upon miR-155 over-expression (e.g. *CCND1* up-regulation), the RNA levels in the IPs of both HEK293T cell lines were normalized to their respective TL fractions, assuming that primary miRNA targets are enriched in the IP and/or degraded in the TL fraction. Accordingly 100 transcripts, including 67 known and putative miR-155 targets, were identified ($p<0.01$, FDR 10%). Notably, of the 67 potential miR-155 targets only 9 (e.g. *BACH1* and *JARID2*) were identified by a significant ($p<0.05$) decay of mRNA in the TL fraction and only minor changes in the IP fractions. In addition, 20 potential miR-155 targets were identified by a strong enrichment in the IP of HEK239T pREP4miR-155 without significant ($p<0.05$) changes in the TL fraction (e.g. *PHC2* and *DUSP14*), suggesting that these were rather exclusively regulated by translational repression. Notably, one target gene, *ZFP36*, was simultaneously identified by significant enrichment in IP and decay in the TL fractions of HEK miR-155. The vast majority of putative miR-155 targets showed however a modest enrichment in the IP fraction and a simultaneous and modest degradation in the corresponding TL. Strikingly, according to the pSILAC database (psilac.mdc-berlin.de), PHC2 was identified as a miR-155 target on protein level, however the changes on mRNA levels were very weak with a log2-fold change of -0.04, supporting the present data [192].

Interestingly, *RAB34*, which was identified as a putative miR-155 target in MEC-1 cells using qRT-PCR and luciferase sensor assays, was also identified as a miR-155 target in HEK-miR-155 by RIP-Seq, supporting the assumption that *RAB34* is a true miR-155 target in HEK293T cells. Furthermore four miR-155 targets identified by RIP-Seq (*DUSP14*, *MAP3K14*, *PHC2* and *CEBPB*) could be confirmed by luciferase sensor assays and two miR-155 targets (TCF4 and MAP3K14) were confirmed by Western blot analyses.

Even though the RIP-Seq method offers many advantages for identifying miRNA targets, it has caveats as well. In comparison to the PAR-CLIP method, RIP-Seq cannot directly specify miRNA-mRNA interactions. Therefore, miRNA target prediction algorithms are necessary to evaluate the targetome of a specific miRNA. But since these prediction algorithms have high false negative and false positive rates, their usage is a drawback of this method. To overcome this problem, a highly stringent strategy was applied, where only those hits were considered as putative miRNA targets, which were predicted by at least three out of five tested prediction tools. This implicates, that some of the real miRNA targets were probably not detected from the analysis. Furthermore, the prediction algorithms used just screen the 3'UTR of putative target genes. But since it was shown that open reading frames (ORF) and 5'UTRs of transcripts contain also, to a lesser extent, miRNA target sites [271], these miRNA-mRNA interactions were missed by the applied method.

Taken together these data indicate that the over-expression of miR-155 alters the expression of hundreds of genes. Many of these were not enriched by RIP and are therefore not directly targeted by miR-155 in this cellular context, even though they contain predicted binding sites for this miRNA. Thus, RIP-Seq is a powerful screening tool to identify direct miRNA targets by combining data on mRNA degradation in TLs and on enrichment of mRNAs in IPs. Furthermore, this technique provides miRNA targets, which might be exclusively translationally inhibited upon miRNA binding.

4.1.5 Known and novel miR-155 targets related to cell proliferation

Phenotypic characterization of the established HEK-miR-155 cell line revealed an enhanced proliferation, as identified by two independent assay types. Interestingly, it was previously reported that miR-155 enhances proliferation of other cell types as well [254,255]. The presented RIP-Seq experiments identified several novel and known miR-155 targets (e.g. ZFP36, CEBPB and CTNND1) with a regulatory function in cellular proliferation. One of the most differentially enriched transcripts is the zinc finger protein ZFP36. This protein is a RNA destabilizing enzyme, recognizing AU-rich elements (ARE) within transcripts [272]. It is frequently decreased in human cancers with a negative prognostic indication for breast cancer. Overexpression of this gene in HeLa cells markedly reduced proliferation partly by limiting the expression of VEGF [273]. Strikingly,

ZFP36 was shown to directly influence the stability of *CCND1* mRNA, a well-known cancer related regulator of cell cycle [274,275]. A miR-155 mediated down regulation of ZFP36 might therefore contribute to the observed increase of *CCND1*. Further, as indicated in 4.1.4, CEBPB negatively regulates *CCND1* expression as well. It is feasible, that the increase of *CCND1*, caused by miR-155 mediated reduction of *CCND1* regulating factors, is in part responsible for the enhanced proliferation of HEK-miR-155. However, the effect of *ZFP36* on *CCND1* in HEK293T remains to be tested. Further, the preformed RIP-Seq experiments suggested a subsequent regulation of *CCND1* by endogenous miRNAs. It thus has to be addressed, if the increase of *CCND1* mRNA is reflected by an equal increase of cellular CCND1 protein.

Another highly enriched potential novel miR-155 target is CTNND1, a protein, which is directly regulated by trans-membrane proteins like E-cadherin [276]. In a study using human colon carcinoma cells, it was shown that CTNND1 overexpression was associated with a reduced cell cycle progression [277].

According to the Ingenuity database up to 10 known and novel miR-155 targets, which were identified by the present RIP-Seq experiments, are negatively associated with proliferation. It has to be addressed in future experiments whether the regulation of one of these genes or a combination of several of them (later discussed in 4.3) is responsible for the enhanced proliferation of HEK-miR-155 cells. In addition, it has to by clarified whether the observed phenotype is a long-term effect of miR-155 over-expression, since transient transfection of miR-155 in HEK293T cells did not show any increase in proliferation (data not shown).

4.2 The miRNA targetome of MEC-1 and JEKO-1

It was the primary aim of this study to identify novel transcripts regulated by miR-155 or the miR-17-92 cluster in order to delineate their potential role in chronic lymphocytic leukemia and mantle cell lymphoma. Established mouse models with aberrant miR-155 and miR-17-92 expression already pointed to a contribution of these miRNAs to the development of leukemic B-cells [216,218,219,230]. In the present study, RIP-Seq was used to identify genes regulated by miRNAs in the B cell lines MEC-1 and JEKO-1, including miR-155 and miR-17-92. Thereby, 1,096 AGO2-associated mRNAs were identified in MEC-1, including 144 potential miR-155 targets and 242 potential miR-92a-1 targets, as well as

1,379 potential miRNA target genes, including 118 and 289 potential targets for miR-155 and miR-92a, respectively in JEKO-1 cells. Of these, 688 potential miRNA targets were common to both cell lines. Comparing the RIP-Seq data with published PAR-CLIP results using lymphoblastoid B-cells [278] revealed an overlap of 609 and 607 miRNA targets to MEC-1 and JEKO-1 data, respectively. In general, it is assumed that 30% of the human genes are regulated by miRNAs [278]. PAR-CLIP experiments identified several thousand genes associated to one of the four AGO proteins [147]. For instance, the above mentioned PAR-CLIP study with lymphoblastoid B-cells identified approximately 3,500 miRNA target genes [278]. However, the obtained RIP-Seq data using JEKO-1 and MEC-1 identified roughly 1,000 miRNA targets per cell line. Since RIP-Seq does not include cross-linking of the AGO protein with the attached miRNA and mRNA, the sensitivity of this method might be lower, resulting in the identification of mainly highly regulated miRNA targets genes. PAR-CLIP that is based on cross-linking of protein and RNA, more likely also identifies less stable and more transient miRNA targets.
Finally, likewise to the findings of the RIP-Seq experiments in HEK293T cells (refer to 3.3.7), on average more than 6 miRNAs were predicted to regulate one of the enriched genes again indicating a cooperative regulation of single target genes by several miRNAs.

The *BTG2* mRNA was highly enriched by AGO2 IP in both B-cell lines showing the highest significance. Of the top 30 AGO2-associated miRNAs, 18 were predicted to regulate *BTG2*, including miR-92a-1 and miR-18a of the miR-17-92 cluster, miR-106a and miR-106b as homologues of the miR-17-92 cluster and miR-21, an experimentally verified regulator of *BTG2* [279]. *BTG2* has about 66% homology to *BTG1*, another member of this gene family, which was initially identified to be involved in a chromosomal translocation within a case of CLL [280]. Interestingly, *BTG2* expression was induced by a *TP53* dependent mechanism upon genotoxic stress. Further, the authors suggested, that *BTG2* is a novel tumor suppressor gene with anti-proliferative properties [281]. Years later, *BTG2* was shown involved in gene-specific histone H4 methylation and acetylation and thereby contributing to retinoic acid mediated differentiation of myeloid leukemia cells [282]. In the present work up to 18 of the 30 most highly expressed miRNAs in both leukemic B-cell lines tested were potential regulators of *BTG2*, indicating that this gene is tightly

regulated by miRNAs. A potential pathomechanistic role of *BTG2* in CLL or MCL might be an important aspect to test in future experiments.

Several potential miRNA targets identified by RIP-Seq in MEC-1 and JEKO-1 were previously tested as miR-155, miR-19a or miR-92a-1 targets using qRT-PCR, luciferase sensor assays and Western blot analyses. Of these transcripts, 8 and 11 were identified by RIP-Seq in JEKO-1 and MEC-1, respectively. Especially *FBXW7,* a known tumor suppressor gene [283] and *RAB5C* were down regulated in MCL and CLL patients and identified by RIP-Seq in leukemic B-cell lines. *FBXW7* was tested as potential miR-92a-1 target in MCL by qRT-PCR and luciferase sensor assays (refer to 3.2.2.2 and 3.2.2.3). As detected by qRT-PCR, transfection of pre-miR-92a-1 and anti-miR-92a-1 in MEC-1 cells slightly decreased or increased *FBXW7*, respectively. However, these findings were just a trend, which might be due to the already discussed fine-tuning properties of miRNAs. Surprisingly, luciferase sensor assays indicated a significant increase in FBXW7 expression upon enhanced miR-92a-1 levels. *FBXW7* was further identified as a target of 9 and 12 of the top 30 enriched miRNAs, including miR-92a-1, in JEKO-1 and MEC-1, respectively. Together these data suggest that *FBXW7* is a target of miR-92a-1.

Strikingly, qRT-PCR, luciferase sensor assays, Western blot analyses and RIP-Seq identified *RAB5C* as a miR-155 target in JEKO-1 and MEC-1 cells, suggesting a potential role of this gene in MCL and CLL. Of note, RAB5C protein levels were just rarely affected supporting the general notion that miRNAs are fine-tuners of target genes. RAB5C is a small GTPase of the RAS protein superfamily that shares 86% identity to RAB5A and RAB5B [284]. It was shown that RAB5C is a regulatory component for receptor endocytosis and endosome dynamics [285]. During zebrafish gastrulation, RAB5C was shown to be involved in WNT11 and E-cadherin mediated tissue morphogenesis [286]. Interestingly, RAB34 another GTPase down regulated in CLL patients, which is predicted as a miR-155 target and which was confirmed by luciferase sensor assays and RIP-Seq experiments of HEK-miR-155, was shown to cooperatively regulate macropinocytosis together with *RAB5* in a human epithelial colorectal adenocarcinoma cell line [287]. With respect to B-cells and leukemia the functions of *RAB5C* and *RAB34* were not characterized so far. However, since these proteins were shown involved in receptor internalization and endosome trafficking, potential abnormalities of these cellular functions in CLL and MCL might by interesting characteristics to test. For instance, alterations in B-cell receptor

endocytosis were described, which result in subsequent changes in the outcome of BCR receptor signaling [288].

The transcription factors *CEBPB* and *Pu.1* were among the first miR-155 targets identified in leukemic B-cells [211,216]. However, *CEBPB* was just identified in the IP of JEKO-1, but not MEC-1 cells. Conversely, *Pu.1* was exclusively AGO2 enriched in MEC-1 cells. Interestingly, as discussed in 4.1.5 *CEBPB* is a negative regulator of *CCND1*, which is highly over-expressed in and a hallmark of MCL. In line with this, the novel miR-155 target *ZFP36* (refer to 4.1.5), which is another negative regulator of *CCND1* [275], was identfied by RIP-Seq of JEKO-1 and MEC-1. Besides that, several other potential miR-155 targets related to proliferation (e.g. *CTNND1* and *RAPGEF2*) and identifed by RIP-Seq of HEK-miR-155, were highly enriched in the AGO2 IPs of both B-cell lines. In contrast, *SHIP1,* a well-known miR-155 target involved in myeloproliferative disorders [214] was not identified by RIP-Seq of JEKO-1 and MEC-1 cells, suggesting that this miR-155 targets plays an inferior role in the B-cell lines tested.

Interestingly, several components of the miRNA biogenesis pathway were also AGO2-associated in JEKO-1 and MEC-1. DICER1, a central factor facilitating miRNA maturation (refer to 1.6.1) was significantly enriched in the AGO2 IPs of both cell lines. Furthermore, the mRNA of *AGO2* itself was highly and significantly enriched in the IP of JEKO-1 and MEC-1, indicating that the miRNA biogenesis and activity is regulated in negative feedback loops as previously suggested by other groups [155,156,157].

To confirm the relevance of known and newly identified miRNA targets in B cell lymphomas, future RIP-Seq experiments using primary leukemic cells of CLL and MCL patients are planned. These studies will shed more light onto the role of miRNAs and their target genes in these cancer types.

4.3 MicroRNAs with limited regulatory abilities for single transcripts and severe phenotypic effects: a paradox?

The manipulation of miRNA levels in animal models has frequently resulted in severe phenotypes. For instance, mice lacking miR-155 show impaired immune responses, whereas mice over-expressing miR-155 exhibit perturbed peripheral blood cell populations [216,219]. Mice deficient for the miR-17-92 cluster die directly after birth, showing hypoplastic lungs and reduced amounts of pre-B-cells. Conversely, mice with enhanced expression of miR-17-92 in lymphocytes exhibit a lymphoproliferative phenotype coupled with autoimmunity and premature death [5,230]. These observations suggest miRNAs as important regulators that control normal development and homeostasis. Knowing this, it is astonishing that data from this study and also from other groups show that miRNAs have a very limited impact on the expression levels of their target mRNAs and proteins [264]. Indeed, miRNAs are believed to act as switches and fine-tuners of target genes with dependence on the mRNA expression levels [263]. In general, the interaction of a single miRNA with a single target mRNA might not explain the observed phenotypes. Rather the tightly coordinated regulation of many target genes as for instance suggested by Linsley and colleagues [289] and the mutual modulation and control of miRNAs and mRNAs [290], including feedback loops [291,292] (refer to 1.6.1), are responsible for keeping the balance, that prevents aberrant developments.

It was previously reported that single miRNAs or miRNA clusters act on several positions within a single signaling cascade or alternatively in functionally "redundant" pathways and thereby regulate a specific cellular phenotype [293]. Furthermore, *in silico* miRNA target predictions for the top 30 AGO2-assciated miRNAs were performed with the list of mRNAs enriched by RIP, in order to estimate the contribution of endogenously expressed miRNAs to the enrichment of the 100 putative miRNA target genes in HEK-miR-155 cells. This analysis revealed that on average more than 4 miRNAs have the potential to regulate one target gene. Single transcripts of these datasets were predicted to be regulated by up to 20 of the top 30 AGO2-associated miRNAs. Furthermore, similar results were obtained in RIP-Seq experiments with MEC-1 and JEKO-1 cells. These data support previously published findings of a cooperative miRNA activity on target genes [290]. It is

feasible that the regulation of one target gene by multiple miRNAs enhances the effects of miRNA mediated gene repression.

RNA-Seq and TaqMan arrays of HEK-vector and pREP4miR-155 cells identified changes in mRNA and miRNA profiles, presumably as a secondary event triggered by miR-155 over-expression. Approximately 20% of all miRNAs tested and more than 400 of approximately 10,000 quantified mRNAs were differentially expressed. For instance, *CCND1* or the *ETS* transcription factor sub-family *PEA3* (*ETV1*, *ETV4* and *ETV5*) were highly up regulated in HEK-miR-155 cells. *PEA3* genes *ETV4* and *ETV5* were shown involved in kidney development [294]. Furthermore, over-expression of *PEA3* gene family members was detected in several cancer entities and associated with cancer related features like proliferation and migration [295]. However, the causality of a miR-155 induced expression of *PEA3* genes was not known so far.

The observation that the over-expression of a single miRNA leads to secondary changes in the expression profiles of other miRNAs and mRNAs can be explained by the existence of a tightly controlled miRNA-mRNA interaction network, as previously proposed by other groups [290]. Deforming this network by ectopic expression of single miRNAs might result in and explain changes in cellular phenotypes. Furthermore, the miRNA biogenesis is a tightly regulated process as described in section 1.6. RIP-Seq of JEKO-1 and MEC-1 showed that several factors of the biogenesis pathway are regulated by miRNAs themselves in negative feedback loops. Recently, it was shown that pseudogenes and competing endogenous RNAs (ceRNA) are of relevance for modulating the activity of miRNAs within cells, suggesting their involvement in fine-tuning of the fine tuners [296,297].

4.4 Disproportional association of miRNAs to AGO2

Expression profiling of miRNAs is extensively used to screen for aberrations in miRNA properties, which might be of relevance in diseases like diabetes, tuberculosis, AIDS and cancer. Cancer related miRNAs were characterized as oncomiRNAs or tumor suppressors. For instance miR-21 and miR-155 were shown up regulated in lung cancers, breast cancers and leukemias [255,298,299,300,301]. Furthermore, miRNA expression profiles were used to predict tumor tissues of origin [302], outcome [303] and over-all survival [304].

In the presented work, miRNA specific TaqMan arrays were used to generate miRNA expression profiles of those cells tested by RIP-Seq. In addition, an activity profile of miRNAs was obtained simultaneously by quantifying miRNAs that co-IP with AGO2. The comparison of these two data sets allowed to investigate whether all miRNAs that are expressed in cells are equally frequent bound to AGO2 and therefore active. Interestingly, this comparison revealed that several miRNAs, including miR-155 and miR-17, were over-proportionally associated with AGO2. Strikingly, similar results were obtained with HEK293T cells and the two B cell lines, suggesting that among others, miR-155, miR-17, miR-20a and miR-92a-1 are recurrently over-represented in AGO2-containing complexes. Furthermore, these results are in line with a published study using embryonic and neuronal stem cells that identified disproportionally enriched miRNAs as well. Interestingly, miR-320, one of the over-proportionally enriched miRNAs in HEK293T, MEC-1 and JEKO-1 IPs, was also disproportionally enriched in their dataset [305].

However, even though TaqMan arrays were reported for being highly reproducible [306], additional technical replicates have to be performed to obtain robust statistics for the data, before firm conclusions can be drawn. Furthermore the mechanisms potentially leading to this observed effect are unknown so far.

Taken together these results indicate that miRNA expression profiles might not exactly reflect the actual miRNA activity.

4.5 Future directions

4.5.1 Improvement of the RIP-Seq method

Screening for miRNA targets in HEK293T, JEKO-1 and MEC-1 cells using the RIP-Seq method identified hundreds of protein coding genes presumably regulated by miRNAs. To analyze the co-precipitated RNAs after RIP, sequencing libraries were generated applying poly(A) enrichment in order to deplete ribosomal RNAs (rRNA). Since the vast majority of non-coding RNAs is not poly-adenylated, these fractions were not analyzed. However, recent publications suggest that non-coding RNAs are also regulated by miRNAs and then in turn might modulate miRNA activities on protein coding genes [296,297]. Thus, modifying the RIP-Seq protocol circumventing the poly(A)-enrichment would significantly improve this technique and allow for a more comprehensive analysis

of the interdependent miRNOME-targetome network. Using the RiboMinus kit from Invitrogen, in order to deplete the rRNA fraction from the total RNA prior to sequencing library generation, might be a suitable option for this purpose.

4.5.2 Functional relevant targets of miR-155 and miR-17-92 in CLL and MCL

MicroRNA-155 and the miR-17-92 cluster are well known in the context of leukemias and lymphomas (refer to 1.6.4 and 1.6.5) and several relevant target genes like *AID*, *SHIP1* or *SPI1* (*PU.1*) have been identified [212,214,216]. However, the identification of single miRNA targets so far just partly explained the molecular mechanism of how these miRNAs drive the development of leukemias and lymphomas. With regard to the results of this study and previous findings by others [290,293], miRNAs act in networks simultaneously regulating thousands of genes, suggesting that multiple miRNA-mRNA interactions are leading to phenotypic changes. RIP-Seq analysis of the B-cell lymphoma lines JEKO-1 and MEC-1 revealed more than hundred genes potentially regulated by miR-155 and the miR-17-92 cluster (e.g. *ZFP36*). In order to identify those targets with pathomechanistic relevance, the dataset needs to be extended to a cohort of patients to identify commonly regulated miRNA targets. Furthermore, the RIP-Seq experiments of the presented work suggested a cooperative activity of multiple miRNAs on single targets. Thus, the identification of such target genes that are cooperatively regulated by miRNAs (e.g. *BTG2*), especially if an association of these miRNAs with cancer was already described (e.g. miR-34a or miR-21), might lead to the discovery of genes with relevance in CLL or MCL.

4.5.3 Disproportional association of miRNAs with AGO2

In the present study, RIP-Seq experiments revealed a disproportional enrichment of miRNAs, including miR-155, miR-92a-1 and miR-320, in the AGO2 IP fractions. However, the lack of biological and technical replicates is a drawback so far. Interestingly, the general phenomenon was recurrently described by another group, identifying several miRNAs, including miR-320, as over-proportionally enriched in AGO2 precipitates [305]. Whether these findings are AGO2 specific or a general phenomenon for all human AGO proteins needs to be tested. However, data resulting from PAR-CLIP experiments so far suggested

no prevalent association of specific miRNAs to single AGO proteins, indicating that the disproportional loading could be a general feature [147].

The mechanism(s) responsible for these findings remain elusive. Feasible explanations are variations in AGO2-miRNA stabilities [307], different miRNA accessibilities due to sub-cellular distribution [308], miRNA specific AGO2 loading efficiencies or the differential expression of co-factors involved in miRNA loading processes.

Taken together these data indicate that the activity of certain miRNAs, which are over-proportionally associated with AGO2, is higher than suggested by their expression levels. It thus remains to be tested, whether these observations are *de facto* reflected by a higher impact of these miRNAs on the miRNA targetome and which molecular mechanisms are responsible for the disproportional residence of specific miRNA in AGO proteins.

5 References

1. Boyle P (2006) The globalisation of cancer. Lancet 368: 629-630.
2. Hanahan D, Weinberg RA (2000) The hallmarks of cancer. Cell 100: 57-70.
3. Gronych J, Korshunov A, Bageritz J, Milde T, Jugold M, *et al.* (2011) An activated mutant BRAF kinase domain is sufficient to induce pilocytic astrocytoma in mice. J Clin Invest 121: 1344-1348.
4. Jiang BH, Liu LZ (2009) PI3K/PTEN signaling in angiogenesis and tumorigenesis. Adv Cancer Res 102: 19-65.
5. Xiao C, Srinivasan L, Calado DP, Patterson HC, Zhang B, *et al.* (2008) Lymphoproliferative disease and autoimmunity in mice with increased miR-17-92 expression in lymphocytes. Nat Immunol 9: 405-414.
6. Yuan TL, Cantley LC (2008) PI3K pathway alterations in cancer: variations on a theme. Oncogene 27: 5497-5510.
7. Adams JM, Cory S (2007) The Bcl-2 apoptotic switch in cancer development and therapy. Oncogene 26: 1324-1337.
8. Calin GA, Dumitru CD, Shimizu M, Bichi R, Zupo S, *et al.* (2002) Frequent deletions and down-regulation of micro- RNA genes miR15 and miR16 at 13q14 in chronic lymphocytic leukemia. Proc Natl Acad Sci U S A 99: 15524-15529.
9. Blasco MA (2005) Telomeres and human disease: ageing, cancer and beyond. Nat Rev Genet 6: 611-622.
10. Carmeliet P (2005) VEGF as a key mediator of angiogenesis in cancer. Oncology 69 Suppl 3: 4-10.
11. Polyak K, Weinberg RA (2009) Transitions between epithelial and mesenchymal states: acquisition of malignant and stem cell traits. Nat Rev Cancer 9: 265-273.
12. Berx G, van Roy F (2009) Involvement of members of the cadherin superfamily in cancer. Cold Spring Harb Perspect Biol 1: a003129.
13. Hanahan D, Weinberg RA (2011) Hallmarks of cancer: the next generation. Cell 144: 646-674.
14. Negrini S, Gorgoulis VG, Halazonetis TD (2010) Genomic instability--an evolving hallmark of cancer. Nat Rev Mol Cell Biol 11: 220-228.
15. Miki Y, Swensen J, Shattuck-Eidens D, Futreal PA, Harshman K, *et al.* (1994) A strong candidate for the breast and ovarian cancer susceptibility gene BRCA1. Science 266: 66-71.
16. Wang B, Matsuoka S, Ballif BA, Zhang D, Smogorzewska A, *et al.* (2007) Abraxas and RAP80 form a BRCA1 protein complex required for the DNA damage response. Science 316: 1194-1198.
17. Artandi SE, DePinho RA (2010) Telomeres and telomerase in cancer. Carcinogenesis 31: 9-18.
18. Seiffert M, Schulz A, Ohl S, Dohner H, Stilgenbauer S, *et al.* (2010) Soluble CD14 is a novel monocyte-derived survival factor for chronic lymphocytic leukemia cells, which is induced by CLL cells in vitro and present at abnormally high levels in vivo. Blood 116: 4223-4230.
19. Schulz A, Toedt G, Zenz T, Stilgenbauer S, Lichter P, *et al.* (2011) Inflammatory cytokines and signaling pathways are associated with survival of primary chronic lymphocytic leukemia cells in vitro: a dominant role of CCL2. Haematologica 96: 408-416.
20. Grivennikov SI, Greten FR, Karin M (2010) Immunity, inflammation, and cancer. Cell 140: 883-899.
21. Warburg O (1956) On respiratory impairment in cancer cells. Science 124: 269-270.
22. Bonadonna G (2000) Historical review of Hodgkin's disease. Br J Haematol 110: 504-511.
23. Stansfeld AG, Diebold J, Noel H, Kapanci Y, Rilke F, *et al.* (1988) Updated Kiel classification for lymphomas. Lancet 1: 292-293.
24. (1982) National Cancer Institute sponsored study of classifications of non-Hodgkin's lymphomas: summary and description of a working formulation for clinical usage. The Non-Hodgkin's Lymphoma Pathologic Classification Project. Cancer 49: 2112-2135.
25. Sabattini E, Bacci F, Sagramoso C, Pileri SA (2010) WHO classification of tumours of haematopoietic and lymphoid tissues in 2008: an overview. Pathologica 102: 83-87.
26. Rajewsky K (1996) Clonal selection and learning in the antibody system. Nature 381: 751-758.
27. Kuppers R, Zhao M, Hansmann ML, Rajewsky K (1993) Tracing B cell development in human germinal centres by molecular analysis of single cells picked from histological sections. EMBO J 12: 4955-4967.

28. Liu YJ, Arpin C, de Bouteiller O, Guret C, Banchereau J, *et al.* (1996) Sequential triggering of apoptosis, somatic mutation and isotype switch during germinal center development. Semin Immunol 8: 169-177.
29. Kuppers R (2005) Mechanisms of B-cell lymphoma pathogenesis. Nat Rev Cancer 5: 251-262.
30. Kuppers R, Klein U, Hansmann ML, Rajewsky K (1999) Cellular origin of human B-cell lymphomas. N Engl J Med 341: 1520-1529.
31. Kuppers R, Dalla-Favera R (2001) Mechanisms of chromosomal translocations in B cell lymphomas. Oncogene 20: 5580-5594.
32. Tsujimoto Y, Louie E, Bashir MM, Croce CM (1988) The reciprocal partners of both the t(14; 18) and the t(11; 14) translocations involved in B-cell neoplasms are rearranged by the same mechanism. Oncogene 2: 347-351.
33. Goossens T, Klein U, Kuppers R (1998) Frequent occurrence of deletions and duplications during somatic hypermutation: implications for oncogene translocations and heavy chain disease. Proc Natl Acad Sci U S A 95: 2463-2468.
34. Papavasiliou FN, Schatz DG (2000) Cell-cycle-regulated DNA double-stranded breaks in somatic hypermutation of immunoglobulin genes. Nature 408: 216-221.
35. Gaidano G, Ballerini P, Gong JZ, Inghirami G, Neri A, *et al.* (1991) p53 mutations in human lymphoid malignancies: association with Burkitt lymphoma and chronic lymphocytic leukemia. Proc Natl Acad Sci U S A 88: 5413-5417.
36. Schaffner C, Stilgenbauer S, Rappold GA, Dohner H, Lichter P (1999) Somatic ATM mutations indicate a pathogenic role of ATM in B-cell chronic lymphocytic leukemia. Blood 94: 748-753.
37. Schaffner C, Idler I, Stilgenbauer S, Dohner H, Lichter P (2000) Mantle cell lymphoma is characterized by inactivation of the ATM gene. Proc Natl Acad Sci U S A 97: 2773-2778.
38. Stilgenbauer S, Schaffner C, Winkler D, Ott G, Leupolt E, *et al.* (2000) The ATM gene in the pathogenesis of mantle-cell lymphoma. Ann Oncol 11 Suppl 1: 127-130.
39. Gunven P, Klein G, Klein E, Norin T, Singh S (1980) Surface immunoglobulins on Burkitt's lymphoma biopsy cells from 91 patients. Int J Cancer 25: 711-719.
40. Sthoeger ZM, Wakai M, Tse DB, Vinciguerra VP, Allen SL, *et al.* (1989) Production of autoantibodies by CD5-expressing B lymphocytes from patients with chronic lymphocytic leukemia. J Exp Med 169: 255-268.
41. Dighiero G, Hart S, Lim A, Borche L, Levy R, *et al.* (1991) Autoantibody activity of immunoglobulins isolated from B-cell follicular lymphomas. Blood 78: 581-585.
42. Hussell T, Isaacson PG, Crabtree JE, Spencer J (1996) Helicobacter pylori-specific tumour-infiltrating T cells provide contact dependent help for the growth of malignant B cells in low-grade gastric lymphoma of mucosa-associated lymphoid tissue. J Pathol 178: 122-127.
43. Caldwell RG, Wilson JB, Anderson SJ, Longnecker R (1998) Epstein-Barr virus LMP2A drives B cell development and survival in the absence of normal B cell receptor signals. Immunity 9: 405-411.
44. Brauninger A, Spieker T, Mottok A, Baur AS, Kuppers R, *et al.* (2003) Epstein-Barr virus (EBV)-positive lymphoproliferations in post-transplant patients show immunoglobulin V gene mutation patterns suggesting interference of EBV with normal B cell differentiation processes. Eur J Immunol 33: 1593-1602.
45. Linnstaedt SD, Gottwein E, Skalsky RL, Luftig MA, Cullen BR (2010) Virally induced cellular microRNA miR-155 plays a key role in B-cell immortalization by Epstein-Barr virus. J Virol 84: 11670-11678.
46. Gatto G, Rossi A, Rossi D, Kroening S, Bonatti S, *et al.* (2008) Epstein-Barr virus latent membrane protein 1 trans-activates miR-155 transcription through the NF-kappaB pathway. Nucleic Acids Res 36: 6608-6619.
47. Lu F, Weidmer A, Liu CG, Volinia S, Croce CM, *et al.* (2008) Epstein-Barr virus-induced miR-155 attenuates NF-kappaB signaling and stabilizes latent virus persistence. J Virol 82: 10436-10443.
48. Johnson PW, Watt SM, Betts DR, Davies D, Jordan S, *et al.* (1993) Isolated follicular lymphoma cells are resistant to apoptosis and can be grown in vitro in the CD40/stromal cell system. Blood 82: 1848-1857.
49. Redaelli A, Laskin BL, Stephens JM, Botteman MF, Pashos CL (2004) The clinical and epidemiological burden of chronic lymphocytic leukaemia. Eur J Cancer Care (Engl) 13: 279-287.
50. Inamdar KV, Bueso-Ramos CE (2007) Pathology of chronic lymphocytic leukemia: an update. Ann Diagn Pathol 11: 363-389.
51. Hudson RP, Wilson SJ (1960) Hypogammaglobulinemia and chronic lymphatic leukemia. Cancer 13: 200-204.

52. Dameshek W, Schwartz RS (1959) Leukemia and auto-immunization- some possible relationships. Blood 14: 1151-1158.
53. Dighiero G, Charron D, Debre P, Le Porrier M, Vaugier G, *et al.* (1979) Identification of a pure splenic form of chronic lymphocytic leukaemia. Br J Haematol 41: 169-176.
54. Swerdlow SH, Zellner DC, Hurtubise PE, Kennealy J (1986) Pleural involvement in B-cell chronic lymphocytic leukemia associated with a T-cell-rich "reactive" pleural effusion. Am Rev Respir Dis 134: 172-174.
55. Rai KR, Sawitsky A, Cronkite EP, Chanana AD, Levy RN, *et al.* (1975) Clinical staging of chronic lymphocytic leukemia. Blood 46: 219-234.
56. Binet JL, Auquier A, Dighiero G, Chastang C, Piguet H, *et al.* (1981) A new prognostic classification of chronic lymphocytic leukemia derived from a multivariate survival analysis. Cancer 48: 198-206.
57. Hallek M, Cheson BD, Catovsky D, Caligaris-Cappio F, Dighiero G, *et al.* (2008) Guidelines for the diagnosis and treatment of chronic lymphocytic leukemia: a report from the International Workshop on Chronic Lymphocytic Leukemia updating the National Cancer Institute-Working Group 1996 guidelines. Blood 111: 5446-5456.
58. Damle RN, Wasil T, Fais F, Ghiotto F, Valetto A, *et al.* (1999) Ig V gene mutation status and CD38 expression as novel prognostic indicators in chronic lymphocytic leukemia. Blood 94: 1840-1847.
59. Rosenwald A, Alizadeh AA, Widhopf G, Simon R, Davis RE, *et al.* (2001) Relation of gene expression phenotype to immunoglobulin mutation genotype in B cell chronic lymphocytic leukemia. J Exp Med 194: 1639-1647.
60. Klein U, Tu Y, Stolovitzky GA, Mattioli M, Cattoretti G, *et al.* (2001) Gene expression profiling of B cell chronic lymphocytic leukemia reveals a homogeneous phenotype related to memory B cells. The Journal of experimental medicine 194: 1625-1638.
61. Lichter P, Cremer T, Borden J, Manuelidis L, Ward DC (1988) Delineation of individual human chromosomes in metaphase and interphase cells by in situ suppression hybridization using recombinant DNA libraries. Hum Genet 80: 224-234.
62. Dohner H, Stilgenbauer S, Benner A, Leupolt E, Krober A, *et al.* (2000) Genomic aberrations and survival in chronic lymphocytic leukemia. N Engl J Med 343: 1910-1916.
63. Schwaenen C, Nessling M, Wessendorf S, Salvi T, Wrobel G, *et al.* (2004) Automated array-based genomic profiling in chronic lymphocytic leukemia: development of a clinical tool and discovery of recurrent genomic alterations. Proc Natl Acad Sci U S A 101: 1039-1044.
64. Stilgenbauer S, Sander S, Bullinger L, Benner A, Leupolt E, *et al.* (2007) Clonal evolution in chronic lymphocytic leukemia: acquisition of high-risk genomic aberrations associated with unmutated VH, resistance to therapy, and short survival. Haematologica 92: 1242-1245.
65. Klein U, Lia M, Crespo M, Siegel R, Shen Q, *et al.* (2010) The DLEU2/miR-15a/16-1 cluster controls B cell proliferation and its deletion leads to chronic lymphocytic leukemia. Cancer Cell 17: 28-40.
66. Hallek M, Fischer K, Fingerle-Rowson G, Fink AM, Busch R, *et al.* (2010) Addition of rituximab to fludarabine and cyclophosphamide in patients with chronic lymphocytic leukaemia: a randomised, open-label, phase 3 trial. Lancet 376: 1164-1174.
67. Dohner H, Stilgenbauer S, James MR, Benner A, Weilguni T, *et al.* (1997) 11q deletions identify a new subset of B-cell chronic lymphocytic leukemia characterized by extensive nodal involvement and inferior prognosis. Blood 89: 2516-2522.
68. Austen B, Powell JE, Alvi A, Edwards I, Hooper L, *et al.* (2005) Mutations in the ATM gene lead to impaired overall and treatment-free survival that is independent of IGVH mutation status in patients with B-CLL. Blood 106: 3175-3182.
69. Zenz T, Mertens D, Kuppers R, Dohner H, Stilgenbauer S (2010) From pathogenesis to treatment of chronic lymphocytic leukaemia. Nat Rev Cancer 10: 37-50.
70. Schweighofer CD, Huh YO, Luthra R, Sargent RL, Ketterling RP, *et al.* (2011) The B cell antigen receptor in atypical chronic lymphocytic leukemia with t(14;19)(q32;q13) demonstrates remarkable stereotypy. Int J Cancer 128: 2759-2764.
71. Puente XS, Pinyol M, Quesada V, Conde L, Ordonez GR, *et al.* (2011) Whole-genome sequencing identifies recurrent mutations in chronic lymphocytic leukaemia. Nature 475: 101-105.
72. Fabbri G, Rasi S, Rossi D, Trifonov V, Khiabanian H, *et al.* (2011) Analysis of the chronic lymphocytic leukemia coding genome: role of NOTCH1 mutational activation. The Journal of experimental medicine 208: 1389-1401.
73. Korz C, Pscherer A, Benner A, Mertens D, Schaffner C, *et al.* (2002) Evidence for distinct pathomechanisms in B-cell chronic lymphocytic leukemia and mantle cell lymphoma by quantitative expression analysis of cell cycle and apoptosis-associated genes. Blood 99: 4554-4561.

74. Schmid C, Isaacson PG (1994) Proliferation centres in B-cell malignant lymphoma, lymphocytic (B-CLL): an immunophenotypic study. Histopathology 24: 445-451.
75. Seiffert M, Stilgenbauer S, Dohner H, Lichter P (2007) Efficient nucleofection of primary human B cells and B-CLL cells induces apoptosis, which depends on the microenvironment and on the structure of transfected nucleic acids. Leukemia 21: 1977-1983.
76. Munk Pedersen I, Reed J (2004) Microenvironmental interactions and survival of CLL B-cells. Leuk Lymphoma 45: 2365-2372.
77. Pedersen IM, Kitada S, Leoni LM, Zapata JM, Karras JG, *et al.* (2002) Protection of CLL B cells by a follicular dendritic cell line is dependent on induction of Mcl-1. Blood 100: 1795-1801.
78. Schena M, Larsson LG, Gottardi D, Gaidano G, Carlsson M, *et al.* (1992) Growth- and differentiation-associated expression of bcl-2 in B-chronic lymphocytic leukemia cells. Blood 79: 2981-2989.
79. Giles FJ, O'Brien SM, Keating MJ (1998) Chronic lymphocytic leukemia in (Richter's) transformation. Semin Oncol 25: 117-125.
80. Herrmann A, Hoster E, Zwingers T, Brittinger G, Engelhard M, *et al.* (2009) Improvement of overall survival in advanced stage mantle cell lymphoma. J Clin Oncol 27: 511-518.
81. Rosenwald A, Wright G, Wiestner A, Chan WC, Connors JM, *et al.* (2003) The proliferation gene expression signature is a quantitative integrator of oncogenic events that predicts survival in mantle cell lymphoma. Cancer Cell 3: 185-197.
82. Campo E, Raffeld M, Jaffe ES (1999) Mantle-cell lymphoma. Semin Hematol 36: 115-127.
83. Bosch F, Lopez-Guillermo A, Campo E, Ribera JM, Conde E, *et al.* (1998) Mantle cell lymphoma: presenting features, response to therapy, and prognostic factors. Cancer 82: 567-575.
84. Kienle D, Krober A, Katzenberger T, Ott G, Leupolt E, *et al.* (2003) VH mutation status and VDJ rearrangement structure in mantle cell lymphoma: correlation with genomic aberrations, clinical characteristics, and outcome. Blood 102: 3003-3009.
85. Jares P, Colomer D, Campo E (2007) Genetic and molecular pathogenesis of mantle cell lymphoma: perspectives for new targeted therapeutics. Nat Rev Cancer 7: 750-762.
86. Bea S, Ribas M, Hernandez JM, Bosch F, Pinyol M, *et al.* (1999) Increased number of chromosomal imbalances and high-level DNA amplifications in mantle cell lymphoma are associated with blastoid variants. Blood 93: 4365-4374.
87. Kohlhammer H, Schwaenen C, Wessendorf S, Holzmann K, Kestler HA, *et al.* (2004) Genomic DNA-chip hybridization in t(11;14)-positive mantle cell lymphomas shows a high frequency of aberrations and allows a refined characterization of consensus regions. Blood 104: 795-801.
88. Sander S, Bullinger L, Leupolt E, Benner A, Kienle D, *et al.* (2008) Genomic aberrations in mantle cell lymphoma detected by interphase fluorescence in situ hybridization. Incidence and clinicopathological correlations. Haematologica 93: 680-687.
89. Salaverria I, Zettl A, Bea S, Moreno V, Valls J, *et al.* (2007) Specific secondary genetic alterations in mantle cell lymphoma provide prognostic information independent of the gene expression-based proliferation signature. J Clin Oncol 25: 1216-1222.
90. Pinyol M, Hernandez L, Cazorla M, Balbin M, Jares P, *et al.* (1997) Deletions and loss of expression of p16INK4a and p21Waf1 genes are associated with aggressive variants of mantle cell lymphomas. Blood 89: 272-280.
91. Hernandez L, Bea S, Pinyol M, Ott G, Katzenberger T, *et al.* (2005) CDK4 and MDM2 gene alterations mainly occur in highly proliferative and aggressive mantle cell lymphomas with wild-type INK4a/ARF locus. Cancer Res 65: 2199-2206.
92. Au WY, Horsman DE, Viswanatha DS, Connors JM, Klasa RJ, *et al.* (2000) 8q24 translocations in blastic transformation of mantle cell lymphoma. Haematologica 85: 1225-1227.
93. Tagawa H, Karnan S, Suzuki R, Matsuo K, Zhang X, *et al.* (2005) Genome-wide array-based CGH for mantle cell lymphoma: identification of homozygous deletions of the proapoptotic gene BIM. Oncogene 24: 1348-1358.
94. Rudelius M, Pittaluga S, Nishizuka S, Pham TH, Fend F, *et al.* (2006) Constitutive activation of Akt contributes to the pathogenesis and survival of mantle cell lymphoma. Blood 108: 1668-1676.
95. Rizzatti EG, Falcao RP, Panepucci RA, Proto-Siqueira R, Anselmo-Lima WT, *et al.* (2005) Gene expression profiling of mantle cell lymphoma cells reveals aberrant expression of genes from the PI3K-AKT, WNT and TGFbeta signalling pathways. Br J Haematol 130: 516-526.
96. Lander ES, Linton LM, Birren B, Nusbaum C, Zody MC, *et al.* (2001) Initial sequencing and analysis of the human genome. Nature 409: 860-921.
97. Venter JC, Adams MD, Myers EW, Li PW, Mural RJ, *et al.* (2001) The sequence of the human genome. Science 291: 1304-1351.

98. Clamp M, Fry B, Kamal M, Xie X, Cuff J, *et al.* (2007) Distinguishing protein-coding and noncoding genes in the human genome. Proc Natl Acad Sci U S A 104: 19428-19433.
99. Siepel A, Bejerano G, Pedersen JS, Hinrichs AS, Hou M, *et al.* (2005) Evolutionarily conserved elements in vertebrate, insect, worm, and yeast genomes. Genome Res 15: 1034-1050.
100. Lander ES (2011) Initial impact of the sequencing of the human genome. Nature 470: 187-197.
101. Carmell MA, Girard A, van de Kant HJ, Bourc'his D, Bestor TH, *et al.* (2007) MIWI2 is essential for spermatogenesis and repression of transposons in the mouse male germline. Dev Cell 12: 503-514.
102. Kuramochi-Miyagawa S, Watanabe T, Gotoh K, Totoki Y, Toyoda A, *et al.* (2008) DNA methylation of retrotransposon genes is regulated by Piwi family members MILI and MIWI2 in murine fetal testes. Genes Dev 22: 908-917.
103. Watanabe T, Totoki Y, Toyoda A, Kaneda M, Kuramochi-Miyagawa S, *et al.* (2008) Endogenous siRNAs from naturally formed dsRNAs regulate transcripts in mouse oocytes. Nature 453: 539-543.
104. Tam OH, Aravin AA, Stein P, Girard A, Murchison EP, *et al.* (2008) Pseudogene-derived small interfering RNAs regulate gene expression in mouse oocytes. Nature 453: 534-538.
105. Orom UA, Derrien T, Beringer M, Gumireddy K, Gardini A, *et al.* (2010) Long noncoding RNAs with enhancer-like function in human cells. Cell 143: 46-58.
106. Kim TK, Hemberg M, Gray JM, Costa AM, Bear DM, *et al.* (2010) Widespread transcription at neuronal activity-regulated enhancers. Nature 465: 182-187.
107. Bertone P, Stolc V, Royce TE, Rozowsky JS, Urban AE, *et al.* (2004) Global identification of human transcribed sequences with genome tiling arrays. Science 306: 2242-2246.
108. Guttman M, Amit I, Garber M, French C, Lin MF, *et al.* (2009) Chromatin signature reveals over a thousand highly conserved large non-coding RNAs in mammals. Nature 458: 223-227.
109. Sotomaru Y, Katsuzawa Y, Hatada I, Obata Y, Sasaki H, *et al.* (2002) Unregulated expression of the imprinted genes H19 and Igf2r in mouse uniparental fetuses. J Biol Chem 277: 12474-12478.
110. Brown CJ, Ballabio A, Rupert JL, Lafreniere RG, Grompe M, *et al.* (1991) A gene from the region of the human X inactivation centre is expressed exclusively from the inactive X chromosome. Nature 349: 38-44.
111. Rinn JL, Kertesz M, Wang JK, Squazzo SL, Xu X, *et al.* (2007) Functional demarcation of active and silent chromatin domains in human HOX loci by noncoding RNAs. Cell 129: 1311-1323.
112. Bartel DP (2004) MicroRNAs: genomics, biogenesis, mechanism, and function. Cell 116: 281-297.
113. Wightman B, Ha I, Ruvkun G (1993) Posttranscriptional regulation of the heterochronic gene lin-14 by lin-4 mediates temporal pattern formation in C. elegans. Cell 75: 855-862.
114. Lee RC, Feinbaum RL, Ambros V (1993) The C. elegans heterochronic gene lin-4 encodes small RNAs with antisense complementarity to lin-14. Cell 75: 843-854.
115. Lagos-Quintana M, Rauhut R, Lendeckel W, Tuschl T (2001) Identification of novel genes coding for small expressed RNAs. Science 294: 853-858.
116. Lau NC, Lim LP, Weinstein EG, Bartel DP (2001) An abundant class of tiny RNAs with probable regulatory roles in Caenorhabditis elegans. Science 294: 858-862.
117. Lee RC, Ambros V (2001) An extensive class of small RNAs in Caenorhabditis elegans. Science 294: 862-864.
118. Ruvkun G (2001) Molecular biology. Glimpses of a tiny RNA world. Science 294: 797-799.
119. Tam W (2001) Identification and characterization of human BIC, a gene on chromosome 21 that encodes a noncoding RNA. Gene 274: 157-167.
120. Tanzer A, Stadler PF (2004) Molecular evolution of a microRNA cluster. J Mol Biol 339: 327-335.
121. Lee Y, Jeon K, Lee JT, Kim S, Kim VN (2002) MicroRNA maturation: stepwise processing and subcellular localization. EMBO J 21: 4663-4670.
122. He L, Thomson JM, Hemann MT, Hernando-Monge E, Mu D, *et al.* (2005) A microRNA polycistron as a potential human oncogene. Nature 435: 828-833.
123. Lee Y, Kim M, Han J, Yeom KH, Lee S, *et al.* (2004) MicroRNA genes are transcribed by RNA polymerase II. EMBO J 23: 4051-4060.
124. Cai X, Hagedorn CH, Cullen BR (2004) Human microRNAs are processed from capped, polyadenylated transcripts that can also function as mRNAs. RNA 10: 1957-1966.
125. Borchert GM, Lanier W, Davidson BL (2006) RNA polymerase III transcribes human microRNAs. Nat Struct Mol Biol 13: 1097-1101.
126. Lee Y, Ahn C, Han J, Choi H, Kim J, *et al.* (2003) The nuclear RNase III Drosha initiates microRNA processing. Nature 425: 415-419.
127. Han J, Lee Y, Yeom KH, Kim YK, Jin H, *et al.* (2004) The Drosha-DGCR8 complex in primary microRNA processing. Genes Dev 18: 3016-3027.

128. Gregory RI, Yan KP, Amuthan G, Chendrimada T, Doratotaj B, *et al.* (2004) The Microprocessor complex mediates the genesis of microRNAs. Nature 432: 235-240.
129. Han J, Lee Y, Yeom KH, Nam JW, Heo I, *et al.* (2006) Molecular basis for the recognition of primary microRNAs by the Drosha-DGCR8 complex. Cell 125: 887-901.
130. Zeng Y, Cullen BR (2005) Efficient processing of primary microRNA hairpins by Drosha requires flanking nonstructured RNA sequences. J Biol Chem 280: 27595-27603.
131. Morlando M, Ballarino M, Gromak N, Pagano F, Bozzoni I, *et al.* (2008) Primary microRNA transcripts are processed co-transcriptionally. Nat Struct Mol Biol 15: 902-909.
132. Michlewski G, Guil S, Semple CA, Caceres JF (2008) Posttranscriptional regulation of miRNAs harboring conserved terminal loops. Mol Cell 32: 383-393.
133. Guil S, Caceres JF (2007) The multifunctional RNA-binding protein hnRNP A1 is required for processing of miR-18a. Nat Struct Mol Biol 14: 591-596.
134. Michlewski G, Caceres JF (2010) Antagonistic role of hnRNP A1 and KSRP in the regulation of let-7a biogenesis. Nat Struct Mol Biol 17: 1011-1018.
135. Trabucchi M, Briata P, Garcia-Mayoral M, Haase AD, Filipowicz W, *et al.* (2009) The RNA-binding protein KSRP promotes the biogenesis of a subset of microRNAs. Nature 459: 1010-1014.
136. Bohnsack MT, Czaplinski K, Gorlich D (2004) Exportin 5 is a RanGTP-dependent dsRNA-binding protein that mediates nuclear export of pre-miRNAs. RNA 10: 185-191.
137. Lund E, Guttinger S, Calado A, Dahlberg JE, Kutay U (2004) Nuclear export of microRNA precursors. Science 303: 95-98.
138. Zeng Y, Cullen BR (2004) Structural requirements for pre-microRNA binding and nuclear export by Exportin 5. Nucleic Acids Res 32: 4776-4785.
139. Hutvagner G, McLachlan J, Pasquinelli AE, Balint E, Tuschl T, *et al.* (2001) A cellular function for the RNA-interference enzyme Dicer in the maturation of the let-7 small temporal RNA. Science 293: 834-838.
140. Ketting RF, Fischer SE, Bernstein E, Sijen T, Hannon GJ, *et al.* (2001) Dicer functions in RNA interference and in synthesis of small RNA involved in developmental timing in C. elegans. Genes Dev 15: 2654-2659.
141. Bernstein E, Caudy AA, Hammond SM, Hannon GJ (2001) Role for a bidentate ribonuclease in the initiation step of RNA interference. Nature 409: 363-366.
142. Chendrimada TP, Gregory RI, Kumaraswamy E, Norman J, Cooch N, *et al.* (2005) TRBP recruits the Dicer complex to Ago2 for microRNA processing and gene silencing. Nature 436: 740-744.
143. Lee Y, Hur I, Park SY, Kim YK, Suh MR, *et al.* (2006) The role of PACT in the RNA silencing pathway. EMBO J 25: 522-532.
144. MacRae IJ, Ma E, Zhou M, Robinson CV, Doudna JA (2008) In vitro reconstitution of the human RISC-loading complex. Proc Natl Acad Sci U S A 105: 512-517.
145. Khvorova A, Reynolds A, Jayasena SD (2003) Functional siRNAs and miRNAs exhibit strand bias. Cell 115: 209-216.
146. Azuma-Mukai A, Oguri H, Mituyama T, Qian ZR, Asai K, *et al.* (2008) Characterization of endogenous human Argonautes and their miRNA partners in RNA silencing. Proc Natl Acad Sci U S A 105: 7964-7969.
147. Hafner M, Landthaler M, Burger L, Khorshid M, Hausser J, *et al.* (2010) Transcriptome-wide identification of RNA-binding protein and microRNA target sites by PAR-CLIP. Cell 141: 129-141.
148. Song JJ, Smith SK, Hannon GJ, Joshua-Tor L (2004) Crystal structure of Argonaute and its implications for RISC slicer activity. Science 305: 1434-1437.
149. Berezikov E, Chung WJ, Willis J, Cuppen E, Lai EC (2007) Mammalian mirtron genes. Mol Cell 28: 328-336.
150. Ruby JG, Jan CH, Bartel DP (2007) Intronic microRNA precursors that bypass Drosha processing. Nature 448: 83-86.
151. Landgraf P, Rusu M, Sheridan R, Sewer A, Iovino N, *et al.* (2007) A mammalian microRNA expression atlas based on small RNA library sequencing. Cell 129: 1401-1414.
152. Weber B, Stresemann C, Brueckner B, Lyko F (2007) Methylation of human microRNA genes in normal and neoplastic cells. Cell Cycle 6: 1001-1005.
153. Davis BN, Hilyard AC, Lagna G, Hata A (2008) SMAD proteins control DROSHA-mediated microRNA maturation. Nature 454: 56-61.
154. Han J, Pedersen JS, Kwon SC, Belair CD, Kim YK, *et al.* (2009) Posttranscriptional crossregulation between Drosha and DGCR8. Cell 136: 75-84.
155. Yeom KH, Lee Y, Han J, Suh MR, Kim VN (2006) Characterization of DGCR8/Pasha, the essential cofactor for Drosha in primary miRNA processing. Nucleic Acids Res 34: 4622-4629.

156. Tokumaru S, Suzuki M, Yamada H, Nagino M, Takahashi T (2008) let-7 regulates Dicer expression and constitutes a negative feedback loop. Carcinogenesis 29: 2073-2077.
157. Kovaleva V, Mora R, Park YJ, Plass C, Chiramel A, *et al.* (2012) MicroRNA-130a targets ATG2B and DICER1 to inhibit autophagy and trigger killing of chronic lymphocytic leukemia cells. Cancer research.
158. Viswanathan SR, Daley GQ, Gregory RI (2008) Selective blockade of microRNA processing by Lin28. Science 320: 97-100.
159. Heo I, Joo C, Cho J, Ha M, Han J, *et al.* (2008) Lin28 mediates the terminal uridylation of let-7 precursor MicroRNA. Mol Cell 32: 276-284.
160. Rybak A, Fuchs H, Smirnova L, Brandt C, Pohl EE, *et al.* (2008) A feedback loop comprising lin-28 and let-7 controls pre-let-7 maturation during neural stem-cell commitment. Nat Cell Biol 10: 987-993.
161. Diederichs S, Haber DA (2007) Dual role for argonautes in microRNA processing and posttranscriptional regulation of microRNA expression. Cell 131: 1097-1108.
162. Scadden AD (2005) The RISC subunit Tudor-SN binds to hyper-edited double-stranded RNA and promotes its cleavage. Nat Struct Mol Biol 12: 489-496.
163. Kawahara Y, Megraw M, Kreider E, Iizasa H, Valente L, *et al.* (2008) Frequency and fate of microRNA editing in human brain. Nucleic Acids Res 36: 5270-5280.
164. Ramachandran V, Chen X (2008) Degradation of microRNAs by a family of exoribonucleases in Arabidopsis. Science 321: 1490-1492.
165. Kennedy S, Wang D, Ruvkun G (2004) A conserved siRNA-degrading RNase negatively regulates RNA interference in C. elegans. Nature 427: 645-649.
166. Kim YK, Heo I, Kim VN (2010) Modifications of small RNAs and their associated proteins. Cell 143: 703-709.
167. Lewis BP, Burge CB, Bartel DP (2005) Conserved seed pairing, often flanked by adenosines, indicates that thousands of human genes are microRNA targets. Cell 120: 15-20.
168. Bartel DP (2009) MicroRNAs: target recognition and regulatory functions. Cell 136: 215-233.
169. Doench JG, Sharp PA (2004) Specificity of microRNA target selection in translational repression. Genes Dev 18: 504-511.
170. Grimson A, Farh KK, Johnston WK, Garrett-Engele P, Lim LP, *et al.* (2007) MicroRNA targeting specificity in mammals: determinants beyond seed pairing. Mol Cell 27: 91-105.
171. Nelson PT, Wang WX, Mao G, Wilfred BR, Xie K, *et al.* (2011) Specific sequence determinants of miR-15/107 microRNA gene group targets. Nucleic Acids Res.
172. Sandberg R, Neilson JR, Sarma A, Sharp PA, Burge CB (2008) Proliferating cells express mRNAs with shortened 3' untranslated regions and fewer microRNA target sites. Science 320: 1643-1647.
173. Hock J, Meister G (2008) The Argonaute protein family. Genome biology 9: 210.
174. Liu J, Carmell MA, Rivas FV, Marsden CG, Thomson JM, *et al.* (2004) Argonaute2 is the catalytic engine of mammalian RNAi. Science 305: 1437-1441.
175. Eulalio A, Helms S, Fritzsch C, Fauser M, Izaurralde E (2009) A C-terminal silencing domain in GW182 is essential for miRNA function. RNA 15: 1067-1077.
176. Zipprich JT, Bhattacharyya S, Mathys H, Filipowicz W (2009) Importance of the C-terminal domain of the human GW182 protein TNRC6C for translational repression. RNA 15: 781-793.
177. Lazzaretti D, Tournier I, Izaurralde E (2009) The C-terminal domains of human TNRC6A, TNRC6B, and TNRC6C silence bound transcripts independently of Argonaute proteins. RNA 15: 1059-1066.
178. Behm-Ansmant I, Rehwinkel J, Doerks T, Stark A, Bork P, *et al.* (2006) mRNA degradation by miRNAs and GW182 requires both CCR4:NOT deadenylase and DCP1:DCP2 decapping complexes. Genes Dev 20: 1885-1898.
179. Fabian MR, Cieplak MK, Frank F, Morita M, Green J, *et al.* (2011) miRNA-mediated deadenylation is orchestrated by GW182 through two conserved motifs that interact with CCR4-NOT. Nature structural & molecular biology 18: 1211-1217.
180. Chekulaeva M, Mathys H, Zipprich JT, Attig J, Colic M, *et al.* (2011) miRNA repression involves GW182-mediated recruitment of CCR4-NOT through conserved W-containing motifs. Nature structural & molecular biology 18: 1218-1226.
181. Filipowicz W, Bhattacharyya SN, Sonenberg N (2008) Mechanisms of post-transcriptional regulation by microRNAs: are the answers in sight? Nat Rev Genet 9: 102-114.
182. Pillai RS, Bhattacharyya SN, Artus CG, Zoller T, Cougot N, *et al.* (2005) Inhibition of translational initiation by Let-7 MicroRNA in human cells. Science 309: 1573-1576.
183. Kiriakidou M, Tan GS, Lamprinaki S, De Planell-Saguer M, Nelson PT, *et al.* (2007) An mRNA m7G cap binding-like motif within human Ago2 represses translation. Cell 129: 1141-1151.

184. Thermann R, Hentze MW (2007) Drosophila miR2 induces pseudo-polysomes and inhibits translation initiation. Nature 447: 875-878.
185. Mathonnet G, Fabian MR, Svitkin YV, Parsyan A, Huck L, *et al.* (2007) MicroRNA inhibition of translation initiation in vitro by targeting the cap-binding complex eIF4F. Science 317: 1764-1767.
186. Beilharz TH, Humphreys DT, Clancy JL, Thermann R, Martin DI, *et al.* (2009) microRNA-mediated messenger RNA deadenylation contributes to translational repression in mammalian cells. PLoS One 4: e6783.
187. Petersen CP, Bordeleau ME, Pelletier J, Sharp PA (2006) Short RNAs repress translation after initiation in mammalian cells. Mol Cell 21: 533-542.
188. Nottrott S, Simard MJ, Richter JD (2006) Human let-7a miRNA blocks protein production on actively translating polyribosomes. Nat Struct Mol Biol 13: 1108-1114.
189. Fabian MR, Mathonnet G, Sundermeier T, Mathys H, Zipprich JT, *et al.* (2009) Mammalian miRNA RISC recruits CAF1 and PABP to affect PABP-dependent deadenylation. Mol Cell 35: 868-880.
190. Eulalio A, Behm-Ansmant I, Izaurralde E (2007) P bodies: at the crossroads of post-transcriptional pathways. Nat Rev Mol Cell Biol 8: 9-22.
191. Parker R, Sheth U (2007) P bodies and the control of mRNA translation and degradation. Mol Cell 25: 635-646.
192. Selbach M, Schwanhausser B, Thierfelder N, Fang Z, Khanin R, *et al.* (2008) Widespread changes in protein synthesis induced by microRNAs. Nature 455: 58-63.
193. Hendrickson DG, Hogan DJ, McCullough HL, Myers JW, Herschlag D, *et al.* (2009) Concordant regulation of translation and mRNA abundance for hundreds of targets of a human microRNA. PLoS Biol 7: e1000238.
194. Guo H, Ingolia NT, Weissman JS, Bartel DP (2010) Mammalian microRNAs predominantly act to decrease target mRNA levels. Nature 466: 835-840.
195. Eiring AM, Harb JG, Neviani P, Garton C, Oaks JJ, *et al.* (2010) miR-328 functions as an RNA decoy to modulate hnRNP E2 regulation of mRNA translation in leukemic blasts. Cell 140: 652-665.
196. Calin GA, Liu CG, Sevignani C, Ferracin M, Felli N, *et al.* (2004) MicroRNA profiling reveals distinct signatures in B cell chronic lymphocytic leukemias. Proc Natl Acad Sci U S A 101: 11755-11760.
197. Calin GA, Sevignani C, Dumitru CD, Hyslop T, Noch E, *et al.* (2004) Human microRNA genes are frequently located at fragile sites and genomic regions involved in cancers. Proc Natl Acad Sci U S A 101: 2999-3004.
198. Cimmino A, Calin GA, Fabbri M, Iorio MV, Ferracin M, *et al.* (2005) miR-15 and miR-16 induce apoptosis by targeting BCL2. Proc Natl Acad Sci U S A 102: 13944-13949.
199. Saunders MA, Liang H, Li WH (2007) Human polymorphism at microRNAs and microRNA target sites. Proc Natl Acad Sci U S A 104: 3300-3305.
200. Ventura A, Jacks T (2009) MicroRNAs and cancer: short RNAs go a long way. Cell 136: 586-591.
201. Schetter AJ, Leung SY, Sohn JJ, Zanetti KA, Bowman ED, *et al.* (2008) MicroRNA expression profiles associated with prognosis and therapeutic outcome in colon adenocarcinoma. JAMA 299: 425-436.
202. Lawrie CH, Gal S, Dunlop HM, Pushkaran B, Liggins AP, *et al.* (2008) Detection of elevated levels of tumour-associated microRNAs in serum of patients with diffuse large B-cell lymphoma. Br J Haematol 141: 672-675.
203. Clurman BE, Hayward WS (1989) Multiple proto-oncogene activations in avian leukosis virus-induced lymphomas: evidence for stage-specific events. Mol Cell Biol 9: 2657-2664.
204. Tam W, Ben-Yehuda D, Hayward WS (1997) bic, a novel gene activated by proviral insertions in avian leukosis virus-induced lymphomas, is likely to function through its noncoding RNA. Mol Cell Biol 17: 1490-1502.
205. Eis PS, Tam W, Sun L, Chadburn A, Li Z, *et al.* (2005) Accumulation of miR-155 and BIC RNA in human B cell lymphomas. Proc Natl Acad Sci U S A 102: 3627-3632.
206. Kluiver J, Poppema S, de Jong D, Blokzijl T, Harms G, *et al.* (2005) BIC and miR-155 are highly expressed in Hodgkin, primary mediastinal and diffuse large B cell lymphomas. J Pathol 207: 243-249.
207. Kluiver J, Haralambieva E, de Jong D, Blokzijl T, Jacobs S, *et al.* (2006) Lack of BIC and microRNA miR-155 expression in primary cases of Burkitt lymphoma. Genes Chromosomes Cancer 45: 147-153.
208. Kluiver J, van den Berg A, de Jong D, Blokzijl T, Harms G, *et al.* (2007) Regulation of pri-microRNA BIC transcription and processing in Burkitt lymphoma. Oncogene 26: 3769-3776.
209. O'Connell RM, Taganov KD, Boldin MP, Cheng G, Baltimore D (2007) MicroRNA-155 is induced during the macrophage inflammatory response. Proc Natl Acad Sci U S A 104: 1604-1609.
210. Yin Q, Wang X, McBride J, Fewell C, Flemington E (2008) B-cell receptor activation induces BIC/miR-155 expression through a conserved AP-1 element. J Biol Chem 283: 2654-2662.

211. Yin Q, McBride J, Fewell C, Lacey M, Wang X, *et al.* (2008) MicroRNA-155 is an Epstein-Barr virus-induced gene that modulates Epstein-Barr virus-regulated gene expression pathways. J Virol 82: 5295-5306.
212. Dorsett Y, McBride KM, Jankovic M, Gazumyan A, Thai TH, *et al.* (2008) MicroRNA-155 suppresses activation-induced cytidine deaminase-mediated Myc-Igh translocation. Immunity 28: 630-638.
213. Gibcus JH, Tan LP, Harms G, Schakel RN, de Jong D, *et al.* (2009) Hodgkin lymphoma cell lines are characterized by a specific miRNA expression profile. Neoplasia 11: 167-176.
214. O'Connell RM, Chaudhuri AA, Rao DS, Baltimore D (2009) Inositol phosphatase SHIP1 is a primary target of miR-155. Proc Natl Acad Sci U S A 106: 7113-7118.
215. Tili E, Michaille JJ, Wernicke D, Alder H, Costinean S, *et al.* (2011) Mutator activity induced by microRNA-155 (miR-155) links inflammation and cancer. Proc Natl Acad Sci U S A 108: 4908-4913.
216. Vigorito E, Perks KL, Abreu-Goodger C, Bunting S, Xiang Z, *et al.* (2007) microRNA-155 regulates the generation of immunoglobulin class-switched plasma cells. Immunity 27: 847-859.
217. Louafi F, Martinez-Nunez RT, Sanchez-Elsner T (2010) MicroRNA-155 targets SMAD2 and modulates the response of macrophages to transforming growth factor-{beta}. J Biol Chem 285: 41328-41336.
218. Costinean S, Sandhu SK, Pedersen IM, Tili E, Trotta R, *et al.* (2009) Src homology 2 domain-containing inositol-5-phosphatase and CCAAT enhancer-binding protein beta are targeted by miR-155 in B cells of Emicro-MiR-155 transgenic mice. Blood 114: 1374-1382.
219. Costinean S, Zanesi N, Pekarsky Y, Tili E, Volinia S, *et al.* (2006) Pre-B cell proliferation and lymphoblastic leukemia/high-grade lymphoma in E(mu)-miR155 transgenic mice. Proceedings of the National Academy of Sciences of the United States of America 103: 7024-7029.
220. Ota A, Tagawa H, Karnan S, Tsuzuki S, Karpas A, *et al.* (2004) Identification and characterization of a novel gene, C13orf25, as a target for 13q31-q32 amplification in malignant lymphoma. Cancer Res 64: 3087-3095.
221. Wang M, Tan LP, Dijkstra MK, van Lom K, Robertus JL, *et al.* (2008) miRNA analysis in B-cell chronic lymphocytic leukaemia: proliferation centres characterized by low miR-150 and high BIC/miR-155 expression. J Pathol 215: 13-20.
222. Pichiorri F, Suh SS, Ladetto M, Kuehl M, Palumbo T, *et al.* (2008) MicroRNAs regulate critical genes associated with multiple myeloma pathogenesis. Proc Natl Acad Sci U S A 105: 12885-12890.
223. Ghosh AK, Shanafelt TD, Cimmino A, Taccioli C, Volinia S, *et al.* (2009) Aberrant regulation of pVHL levels by microRNA promotes the HIF/VEGF axis in CLL B cells. Blood 113: 5568-5574.
224. Liu WH, Yeh SH, Lu CC, Yu SL, Chen HY, *et al.* (2009) MicroRNA-18a prevents estrogen receptor-alpha expression, promoting proliferation of hepatocellular carcinoma cells. Gastroenterology 136: 683-693.
225. Navarro A, Marrades RM, Vinolas N, Quera A, Agusti C, *et al.* (2009) MicroRNAs expressed during lung cancer development are expressed in human pseudoglandular lung embryogenesis. Oncology 76: 162-169.
226. Northcott PA, Fernandez LA, Hagan JP, Ellison DW, Grajkowska W, *et al.* (2009) The miR-17/92 polycistron is up-regulated in sonic hedgehog-driven medulloblastomas and induced by N-myc in sonic hedgehog-treated cerebellar neural precursors. Cancer Res 69: 3249-3255.
227. O'Donnell KA, Wentzel EA, Zeller KI, Dang CV, Mendell JT (2005) c-Myc-regulated microRNAs modulate E2F1 expression. Nature 435: 839-843.
228. Dews M, Homayouni A, Yu D, Murphy D, Sevignani C, *et al.* (2006) Augmentation of tumor angiogenesis by a Myc-activated microRNA cluster. Nat Genet 38: 1060-1065.
229. Diosdado B, van de Wiel MA, Terhaar Sive Droste JS, Mongera S, Postma C, *et al.* (2009) MiR-17-92 cluster is associated with 13q gain and c-myc expression during colorectal adenoma to adenocarcinoma progression. Br J Cancer 101: 707-714.
230. Ventura A, Young AG, Winslow MM, Lintault L, Meissner A, *et al.* (2008) Targeted deletion reveals essential and overlapping functions of the miR-17 through 92 family of miRNA clusters. Cell 132: 875-886.
231. Ernst A, Campos B, Meier J, Devens F, Liesenberg F, *et al.* (2010) De-repression of CTGF via the miR-17-92 cluster upon differentiation of human glioblastoma spheroid cultures. Oncogene 29: 3411-3422.
232. Fontana L, Fiori ME, Albini S, Cifaldi L, Giovinazzi S, *et al.* (2008) Antagomir-17-5p abolishes the growth of therapy-resistant neuroblastoma through p21 and BIM. PLoS One 3: e2236.
233. Taguchi A, Yanagisawa K, Tanaka M, Cao K, Matsuyama Y, *et al.* (2008) Identification of hypoxia-inducible factor-1 alpha as a novel target for miR-17-92 microRNA cluster. Cancer Res 68: 5540-5545.
234. Yu Z, Wang C, Wang M, Li Z, Casimiro MC, *et al.* (2008) A cyclin D1/microRNA 17/20 regulatory feedback loop in control of breast cancer cell proliferation. J Cell Biol 182: 509-517.

235. Farfsing A (2009) Identification and functional characterization of candidate genes in recurrently gained genomic regions of mantle cell lymphoma and chronic lymphocytic leukemia.
236. Zuker M, Stiegler P (1981) Optimal computer folding of large RNA sequences using thermodynamics and auxiliary information. Nucleic Acids Res 9: 133-148.
237. Maragkakis M, Alexiou P, Papadopoulos GL, Reczko M, Dalamagas T, *et al.* (2009) Accurate microRNA target prediction correlates with protein repression levels. BMC Bioinformatics 10: 295.
238. Maragkakis M, Reczko M, Simossis VA, Alexiou P, Papadopoulos GL, *et al.* (2009) DIANA-microT web server: elucidating microRNA functions through target prediction. Nucleic Acids Res 37: W273-276.
239. Dweep H, Sticht C, Pandey P, Gretz N (2011) miRWalk--database: prediction of possible miRNA binding sites by "walking" the genes of three genomes. Journal of biomedical informatics 44: 839-847.
240. Kertesz M, Iovino N, Unnerstall U, Gaul U, Segal E (2007) The role of site accessibility in microRNA target recognition. Nat Genet 39: 1278-1284.
241. Betel D, Koppal A, Agius P, Sander C, Leslie C (2010) Comprehensive modeling of microRNA targets predicts functional non-conserved and non-canonical sites. Genome Biol 11: R90.
242. Krek A, Grun D, Poy MN, Wolf R, Rosenberg L, *et al.* (2005) Combinatorial microRNA target predictions. Nature genetics 37: 495-500.
243. Miranda KC, Huynh T, Tay Y, Ang YS, Tam WL, *et al.* (2006) A pattern-based method for the identification of MicroRNA binding sites and their corresponding heteroduplexes. Cell 126: 1203-1217.
244. Rehmsmeier M, Steffen P, Hochsmann M, Giegerich R (2004) Fast and effective prediction of microRNA/target duplexes. RNA 10: 1507-1517.
245. Trapnell C, Pachter L, Salzberg SL (2009) TopHat: discovering splice junctions with RNA-Seq. Bioinformatics 25: 1105-1111.
246. Anders S, Huber W (2010) Differential expression analysis for sequence count data. Genome biology 11: R106.
247. Farfsing A, Engel F, Seiffert M, Hartmann E, Ott G, *et al.* (2009) Gene knockdown studies revealed CCDC50 as a candidate gene in mantle cell lymphoma and chronic lymphocytic leukemia. Leukemia 23: 2018-2026.
248. Rozen S, Skaletsky H (2000) Primer3 on the WWW for general users and for biologist programmers. Methods Mol Biol 132: 365-386.
249. Saiki RK, Gelfand DH, Stoffel S, Scharf SJ, Higuchi R, *et al.* (1988) Primer-directed enzymatic amplification of DNA with a thermostable DNA polymerase. Science 239: 487-491.
250. Sanger F, Nicklen S, Coulson AR (1977) DNA sequencing with chain-terminating inhibitors. Proc Natl Acad Sci U S A 74: 5463-5467.
251. Meier J (2007) Charakterisierung der MikroRNA-Expression von miR-155 und miR-17-92 in B-Zell-Non-Hodgkin-Lymphomen.
252. Tan LP, Seinen E, Duns G, de Jong D, Sibon OC, *et al.* (2009) A high throughput experimental approach to identify miRNA targets in human cells. Nucleic Acids Res 37: e137.
253. Wang WX, Wilfred BR, Hu Y, Stromberg AJ, Nelson PT (2010) Anti-Argonaute RIP-Chip shows that miRNA transfections alter global patterns of mRNA recruitment to microribonucleoprotein complexes. RNA 16: 394-404.
254. Willimott S, Wagner SD (2012) miR-125b and miR-155 contribute to BCL2 repression and proliferation in response to CD40 ligand (CD154) in human leukemic B-cells. The Journal of biological chemistry 287: 2608-2617.
255. Jiang S, Zhang HW, Lu MH, He XH, Li Y, *et al.* (2010) MicroRNA-155 functions as an OncomiR in breast cancer by targeting the suppressor of cytokine signaling 1 gene. Cancer Res 70: 3119-3127.
256. O'Connell RM, Rao DS, Chaudhuri AA, Boldin MP, Taganov KD, *et al.* (2008) Sustained expression of microRNA-155 in hematopoietic stem cells causes a myeloproliferative disorder. J Exp Med 205: 585-594.
257. Qin X, Wang X, Wang Y, Tang Z, Cui Q, *et al.* (2010) MicroRNA-19a mediates the suppressive effect of laminar flow on cyclin D1 expression in human umbilical vein endothelial cells. Proceedings of the National Academy of Sciences of the United States of America 107: 3240-3244.
258. Deshpande A, Pastore A, Deshpande AJ, Zimmermann Y, Hutter G, *et al.* (2009) 3'UTR mediated regulation of the cyclin D1 proto-oncogene. Cell Cycle 8: 3584-3592.
259. Gutsch R, Kandemir JD, Pietsch D, Cappello C, Meyer J, *et al.* (2011) CCAAT/enhancer-binding protein beta inhibits proliferation in monocytic cells by affecting the retinoblastoma protein/E2F/cyclin E pathway but is not directly required for macrophage morphology. The Journal of biological chemistry 286: 22716-22729.

260. Ebert MS, Neilson JR, Sharp PA (2007) MicroRNA sponges: competitive inhibitors of small RNAs in mammalian cells. Nat Methods 4: 721-726.
261. Diederichs S, Jung S, Rothenberg SM, Smolen GA, Mlody BG, *et al.* (2008) Coexpression of Argonaute-2 enhances RNA interference toward perfect match binding sites. Proceedings of the National Academy of Sciences of the United States of America 105: 9284-9289.
262. Bazzini AA, Lee MT, Giraldez AJ (2012) Ribosome profiling shows that miR-430 reduces translation before causing mRNA decay in zebrafish. Science 336: 233-237.
263. Mukherji S, Ebert MS, Zheng GX, Tsang JS, Sharp PA, *et al.* (2011) MicroRNAs can generate thresholds in target gene expression. Nature genetics 43: 854-859.
264. Baek D, Villen J, Shin C, Camargo FD, Gygi SP, *et al.* (2008) The impact of microRNAs on protein output. Nature 455: 64-71.
265. Ong SE, Blagoev B, Kratchmarova I, Kristensen DB, Steen H, *et al.* (2002) Stable isotope labeling by amino acids in cell culture, SILAC, as a simple and accurate approach to expression proteomics. Mol Cell Proteomics 1: 376-386.
266. Lossner C, Meier J, Warnken U, Rogers MA, Lichter P, *et al.* (2011) Quantitative Proteomics Identify Novel miR-155 Target Proteins. PLoS One 6: e22146.
267. Kishore S, Jaskiewicz L, Burger L, Hausser J, Khorshid M, *et al.* (2011) A quantitative analysis of CLIP methods for identifying binding sites of RNA-binding proteins. Nat Methods.
268. Chi SW, Zang JB, Mele A, Darnell RB (2009) Argonaute HITS-CLIP decodes microRNA-mRNA interaction maps. Nature 460: 479-486.
269. Keene JD, Komisarow JM, Friedersdorf MB (2006) RIP-Chip: the isolation and identification of mRNAs, microRNAs and protein components of ribonucleoprotein complexes from cell extracts. Nat Protoc 1: 302-307.
270. Hershkovitz Rokah O, Granot G, Ovcharenko A, Modai S, Pasmanik-Chor M, *et al.* (2012) Downregulation of mir-31, mir-155, and mir-564 in chronic myeloid leukemia cells. PLoS One 7: e35501.
271. Fang Z, Rajewsky N (2011) The impact of miRNA target sites in coding sequences and in 3'UTRs. PLoS One 6: e18067.
272. Blackshear PJ (2002) Tristetraprolin and other CCCH tandem zinc-finger proteins in the regulation of mRNA turnover. Biochemical Society transactions 30: 945-952.
273. Brennan SE, Kuwano Y, Alkharouf N, Blackshear PJ, Gorospe M, *et al.* (2009) The mRNA-destabilizing protein tristetraprolin is suppressed in many cancers, altering tumorigenic phenotypes and patient prognosis. Cancer research 69: 5168-5176.
274. Kim JK, Diehl JA (2009) Nuclear cyclin D1: an oncogenic driver in human cancer. Journal of cellular physiology 220: 292-296.
275. Marderosian M, Sharma A, Funk AP, Vartanian R, Masri J, *et al.* (2006) Tristetraprolin regulates Cyclin D1 and c-Myc mRNA stability in response to rapamycin in an Akt-dependent manner via p38 MAPK signaling. Oncogene 25: 6277-6290.
276. Reynolds AB, Carnahan RH (2004) Regulation of cadherin stability and turnover by p120ctn: implications in disease and cancer. Seminars in cell & developmental biology 15: 657-663.
277. Chartier NT, Oddou CI, Laine MG, Ducarouge B, Marie CA, *et al.* (2007) Cyclin-dependent kinase 2/cyclin E complex is involved in p120 catenin (p120ctn)-dependent cell growth control: a new role for p120ctn in cancer. Cancer research 67: 9781-9790.
278. Skalsky RL, Corcoran DL, Gottwein E, Frank CL, Kang D, *et al.* (2012) The viral and cellular microRNA targetome in lymphoblastoid cell lines. PLoS pathogens 8: e1002484.
279. Liu M, Wu H, Liu T, Li Y, Wang F, *et al.* (2009) Regulation of the cell cycle gene, BTG2, by miR-21 in human laryngeal carcinoma. Cell research 19: 828-837.
280. Rouault JP, Rimokh R, Tessa C, Paranhos G, Ffrench M, *et al.* (1992) BTG1, a member of a new family of antiproliferative genes. The EMBO journal 11: 1663-1670.
281. Rouault JP, Falette N, Guehenneux F, Guillot C, Rimokh R, *et al.* (1996) Identification of BTG2, an antiproliferative p53-dependent component of the DNA damage cellular response pathway. Nature genetics 14: 482-486.
282. Passeri D, Marcucci A, Rizzo G, Billi M, Panigada M, *et al.* (2006) Btg2 enhances retinoic acid-induced differentiation by modulating histone H4 methylation and acetylation. Molecular and cellular biology 26: 5023-5032.
283. Inuzuka H, Shaik S, Onoyama I, Gao D, Tseng A, *et al.* (2011) SCF(FBW7) regulates cellular apoptosis by targeting MCL1 for ubiquitylation and destruction. Nature 471: 104-109.

284. Han HJ, Sudo K, Inazawa J, Nakamura Y (1996) Isolation and mapping of a human gene (RABL) encoding a small GTP-binding protein homologous to the Ras-related RAB gene. Cytogenetics and cell genetics 73: 137-139.
285. Bucci C, Lutcke A, Steele-Mortimer O, Olkkonen VM, Dupree P, *et al.* (1995) Co-operative regulation of endocytosis by three Rab5 isoforms. FEBS letters 366: 65-71.
286. Ulrich F, Krieg M, Schotz EM, Link V, Castanon I, *et al.* (2005) Wnt11 functions in gastrulation by controlling cell cohesion through Rab5c and E-cadherin. Developmental cell 9: 555-564.
287. Coyne CB, Shen L, Turner JR, Bergelson JM (2007) Coxsackievirus entry across epithelial tight junctions requires occludin and the small GTPases Rab34 and Rab5. Cell host & microbe 2: 181-192.
288. Chaturvedi A, Martz R, Dorward D, Waisberg M, Pierce SK (2011) Endocytosed BCRs sequentially regulate MAPK and Akt signaling pathways from intracellular compartments. Nature immunology 12: 1119-1126.
289. Linsley PS, Schelter J, Burchard J, Kibukawa M, Martin MM, *et al.* (2007) Transcripts targeted by the microRNA-16 family cooperatively regulate cell cycle progression. Molecular and cellular biology 27: 2240-2252.
290. Sumazin P, Yang X, Chiu HS, Chung WJ, Iyer A, *et al.* (2011) An extensive microRNA-mediated network of RNA-RNA interactions regulates established oncogenic pathways in glioblastoma. Cell 147: 370-381.
291. Zhao H, Kalota A, Jin S, Gewirtz AM (2009) The c-myb proto-oncogene and microRNA-15a comprise an active autoregulatory feedback loop in human hematopoietic cells. Blood 113: 505-516.
292. Sylvestre Y, De Guire V, Querido E, Mukhopadhyay UK, Bourdeau V, *et al.* (2007) An E2F/miR-20a autoregulatory feedback loop. The Journal of biological chemistry 282: 2135-2143.
293. Subramanyam D, Lamouille S, Judson RL, Liu JY, Bucay N, *et al.* (2011) Multiple targets of miR-302 and miR-372 promote reprogramming of human fibroblasts to induced pluripotent stem cells. Nature biotechnology 29: 443-448.
294. Lu BC, Cebrian C, Chi X, Kuure S, Kuo R, *et al.* (2009) Etv4 and Etv5 are required downstream of GDNF and Ret for kidney branching morphogenesis. Nature genetics 41: 1295-1302.
295. Oh S, Shin S, Janknecht R (2012) ETV1, 4 and 5: An oncogenic subfamily of ETS transcription factors. Biochimica et biophysica acta 1826: 1-12.
296. Ebert MS, Sharp PA (2010) Emerging roles for natural microRNA sponges. Current biology : CB 20: R858-861.
297. Cesana M, Cacchiarelli D, Legnini I, Santini T, Sthandier O, *et al.* (2011) A long noncoding RNA controls muscle differentiation by functioning as a competing endogenous RNA. Cell 147: 358-369.
298. Yan LX, Huang XF, Shao Q, Huang MY, Deng L, *et al.* (2008) MicroRNA miR-21 overexpression in human breast cancer is associated with advanced clinical stage, lymph node metastasis and patient poor prognosis. RNA 14: 2348-2360.
299. Yanaihara N, Caplen N, Bowman E, Seike M, Kumamoto K, *et al.* (2006) Unique microRNA molecular profiles in lung cancer diagnosis and prognosis. Cancer Cell 9: 189-198.
300. Wang M, Tan LP, Dijkstra MK, van Lom K, Robertus JL, *et al.* (2008) miRNA analysis in B-cell chronic lymphocytic leukaemia: proliferation centres characterized by low miR-150 and high BIC/miR-155 expression. The Journal of pathology 215: 13-20.
301. Bai H, Xu R, Cao Z, Wei D, Wang C (2011) Involvement of miR-21 in resistance to daunorubicin by regulating PTEN expression in the leukaemia K562 cell line. FEBS letters 585: 402-408.
302. Lu J, Getz G, Miska EA, Alvarez-Saavedra E, Lamb J, *et al.* (2005) MicroRNA expression profiles classify human cancers. Nature 435: 834-838.
303. Calin GA, Ferracin M, Cimmino A, Di Leva G, Shimizu M, *et al.* (2005) A MicroRNA signature associated with prognosis and progression in chronic lymphocytic leukemia. The New England journal of medicine 353: 1793-1801.
304. Garzon R, Volinia S, Liu CG, Fernandez-Cymering C, Palumbo T, *et al.* (2008) MicroRNA signatures associated with cytogenetics and prognosis in acute myeloid leukemia. Blood 111: 3183-3189.
305. Goff LA, Davila J, Swerdel MR, Moore JC, Cohen RI, *et al.* (2009) Ago2 immunoprecipitation identifies predicted microRNAs in human embryonic stem cells and neural precursors. PLoS One 4: e7192.
306. Chen Y, Gelfond JA, McManus LM, Shireman PK (2009) Reproducibility of quantitative RT-PCR array in miRNA expression profiling and comparison with microarray analysis. BMC Genomics 10: 407.
307. Winter J, Diederichs S (2011) Argonaute proteins regulate microRNA stability: Increased microRNA abundance by Argonaute proteins is due to microRNA stabilization. RNA biology 8: 1149-1157.
308. Chen B, Zhang B, Luo H, Yuan J, Skogerbo G, *et al.* (2012) Distinct MicroRNA Subcellular Size and Expression Patterns in Human Cancer Cells. International journal of cell biology 2012: 672462.

6 Supplementary

Table S 1: Summary of mapped and quantified reads per sample and replicate of HEK-vector and pREP4miR-155 generated by 2nd generation sequencing

Cell line	Fraction	Replicate	Total count	Useable count	% of total count
HEK-vector	IP	1	38847512	26697792	68.72
HEK-vector	IP	2	35200455	24681908	70.12
HEK-vector	IP	3	34633980	24064313	69.48
HEK-vector	TL	1	77647039	56479074	72.74
HEK-vector	TL	2	51827659	38276456	73.85
HEK-vector	TL	3	66831196	48956322	73.25
HEK-miR-155	IP	1	33679129	23334445	69.28
HEK-miR-155	IP	2	34442706	24432299	70.94
HEK-miR-155	IP	3	35082010	24734154	70.50
HEK-miR-155	TL	1	69955916	50830568	72.66
HEK-miR-155	TL	2	71385945	53103311	74.39
HEK-miR-155	TL	3	72132189	53445065	74.09

Table S 2: List of significantly (p<0.05) enriched mRNAs in HEK-miR-155 compared to the IP of HEK-vector (n= 213). Genes predicted for being miR-155 targets (according to MiRWalk) are marked with bold letters.

Gene	Log2-FC	P-value		Gene	Log2-FC	P-value
TNFRSF11B	6,10E+00	7,99E-17		NDUFAF2	6,54E-01	1,16E-02
FAM78A	1,78E+00	4,29E-16		MRPS18C	6,69E-01	1,19E-02
KCNQ2	1,59E+00	2,20E-15		**ELOVL6**	6,59E-01	1,21E-02
C21orf37	5,59E+00	7,51E-11		RGS3	7,58E-01	1,26E-02
CCND1	3,88E+00	1,03E-10		SYNPO	9,38E-01	1,28E-02
DPYSL3	1,55E+00	5,27E-10		EFNA3	7,07E-01	1,29E-02
TCF4	1,32E+00	5,38E-10		**FBXO9**	6,38E-01	1,38E-02
ALDH1A2	1,23E+00	2,65E-09		NDUFC1	6,33E-01	1,48E-02
ZNF483	1,92E+00	2,65E-09		TCF7L2	6,52E-01	1,48E-02
CA12	1,36E+00	4,84E-09		MMP2	1,15E+00	1,51E-02
AGTRAP	1,20E+00	7,32E-09		ANAPC5	6,41E-01	1,53E-02
COL27A1	1,20E+00	2,67E-08		**CHCHD7**	6,44E-01	1,53E-02
LY6E	1,04E+00	9,23E-07		UROS	6,20E-01	1,54E-02
C12orf39	1,33E+00	1,53E-06		IMPDH1	6,23E-01	1,59E-02
FAM84B	1,02E+00	1,62E-06		C17orf96	6,43E-01	1,64E-02
BMP2	2,18E+00	3,28E-06		EXOSC4	8,37E-01	1,65E-02
PROCR	1,08E+00	3,88E-06		ABCE1	6,23E-01	1,67E-02
NDRG1	1,15E+00	3,96E-06		KLRG2	6,96E-01	1,70E-02
OR2V2	5,02E+00	5,36E-06		NRARP	6,23E-01	1,78E-02
C19orf51	1,06E+00	1,19E-05		APRT	6,01E-01	1,81E-02
PNPT1	8,90E-01	8,07E-05		NELL1	4,33E+00	1,84E-02
COTL1	8,89E-01	9,17E-05		PDZRN3	7,83E-01	1,86E-02
EDA2R	3,64E+00	9,25E-05		CHRNA4	1,54E+00	1,89E-02
USPL1	9,02E-01	9,25E-05		**GNG4**	6,04E-01	1,91E-02

Gene	Log2-FC	P-value	Gene	Log2-FC	P-value
PPA2	8,75E-01	9,25E-05	CHAC2	6,48E-01	1,93E-02
FCRLB	1,46E+00	9,25E-05	CKMT1A	9,27E-01	1,93E-02
HMOX1	1,01E+00	1,50E-04	NDUFA8	6,28E-01	1,99E-02
SOD1	8,45E-01	1,66E-04	UQCRFS1	6,23E-01	2,01E-02
TRMT12	8,80E-01	2,39E-04	**CDC42EP4**	6,41E-01	2,01E-02
ZNF813	1,59E+00	2,71E-04	PRPS2	6,12E-01	2,01E-02
BBS7	8,74E-01	2,79E-04	AL050321.1	9,73E-01	2,01E-02
PHC2	1,50E+00	3,21E-04	MARS2	6,33E-01	2,01E-02
CHST15	8,55E-01	3,25E-04	GABRD	9,27E-01	2,07E-02
FAM150A	2,24E+00	3,26E-04	**DUSP14**	6,46E-01	2,21E-02
ALPL	9,46E-01	3,88E-04	**TPRKB**	6,04E-01	2,25E-02
C3orf18	8,89E-01	4,24E-04	**GPRIN3**	7,97E-01	2,31E-02
ADCYAP1R1	8,63E-01	6,47E-04	FAM179A	1,44E+00	2,34E-02
POLR3G	1,02E+00	7,08E-04	MRPS12	6,27E-01	2,36E-02
FAM49B	7,94E-01	7,91E-04	HRSP12	6,17E-01	2,36E-02
TESC	9,80E-01	8,36E-04	SEH1L	6,14E-01	2,37E-02
MECR	7,88E-01	8,53E-04	ISM2	8,18E-01	2,37E-02
THEM4	7,73E-01	9,61E-04	BOP1	6,51E-01	2,38E-02
INTS10	7,84E-01	1,01E-03	LRIF1	6,14E-01	2,38E-02
C8orf33	7,66E-01	1,20E-03	ETV5	1,92E+00	2,38E-02
VAMP3	7,53E-01	1,30E-03	DCTD	5,95E-01	2,40E-02
SPRED1	8,30E-01	1,37E-03	EGLN3	6,66E-01	2,50E-02
TBC1D14	7,60E-01	1,49E-03	TSKU	6,28E-01	2,51E-02
ARSJ	1,01E+00	1,52E-03	**CTSC**	6,00E-01	2,52E-02
ADA	8,15E-01	1,82E-03	PRR5L	8,74E-01	2,61E-02
MRPL13	7,48E-01	1,96E-03	LSM4	5,89E-01	2,67E-02
ETV1	1,38E+00	1,98E-03	HSPD1	5,79E-01	2,68E-02
BCL6B	7,82E-01	2,02E-03	**EYA2**	7,07E-01	2,69E-02
EIF2C2	9,18E-01	2,24E-03	**ZNF85**	1,49E+00	2,69E-02
KHDRBS3	7,73E-01	2,25E-03	PPID	6,10E-01	2,69E-02
METTL21A	7,54E-01	2,26E-03	WDR77	6,01E-01	2,81E-02
ZNF586	1,09E+00	2,51E-03	MAP2K6	6,31E-01	2,95E-02
DET1	1,48E+00	2,61E-03	LSM12	5,77E-01	2,95E-02
LIPT1	7,88E-01	2,61E-03	GTF2E2	6,07E-01	2,96E-02
COPS2	6,98E-01	2,66E-03	OR7D2	1,93E+00	2,96E-02
SPRY1	7,84E-01	2,82E-03	TNFRSF10D	7,19E-01	2,99E-02
EPHA8	1,32E+00	3,25E-03	SLC25A33	6,02E-01	2,99E-02
TRIM32	7,40E-01	3,38E-03	RPL17	9,59E-01	2,99E-02
FBXO32	8,60E-01	3,56E-03	OAF	5,93E-01	3,06E-02
DSCC1	7,02E-01	3,86E-03	PVRL4	1,55E+00	3,18E-02
ARRDC2	7,77E-01	3,89E-03	TMEM177	5,84E-01	3,21E-02
TSTA3	7,19E-01	3,93E-03	WDYHV1	6,33E-01	3,21E-02
IER5	7,41E-01	3,95E-03	TMEM14B	5,86E-01	3,30E-02
C20orf27	7,05E-01	4,03E-03	SLC25A32	6,13E-01	3,32E-02
TATDN3	7,07E-01	4,05E-03	SLC25A4	6,06E-01	3,35E-02
PYCRL	7,96E-01	4,19E-03	NEIL2	6,21E-01	3,40E-02
TATDN1	7,12E-01	4,37E-03	QPRT	8,78E-01	3,40E-02
HOMEZ	7,35E-01	4,51E-03	ACN9	5,95E-01	3,42E-02
C12orf24	6,99E-01	4,58E-03	RASGEF1A	6,08E-01	3,56E-02
CHRAC1	6,92E-01	4,64E-03	ZNF44	8,05E-01	3,56E-02
UAP1	6,91E-01	4,69E-03	MRPS18A	5,93E-01	3,57E-02
SLIRP	6,95E-01	4,69E-03	CHEK2	5,83E-01	3,57E-02
DCK	7,09E-01	4,69E-03	RRP7A	5,78E-01	3,57E-02
SLC11A1	1,59E+00	4,71E-03	LSM6	5,95E-01	3,64E-02
ATP1A3	7,31E-01	4,89E-03	**SRXN1**	5,81E-01	3,66E-02
EID2	7,31E-01	5,03E-03	SNCB	1,02E+00	3,68E-02
STAP2	1,36E+00	5,24E-03	RNF139	6,69E-01	3,68E-02
CYC1	7,69E-01	5,47E-03	WNT10B	6,49E-01	3,68E-02
GLRX5	6,92E-01	5,55E-03	FRAT2	5,71E-01	3,98E-02
PLCD3	6,88E-01	5,98E-03	MLF1IP	5,54E-01	4,02E-02

Gene	Log2-FC	P-value		Gene	Log2-FC	P-value
MT1X	7,72E-01	6,08E-03		TMEM145	6,91E-01	4,08E-02
CACYBP	6,90E-01	6,15E-03		SH2D5	6,86E-01	4,08E-02
ETV4	2,26E+00	6,51E-03		**RIMS4**	5,89E-01	4,13E-02
PFN2	6,65E-01	6,87E-03		FGFR4	6,04E-01	4,23E-02
EXT1	6,82E-01	7,23E-03		RABEPK	5,84E-01	4,24E-02
EEF1E1	6,76E-01	7,42E-03		BEND4	6,20E-01	4,33E-02
TADA2B	6,78E-01	7,79E-03		FAM155B	5,81E-01	4,33E-02
HSPE1	6,82E-01	7,81E-03		METTL5	5,66E-01	4,33E-02
MYCL1	6,89E-01	8,27E-03		CENPV	5,58E-01	4,33E-02
NCS1	6,71E-01	8,68E-03		**IKBKE**	7,65E-01	4,35E-02
TRIP13	6,63E-01	8,90E-03		PRDX4	5,54E-01	4,41E-02
DHRS2	1,12E+00	9,69E-03		SPRED2	5,82E-01	4,63E-02
FXN	6,64E-01	9,89E-03		ISCA1	5,49E-01	4,68E-02
C3orf14	6,48E-01	1,00E-02		COL14A1	1,05E+00	4,73E-02
C1orf124	6,61E-01	1,01E-02		**TSHZ3**	5,54E-01	4,77E-02
PANK1	6,69E-01	1,01E-02		POP1	5,98E-01	4,87E-02
SRD5A3	6,59E-01	1,02E-02		DFFA	5,39E-01	4,87E-02
CEBPB	1,44E+00	1,02E-02		TOP1MT	5,55E-01	4,87E-02
ZFP36	7,78E-01	1,02E-02		NOP16	5,71E-01	4,92E-02
UBE2V2	7,77E-01	1,03E-02		PNO1	5,60E-01	4,92E-02
ATP6V1E2	7,22E-01	1,03E-02		GPATCH4	5,56E-01	4,92E-02
GAL	6,68E-01	1,10E-02		WDR67	5,57E-01	4,92E-02
PSMB10	6,80E-01	1,15E-02				

Table S 3: List of significantly (p<0.05) enriched mRNAs in HEK-vector compared to the IP of HEK-miR-155 (n= 409).

Gene	Log2-FC	P-value		Gene	Log2-FC	P-value
SPARC	-4.70E+00	3.71E-27		NMI	-1.10E+00	8.68E-03
GALNT13	-2.84E+00	6.11E-26		ZNF536	-1.03E+00	8.68E-03
EPAS1	-2.26E+00	1.28E-22		OPHN1	-8.33E-01	8.90E-03
DOK6	-3.79E+00	1.47E-22		ABCA3	-1.15E+00	8.90E-03
COL2A1	-2.47E+00	6.07E-20		SLC13A4	-1.03E+00	9.21E-03
ULK2	-2.06E+00	2.41E-19		HEATR5B	-7.11E-01	9.25E-03
UBE2QL1	-2.71E+00	2.56E-18		HOXB3	-6.99E-01	9.25E-03
CDO1	-4.58E+00	8.50E-17		SLFN5	-1.46E+00	9.25E-03
CYP26B1	-2.26E+00	1.06E-16		NME5	-1.82E+00	9.32E-03
PCDH10	-1.68E+00	3.30E-15		CBLB	-8.34E-01	9.43E-03
ZFP106	-1.54E+00	1.99E-13		FZD10	-1.32E+00	9.69E-03
PGCP	-3.57E+00	2.24E-12		DMRTA2	-1.78E+00	9.69E-03
FAM20C	-1.62E+00	9.82E-12		CAV1	-9.52E-01	1.00E-02
OAS3	-4.48E+00	1.95E-11		TTC28	-6.87E-01	1.03E-02
EHBP1L1	-1.84E+00	7.74E-11		GOLGA2	-7.04E-01	1.03E-02
STARD9	-1.50E+00	7.74E-11		LRRC57	-7.03E-01	1.05E-02
TTBK2	-1.61E+00	1.35E-10		PLXNA4	-3.18E+00	1.06E-02
MAMLD1	-1.74E+00	1.60E-10		RALGAPA2	-6.94E-01	1.09E-02
CDH2	-1.95E+00	6.45E-10		IFI27L2	-7.54E-01	1.10E-02
OPTN	-1.30E+00	1.78E-09		NEK11	-1.12E+00	1.10E-02
MYO5B	-1.97E+00	1.78E-09		SCAPER	-7.45E-01	1.11E-02
PLA2G4A	-3.32E+00	2.65E-09		CADPS2	-1.32E+00	1.13E-02
APH1B	-1.36E+00	2.65E-09		GAP43	-1.71E+00	1.14E-02
SLIT2	-1.19E+00	4.11E-09		SCN8A	-1.02E+00	1.14E-02
FGF13	-2.68E+00	7.32E-09		HERC1	-7.10E-01	1.15E-02
DMRT3	-3.94E+00	1.17E-08		KIAA0889	-6.92E-01	1.15E-02
VPS39	-1.18E+00	2.67E-08		SLC2A10	-7.85E-01	1.17E-02
OSBPL7	-1.88E+00	8.23E-08		STAT3	-6.51E-01	1.18E-02

Gene	Log2-FC	P-value		Gene	Log2-FC	P-value
DDIT4L	-1.92E+00	1.61E-07		PLCL1	-1.46E+00	1.19E-02
GANC	-1.37E+00	1.87E-07		ANG	-1.56E+00	1.19E-02
LRP1	-1.19E+00	2.38E-07		CBX5	-6.50E-01	1.21E-02
CDAN1	-1.21E+00	2.62E-07		MAP6	-1.10E+00	1.21E-02
PVALB	-2.88E+00	4.56E-07		IGF2R	-6.49E-01	1.22E-02
PRKCB	-1.34E+00	4.67E-07		PAK3	-1.95E+00	1.26E-02
TP53INP1	-1.23E+00	4.73E-07		FBN2	-6.84E-01	1.27E-02
FBXO27	-1.20E+00	5.58E-07		CXorf58	-2.17E+00	1.33E-02
ZSCAN29	-1.12E+00	5.77E-07		C8orf42	-1.11E+00	1.37E-02
UBR1	-1.13E+00	6.99E-07		SBNO1	-6.58E-01	1.39E-02
CCNDBP1	-1.17E+00	8.57E-07		ABCB4	-1.98E+00	1.39E-02
WNT9A	-1.59E+00	8.57E-07		C19orf57	-8.36E-01	1.48E-02
AIFM2	-2.02E+00	9.38E-07		CELSR2	-6.73E-01	1.50E-02
SAMD12	-1.56E+00	1.53E-06		RNF175	-2.16E+00	1.52E-02
NACAD	-1.50E+00	2.22E-06		PLD1	-1.07E+00	1.52E-02
TMSB4X	-1.57E+00	4.63E-06		HERC3	-7.09E-01	1.53E-02
PLCB2	-2.20E+00	5.84E-06		MLL2	-6.23E-01	1.53E-02
KCNQ1	-1.42E+00	6.93E-06		KIAA0913	-6.42E-01	1.53E-02
TMEM62	-1.13E+00	6.93E-06		EPSTI1	-1.28E+00	1.56E-02
TMEM87A	-1.04E+00	6.93E-06		SORT1	-6.14E-01	1.56E-02
CELF2	-1.68E+00	1.09E-05		EFTUD1	-6.88E-01	1.64E-02
RYR2	-2.66E+00	1.09E-05		ABCA5	-7.47E-01	1.64E-02
LCMT2	-1.04E+00	1.25E-05		C12orf51	-6.39E-01	1.64E-02
CLVS2	-3.75E+00	1.25E-05		KNTC1	-6.50E-01	1.64E-02
HOXA5	-1.06E+00	1.28E-05		PPP1R12B	-7.63E-01	1.65E-02
ODZ1	-5.34E+00	1.34E-05		ATF7IP	-6.93E-01	1.65E-02
PDE10A	-1.41E+00	1.34E-05		LMLN	-7.46E-01	1.65E-02
CACNA1G	-1.68E+00	1.37E-05		PRKCH	-8.24E-01	1.66E-02
LMO7	-1.07E+00	1.77E-05		LRRC33	-1.12E+00	1.78E-02
GOS2	-1.84E+00	2.22E-05		KANK1	-6.96E-01	1.79E-02
OTX2	-1.59E+00	2.44E-05		SYTL4	-8.30E-01	1.81E-02
STXBP5L	-2.18E+00	3.24E-05		PGPEP1	-6.89E-01	1.81E-02
IQGAP3	-9.85E-01	3.25E-05		INSR	-7.89E-01	1.83E-02
KCTD12	-9.82E-01	3.75E-05		NMU	-7.22E-01	1.86E-02
MAP7	-9.87E-01	4.98E-05		DDAH2	-7.19E-01	1.86E-02
ST8SIA4	-3.65E+00	5.99E-05		SAMD5	-9.60E-01	1.87E-02
EFEMP2	-1.83E+00	6.79E-05		MYO3A	-1.11E+00	1.93E-02
SNAP91	-1.74E+00	6.80E-05		APBA1	-1.39E+00	1.93E-02
SLC16A5	-4.61E+00	6.85E-05		NTNG1	-3.13E+00	1.93E-02
SLC35F3	-2.71E+00	6.91E-05		RASGRP1	-1.03E+00	1.93E-02
GPRC5C	-1.47E+00	8.07E-05		LTK	-9.18E-01	1.94E-02
TUBGCP4	-9.67E-01	8.08E-05		SLC17A5	-6.47E-01	1.94E-02
ADAL	-9.79E-01	8.57E-05		SZT2	-7.14E-01	2.01E-02
AC010336.1	-1.78E+00	8.57E-05		ANTXR2	-8.25E-01	2.06E-02
OCLN	-1.01E+00	8.57E-05		SLC46A3	-7.09E-01	2.06E-02
SNAP23	-9.04E-01	8.67E-05		ALG1L	-1.05E+00	2.07E-02
FREM2	-1.23E+00	9.17E-05		DOCK8	-9.09E-01	2.09E-02
B3GALT1	-1.92E+00	9.43E-05		PHIP	-6.87E-01	2.11E-02
LONRF2	-1.08E+00	9.54E-05		SRCAP	-5.99E-01	2.14E-02
APOBEC3B	-1.86E+00	9.86E-05		PARD3B	-8.67E-01	2.14E-02
LAMB2	-9.14E-01	1.03E-04		YPEL5	-7.61E-01	2.14E-02
THRB	-1.01E+00	1.09E-04		PTPN14	-7.53E-01	2.14E-02
DCHS1	-1.40E+00	1.10E-04		ZNF396	-9.41E-01	2.14E-02
BEX2	-8.93E-01	1.10E-04		C2orf72	-7.30E-01	2.18E-02
SLITRK5	-9.34E-01	1.10E-04		DKK3	-9.09E-01	2.21E-02
SPINT2	-1.34E+00	1.48E-04		GOLGB1	-8.13E-01	2.22E-02
TTLL7	-1.02E+00	1.48E-04		AFF3	-6.75E-01	2.24E-02
MBP	-1.58E+00	1.50E-04		MAP1A	-1.48E+00	2.24E-02
NKAIN2	-2.57E+00	1.50E-04		GPX3	-5.99E-01	2.25E-02
PRRX1	-2.19E+00	1.58E-04		MAP2	-1.81E+00	2.27E-02

Gene	Log2-FC	P-value	Gene	Log2-FC	P-value
GPR126	-1.56E+00	1.59E-04	EGR2	-1.42E+00	2.31E-02
RAB9B	-1.11E+00	2.42E-04	SERPING1	-2.19E+00	2.34E-02
NPY1R	-5.47E+00	2.45E-04	DIAPH3	-6.52E-01	2.37E-02
CALCOCO1	-9.32E-01	2.66E-04	VGLL2	-1.03E+00	2.37E-02
HIP1	-8.63E-01	2.88E-04	TRIB2	-7.27E-01	2.38E-02
SPEN	-8.13E-01	3.00E-04	LIG4	-6.51E-01	2.38E-02
MCOLN3	-1.04E+00	3.05E-04	SYNJ1	-6.30E-01	2.40E-02
FSTL1	-8.40E-01	3.26E-04	EXOC6B	-6.33E-01	2.47E-02
RAI2	-1.24E+00	3.69E-04	SDK1	-7.43E-01	2.51E-02
PRKG2	-3.28E+00	3.77E-04	RIMBP3	-2.38E+00	2.51E-02
DNAH11	-1.50E+00	4.01E-04	AMOTL2	-7.17E-01	2.51E-02
SYT1	-1.02E+00	4.42E-04	IQGAP1	-6.16E-01	2.51E-02
MNS1	-1.50E+00	4.48E-04	ARL10	-5.98E-01	2.51E-02
NES	-2.08E+00	4.63E-04	GALC	-8.94E-01	2.52E-02
FRAS1	-9.05E-01	4.71E-04	SMC4	-6.18E-01	2.55E-02
PARP9	-1.22E+00	4.84E-04	DAPK1	-6.17E-01	2.57E-02
LGR5	-1.24E+00	5.36E-04	TAP1	-6.30E-01	2.58E-02
HSBP1L1	-1.62E+00	5.49E-04	CYBRD1	-7.84E-01	2.61E-02
TMSB15A	-8.47E-01	5.61E-04	MYO7A	-3.57E+00	2.64E-02
LRRN2	-1.50E+00	5.76E-04	LBH	-9.74E-01	2.66E-02
CA8	-2.74E+00	7.65E-04	BAI3	-8.79E-01	2.67E-02
FOSL2	-1.07E+00	7.71E-04	BCL6	-7.79E-01	2.68E-02
LPL	-2.67E+00	7.71E-04	C7orf46	-8.59E-01	2.68E-02
DUSP10	-9.25E-01	7.73E-04	SLC44A5	-6.37E-01	2.69E-02
CUL9	-8.66E-01	7.82E-04	BICC1	-6.35E-01	2.83E-02
ANKRD1	-1.43E+00	7.91E-04	ARHGAP33	-6.85E-01	2.85E-02
LGALS1	-9.18E-01	8.20E-04	SLC22A23	-6.30E-01	2.89E-02
BRSK1	-9.49E-01	8.33E-04	ARHGAP31	-7.40E-01	2.95E-02
LYPD6	-8.21E-01	8.39E-04	FAM65B	-1.66E+00	2.95E-02
FAT3	-1.21E+00	8.46E-04	ARHGAP27	-7.90E-01	2.95E-02
CAMK4	-1.12E+00	8.51E-04	HDX	-8.43E-01	2.96E-02
ADAMTSL3	-2.54E+00	8.53E-04	ARMCX4	-7.74E-01	2.96E-02
ODZ4	-1.75E+00	9.14E-04	RGS7	-1.15E+00	3.01E-02
AHR	-1.04E+00	9.14E-04	DST	-6.06E-01	3.02E-02
DGKA	-9.66E-01	9.57E-04	TKTL1	-1.65E+00	3.13E-02
HOXA4	-1.17E+00	9.60E-04	GPC5	-1.44E+00	3.13E-02
CXCL12	-6.49E+00	9.72E-04	RAPGEF5	-7.89E-01	3.17E-02
ATP9A	-7.89E-01	9.76E-04	RFX6	-1.93E+00	3.28E-02
MFSD6	-1.36E+00	9.80E-04	NCKAP5L	-6.12E-01	3.29E-02
C8orf4	-4.56E+00	1.00E-03	MDGA1	-6.45E-01	3.32E-02
HOXA6	-1.53E+00	1.01E-03	COL24A1	-1.32E+00	3.40E-02
CXCL16	-8.57E-01	1.03E-03	COLEC12	-7.55E-01	3.43E-02
SRRM2	-7.65E-01	1.04E-03	TOP2A	-5.69E-01	3.44E-02
FAM5C	-5.47E+00	1.12E-03	SPOCK3	-1.58E+00	3.53E-02
ARHGEF17	-8.73E-01	1.19E-03	CHD7	-5.95E-01	3.56E-02
MOB3C	-1.10E+00	1.34E-03	CLSPN	-6.03E-01	3.57E-02
CREBBP	-7.67E-01	1.36E-03	TBC1D5	-6.61E-01	3.57E-02
IRS4	-7.63E-01	1.49E-03	RNASEL	-8.67E-01	3.57E-02
MCTP1	-1.94E+00	1.52E-03	AGTR1	-1.10E+00	3.57E-02
FAM134B	-1.01E+00	1.58E-03	IFITM1	-1.18E+00	3.58E-02
PLEKHB1	-9.16E-01	1.67E-03	FRMPD3	-8.42E-01	3.59E-02
PLD5	-4.92E+00	1.71E-03	KDM5A	-5.78E-01	3.61E-02
EPHB6	-2.62E+00	1.82E-03	CLSTN3	-6.39E-01	3.64E-02
CDHR1	-1.22E+00	1.88E-03	RIPK1	-5.84E-01	3.64E-02
PTH1R	-1.66E+00	1.94E-03	SYNGAP1	-6.82E-01	3.65E-02
NR3C2	-8.99E-01	1.96E-03	CD109	-7.73E-01	3.66E-02
HOXA3	-1.01E+00	1.96E-03	MYO5C	-7.17E-01	3.67E-02
KCNT2	-2.55E+00	1.98E-03	RNF144B	-9.65E-01	3.67E-02
PLEKHA7	-9.72E-01	2.10E-03	ACVR1C	-1.67E+00	3.68E-02
SLIT3	-1.32E+00	2.11E-03	FGF12	-2.56E+00	3.68E-02

Gene	Log2-FC	P-value		Gene	Log2-FC	P-value
CTTNBP2	-9.26E-01	2.16E-03		TCN2	-2.64E+00	3.69E-02
ANK1	-2.69E+00	2.23E-03		FBN1	-6.99E-01	3.73E-02
SLC12A6	-9.55E-01	2.33E-03		MBD5	-6.31E-01	3.74E-02
MED12	-7.72E-01	2.41E-03		PRKCSH	-5.82E-01	3.78E-02
ITGA6	-8.36E-01	2.58E-03		EFNB3	-5.96E-01	3.84E-02
MXD1	-8.09E-01	2.67E-03		DNAJC6	-6.44E-01	3.84E-02
SPTB	-1.09E+00	2.84E-03		LHX8	-8.29E-01	3.85E-02
PPP1R15A	-8.63E-01	2.84E-03		CDKL5	-9.56E-01	3.85E-02
SPTAN1	-7.31E-01	2.91E-03		PROX1	-1.02E+00	3.91E-02
ITGA8	-8.03E-01	2.94E-03		HIF1A	-5.81E-01	4.04E-02
QPCT	-1.20E+00	2.96E-03		ASH1L	-5.75E-01	4.07E-02
CXCR4	-1.87E+00	3.02E-03		KIAA1539	-7.25E-01	4.15E-02
BASP1	-2.46E+00	3.10E-03		PLXNA3	-5.98E-01	4.17E-02
DOCK9	-7.75E-01	3.12E-03		PNPLA8	-8.55E-01	4.17E-02
PKIB	-1.09E+00	3.12E-03		TFAP2A	-6.24E-01	4.20E-02
DYSF	-2.20E+00	3.12E-03		C7orf13	-1.18E+00	4.24E-02
FLT3	-2.17E+00	3.12E-03		EBF4	-6.90E-01	4.25E-02
CLSTN2	-3.42E+00	3.15E-03		C5orf42	-6.20E-01	4.29E-02
AS3MT	-8.31E-01	3.21E-03		MAN1C1	-8.29E-01	4.31E-02
CACNA2D3	-9.55E-01	3.21E-03		MAGI1	-7.91E-01	4.32E-02
L3MBTL4	-1.36E+00	3.21E-03		KAT6B	-5.87E-01	4.33E-02
MTMR11	-1.12E+00	3.25E-03		RAD54L2	-5.87E-01	4.33E-02
KIF13B	-9.17E-01	3.38E-03		KIF14	-6.03E-01	4.34E-02
KIF1A	-2.18E+00	3.75E-03		DNMBP	-6.14E-01	4.35E-02
SEMA6A	-7.97E-01	3.84E-03		TP53BP1	-5.83E-01	4.36E-02
TANC2	-7.80E-01	3.84E-03		FAM71E1	-1.02E+00	4.41E-02
TTC9	-9.66E-01	3.86E-03		TP53INP2	-6.16E-01	4.41E-02
NMNAT2	-1.42E+00	3.89E-03		SH3D21	-9.24E-01	4.42E-02
TMEM132E	-2.65E+00	4.15E-03		CCDC15	-8.52E-01	4.46E-02
KIAA1370	-9.78E-01	4.22E-03		PCDH17	-7.70E-01	4.48E-02
ADRB2	-1.00E+00	4.22E-03		MON2	-5.96E-01	4.56E-02
DLK2	-8.59E-01	4.36E-03		BMF	-1.31E+00	4.61E-02
PLAT	-1.25E+00	4.69E-03		SCD5	-6.03E-01	4.61E-02
EP300	-7.02E-01	4.88E-03		FRY	-8.12E-01	4.62E-02
GPM6A	-1.09E+00	5.10E-03		CYP1B1	-1.99E+00	4.62E-02
BCOR	-6.76E-01	5.37E-03		YWHAG	-5.30E-01	4.62E-02
SIPA1L2	-7.48E-01	5.38E-03		NOTCH2	-5.47E-01	4.63E-02
KIAA1731	-7.25E-01	5.55E-03		KAT6A	-5.59E-01	4.73E-02
ISM1	-1.01E+00	6.08E-03		INPP1	-6.93E-01	4.73E-02
TP73	-7.25E-01	6.08E-03		TAOK1	-6.24E-01	4.73E-02
NUP210	-8.03E-01	6.12E-03		ZZEF1	-5.65E-01	4.77E-02
HAUS2	-7.21E-01	6.12E-03		C15orf42	-5.55E-01	4.77E-02
SMARCA1	-7.18E-01	6.36E-03		ATP1B2	-7.67E-01	4.77E-02
POU4F1	-7.26E-01	6.36E-03		GAS2L3	-6.41E-01	4.77E-02
HES1	-7.06E-01	6.68E-03		NFAT5	-5.90E-01	4.82E-02
STAG3	-1.75E+00	6.70E-03		AMOTL1	-5.54E-01	4.82E-02
KIAA1407	-1.33E+00	6.73E-03		PTPN21	-6.11E-01	4.84E-02
KIAA0355	-7.34E-01	7.17E-03		NNT	-5.69E-01	4.84E-02
CGNL1	-1.12E+00	7.44E-03		ERC1	-5.93E-01	4.87E-02
SLAIN1	-8.50E-01	7.44E-03		VPS13C	-6.20E-01	4.87E-02
CHSY3	-1.09E+00	7.44E-03		MYH10	-5.54E-01	4.87E-02
BEND5	-1.96E+00	7.61E-03		GFRA1	-1.13E+00	4.91E-02
TM6SF2	-2.03E+00	7.61E-03		NRP1	-5.95E-01	4.92E-02
DOPEY1	-7.61E-01	7.64E-03		GCA	-6.25E-01	4.92E-02
DTX1	-3.93E+00	7.90E-03		ASAP2	-6.37E-01	4.93E-02
TSLP	-1.30E+00	8.04E-03		HSPA2	-1.24E+00	4.97E-02
ITGA7	-1.16E+00	8.18E-03				

Table S 4: List of significantly (p<0.05) degraded transcripts in HEK-miR-155 TL compared to the TL of HEK-vector (n= 339). Genes predicted for being miR-155 targets (according to MiRWalk) are marked with bold letters

Gene	Log2-FC	P-value		Gene	Log2-FC	P-value
SPARC	-7,06E+00	7,43E-52		**ATP6V1G1**	-8,16E-01	3,25E-04
DOK6	-4,46E+00	2,05E-46		BRWD3	-8,60E-01	3,40E-04
GALNT13	-3,38E+00	1,16E-43		**HMCN1**	-1,38E+00	1,26E-02
RHBDD2	-7,30E-01	1,81E-02		SLITRK5	-8,45E-01	3,40E-04
CDO1	-5,51E+00	4,50E-32		LYST	-5,97E-01	4,72E-02
COL2A1	-2,56E+00	1,69E-29		ABHD1	-1,12E+00	3,52E-02
PLA2G4A	-4,57E+00	5,43E-25		**RAPGEF2**	-8,49E-01	3,67E-04
TKTL1	-1,63E+00	1,15E-02		**ZNF652**	-8,50E-01	3,91E-04
BAIAP3	-9,28E-01	3,91E-02		**IGSF11**	-3,03E+00	4,00E-04
OAS3	-4,97E+00	9,60E-24		**GAB3**	-1,64E+00	4,62E-04
EPAS1	-2,17E+00	1,09E-23		EFEMP2	-1,62E+00	4,77E-04
CALCOCO1	-6,93E-01	1,00E-02		DTX1	-3,42E+00	4,78E-04
PGCP	-4,30E+00	1,47E-22		TSLP	-9,32E-01	4,57E-02
UBE2QL1	-2,74E+00	1,49E-22		**GPR126**	-1,05E+00	4,78E-04
ULK2	-1,98E+00	4,64E-20		**NR3C2**	-8,98E-01	4,97E-04
IKZF2	-9,76E-01	4,25E-02		GSN	-6,77E-01	2,97E-02
DSG2	-6,17E-01	2,00E-02		CDHR1	-9,69E-01	1,89E-02
FGF13	-3,05E+00	6,31E-18		**TRIM36**	-9,26E-01	5,09E-04
ZFP106	-1,68E+00	4,16E-17		FGF9	-1,78E+00	5,77E-04
ATP9A	-6,35E-01	1,56E-02		HES1	-8,33E-01	5,82E-04
PCDH10	-1,65E+00	2,50E-16		**KCNA6**	-2,64E+00	1,07E-02
CYP26B1	-1,94E+00	3,86E-14		**TMTC2**	-1,29E+00	5,83E-04
MAMLD1	-1,77E+00	4,35E-14		TMEM86A	-8,82E-01	1,61E-02
FAT3	-2,08E+00	2,23E-13		**COL4A4**	-2,14E+00	6,36E-04
PRKCB	-1,61E+00	1,70E-12		MFSD6	-9,51E-01	2,36E-02
SNCAIP	-1,09E+00	2,37E-02		LAMB2	-8,18E-01	6,53E-04
OPTN	-1,36E+00	2,79E-11		HSPB8	-1,48E+00	4,50E-02
PLCB2	-2,78E+00	2,87E-11		**KCNK13**	-1,21E+00	3,10E-02
MGAT4A	-5,78E-01	4,88E-02		GUCY1A2	-1,66E+00	1,28E-02
CYBRD1	-7,80E-01	2,37E-02		IGFBPL1	-5,66E+00	7,70E-04
CLCN4	-1,81E+00	3,68E-02		AHR	-9,12E-01	8,04E-04
PTGS2	-3,46E+00	1,87E-02		GPX3	-7,78E-01	8,04E-04
SAMD12	-1,69E+00	8,51E-11		SLC16A5	-3,42E+00	8,98E-04
FOSL2	-7,67E-01	2,04E-02		**BACH1**	-6,31E-01	2,32E-02
PLD1	-9,16E-01	4,03E-02		PCDH1	-1,20E+00	2,93E-02
B3GALT1	-2,23E+00	1,30E-10		LRRN2	-1,32E+00	8,98E-04
NES	-2,77E+00	2,48E-10		NMNAT2	-1,22E+00	1,00E-02
EDIL3	-4,31E+00	2,49E-10		MAP6	-1,24E+00	8,98E-04
ST8SIA4	-3,77E+00	3,70E-10		**JARID2**	-7,99E-01	9,35E-04
FAM20C	-1,46E+00	2,15E-09		CAMK4	-1,04E+00	9,66E-04
PPP1R15A	-7,31E-01	1,42E-02		**PPP1R9A**	-9,75E-01	3,63E-02
CDH2	-1,74E+00	2,18E-09		PINK1	-6,42E-01	2,04E-02
STXBP5L	-2,22E+00	2,51E-09		L3MBTL4	-1,26E+00	1,00E-03
EBF4	-7,17E-01	2,98E-02		**CA8**	-2,48E+00	1,04E-03
YPEL3	-9,37E-01	2,48E-02		C19orf57	-9,75E-01	1,08E-03
EHBP1L1	-1,46E+00	7,13E-09		ISM1	-1,02E+00	1,13E-03
MYO3A	-9,71E-01	3,09E-02		TM7SF2	-7,81E-01	1,17E-03
MMP11	-6,53E-01	5,00E-02		SCN1B	-1,23E+00	1,18E-03
MYO5B	-1,60E+00	1,15E-08		NPY1R	-2,92E+00	1,24E-03
CELF2	-1,97E+00	1,17E-08		ITGA8	-8,05E-01	1,30E-03
RYR2	-2,72E+00	1,27E-08		SLAIN1	-9,36E-01	1,32E-03
SLC8A3	-2,21E+00	1,77E-02		TUBGCP4	-7,73E-01	1,39E-03
RPS6KA5	-6,65E-01	3,52E-02		**GFI1**	-7,99E-01	2,00E-02
KCNQ1	-1,72E+00	1,82E-08		**LONRF2**	-8,08E-01	1,43E-03

Gene	Log2-FC	P-value		Gene	Log2-FC	P-value
ESRRG	-2,56E+00	2,00E-08		**ANTXR2**	-7,41E-01	2,38E-02
PRKG2	-2,88E+00	2,20E-08		FSTL1	-6,61E-01	1,03E-02
SNPH	-6,92E-01	2,49E-02		LMOD1	-8,31E-01	2,49E-02
JAG1	-8,79E-01	2,65E-02		ZNF513	-6,37E-01	1,96E-02
APH1B	-1,24E+00	2,20E-08		QPCT	-1,19E+00	1,47E-03
CHRDL1	-1,32E+00	1,63E-02		**KLHL32**	-1,75E+00	1,57E-03
SYTL4	-6,71E-01	3,17E-02		SLC46A3	-8,47E-01	1,65E-03
TTBK2	-1,23E+00	2,20E-08		**SYT1**	-8,51E-01	1,67E-03
GALC	-1,55E+00	5,19E-08		CXCL12	-6,09E+00	1,79E-03
AIFM2	-2,15E+00	5,20E-08		FOXQ1	-1,58E+00	4,74E-02
FOXF1	-6,61E-01	2,74E-02		SLC13A4	-9,15E-01	2,51E-02
STARD9	-1,19E+00	6,24E-08		PLAT	-1,28E+00	1,82E-03
SERPING1	-3,40E+00	8,57E-08		MCOLN3	-8,39E-01	1,88E-03
BMF	-1,44E+00	2,05E-02		**HDX**	-7,55E-01	2,26E-02
SPINT2	-1,72E+00	8,66E-08		MAP7	-7,79E-01	1,99E-03
CCNDBP1	-1,20E+00	1,09E-07		KIF1A	-2,26E+00	2,02E-03
WNT9A	-1,61E+00	1,40E-07		CXCR4	-1,73E+00	2,29E-03
DMRT3	-2,91E+00	2,34E-07		PROX1	-9,50E-01	2,38E-03
DDIT4L	-1,62E+00	2,93E-07		MAN1C1	-9,90E-01	2,39E-03
SNAP91	-1,88E+00	3,71E-07		ADAMTS15	-8,46E-01	3,39E-02
CACNA1G	-1,58E+00	5,05E-07		**C10orf26**	-5,69E-01	3,27E-02
C1orf172	-4,00E+00	5,24E-07		KRBA2	-2,32E+00	2,43E-03
DNAH11	-7,99E-01	5,00E-02		TMEM132E	-2,30E+00	2,68E-03
LGALS1	-1,18E+00	5,54E-07		PLEKHA7	-6,73E-01	3,56E-02
SLIT2	-1,04E+00	6,92E-07		SLFN5	-9,40E-01	3,28E-02
UBR1	-1,09E+00	8,39E-07		PIK3CD	-8,07E-01	2,77E-03
EPHB6	-1,61E+00	4,37E-02		DCHS1	-9,49E-01	2,97E-03
HSPB1	-6,79E-01	1,24E-02		**MIDN**	-9,07E-01	5,00E-02
NACAD	-1,33E+00	8,42E-07		CLSTN2	-2,73E+00	2,97E-03
RGP1	-5,63E-01	4,88E-02		NPFFR2	-3,34E+00	2,99E-03
ATRNL1	-6,82E-01	3,07E-02		ABCA3	-1,09E+00	1,40E-02
EFNB3	-6,17E-01	3,00E-02		TAP1	-5,99E-01	4,03E-02
NMU	-6,88E-01	2,26E-02		NPR1	-1,99E+00	3,05E-03
LCMT2	-1,08E+00	1,95E-06		**C18orf1**	-6,81E-01	3,44E-02
PRRX1	-2,33E+00	2,60E-06		ANG	-1,42E+00	3,24E-03
HOXA5	-1,15E+00	2,60E-06		MOB3C	-9,98E-01	3,36E-03
SOX6	-7,06E-01	2,61E-02		**TAPT1**	-6,41E-01	2,32E-02
RAI2	-1,51E+00	3,01E-06		VGLL2	-9,36E-01	3,57E-02
VPS39	-1,01E+00	3,23E-06		MXD1	-7,58E-01	3,36E-03
ODZ1	-4,93E+00	3,35E-06		OCLN	-7,49E-01	3,36E-03
SMOC2	-4,05E+00	3,27E-02		MYO7A	-3,43E+00	3,36E-03
CUL9	-6,73E-01	1,31E-02		S1PR1	-1,03E+00	3,36E-03
OSBPL7	-1,39E+00	3,80E-06		**THRB**	-7,70E-01	3,59E-03
TTC9	-1,34E+00	4,62E-06		KCNS3	-1,09E+00	2,86E-02
SLC27A6	-1,14E+00	1,83E-02		DLK2	-7,06E-01	3,55E-02
GPRC5C	-1,55E+00	4,91E-06		BRSK1	-8,58E-01	3,93E-03
TRIM23	-6,78E-01	1,42E-02		TTLL7	-7,59E-01	4,06E-03
CDAN1	-1,06E+00	5,06E-06		**DPY19L1**	-6,11E-01	3,04E-02
PLCL1	-1,71E+00	5,08E-06		IQGAP3	-7,44E-01	4,22E-03
MBP	-1,54E+00	5,08E-06		FAM131A	-7,00E-01	2,04E-02
GCA	-6,57E-01	3,10E-02		MCTP1	-1,24E+00	1,91E-02
BEX2	-9,82E-01	5,95E-06		PRDM8	-1,41E+00	4,40E-03
PDE10A	-1,34E+00	6,34E-06		KDM5B	-7,20E-01	4,41E-03
TMEM62	-1,08E+00	6,90E-06		CFHR3	-1,94E+00	4,96E-03
CXCL16	-1,04E+00	6,90E-06		BOK	-8,75E-01	3,86E-02
TMEM87A	-9,99E-01	6,90E-06		RPRM	-2,93E+00	3,39E-02
PARD3B	-6,86E-01	3,85E-02		**ZFP36**	-8,59E-01	4,98E-03
SPTAN1	-9,51E-01	1,04E-05		DMRTA2	-1,63E+00	5,04E-03
ADAL	-1,00E+00	1,21E-05		**ACVR1C**	-1,54E+00	5,04E-03
ANKRD1	-1,48E+00	1,22E-05		APOLD1	-7,64E-01	1,27E-02

Gene	Log2-FC	P-value		Gene	Log2-FC	P-value
MNS1	-1,42E+00	1,22E-05		GPM6A	-9,38E-01	5,19E-03
CLVS2	-2,37E+00	1,27E-05		WSCD1	-9,60E-01	1,78E-02
YPEL5	-6,88E-01	4,16E-02		C8orf42	-1,21E+00	2,97E-02
NME5	-2,31E+00	1,49E-05		SLC2A10	-7,82E-01	5,45E-03
LPL	-2,24E+00	1,57E-05		FCGRT	-7,50E-01	5,46E-03
PTGFR	-1,26E+00	1,28E-02		RPH3AL	-8,94E-01	1,23E-02
AS3MT	-1,03E+00	1,57E-05		TMSB15A	-7,33E-01	5,59E-03
LRP1	-5,99E-01	3,92E-02		RFX6	-1,86E+00	5,82E-03
GOS2	-1,86E+00	2,14E-05		PLXNA4	-3,00E+00	5,83E-03
BEND5	-2,59E+00	2,24E-05		ARHGEF17	-7,69E-01	5,83E-03
LSR	-9,72E-01	2,31E-05		**ABAT**	-6,44E-01	4,01E-02
POR	-6,02E-01	3,14E-02		DSCR6	-7,45E-01	1,81E-02
AC010336.1	-1,47E+00	2,63E-05		HAUS2	-7,12E-01	5,85E-03
TMSB4X	-1,40E+00	3,06E-05		NUDT14	-6,64E-01	3,52E-02
ZSCAN29	-9,39E-01	3,23E-05		RIMS1	-2,71E+00	6,11E-03
EPSTI1	-1,61E+00	3,63E-05		LSAMP	-4,01E+00	6,19E-03
STARD8	-7,44E-01	3,39E-02		FGF12	-2,50E+00	6,59E-03
BASP1	-2,88E+00	3,80E-05		ZNF467	-1,30E+00	6,88E-03
PGPEP1	-6,14E-01	3,65E-02		TCN2	-2,76E+00	2,35E-02
PLXNA3	-6,54E-01	1,52E-02		**HS6ST3**	-1,72E+00	1,00E-02
GANC	-1,04E+00	3,80E-05		METTL7A	-7,81E-01	4,32E-02
TP53INP1	-9,90E-01	4,09E-05		HOXA4	-1,02E+00	7,00E-03
LGALS3	-8,44E-01	1,48E-02		RAB9B	-8,09E-01	7,00E-03
LRRTM4	-1,73E+00	4,57E-05		PAK3	-1,42E+00	7,34E-03
ITGB4	-9,06E-01	1,80E-02		CAV1	-9,22E-01	7,39E-03
LYPD6	-9,44E-01	4,62E-05		SPOCK3	-1,44E+00	7,44E-03
INADL	-6,00E-01	4,51E-02		ALG1L	-9,00E-01	4,33E-02
MTMR11	-1,30E+00	5,23E-05		SLC35F1	-6,26E-01	2,54E-02
APOBEC3B	-1,69E+00	5,41E-05		PARD6A	-1,06E+00	7,91E-03
SORT1	-5,46E-01	4,57E-02		ARHGAP33	-7,68E-01	8,02E-03
FBXO27	-1,03E+00	5,90E-05		GALNT3	-3,05E+00	8,19E-03
AHRR	-9,02E-01	5,96E-05		GMCL1	-7,08E-01	8,21E-03
EDNRB	-4,91E+00	4,40E-02		LGR5	-8,71E-01	8,42E-03
MIXL1	-1,78E+00	5,96E-05		DTX3L	-7,66E-01	8,46E-03
LRRC57	-9,43E-01	8,24E-05		CHSY3	-7,78E-01	4,03E-02
SLC22A23	-6,19E-01	3,00E-02		KIAA1539	-8,79E-01	8,66E-03
SPTB	-1,16E+00	9,61E-05		MT1F	-1,20E+00	1,43E-02
PLD5	-3,79E+00	1,09E-04		PTPRO	-1,65E+00	8,72E-03
TCP11L2	-1,09E+00	1,12E-04		**LHX9**	-1,15E+00	8,86E-03
KCTD12	-9,23E-01	1,22E-04		C2orf72	-7,59E-01	1,80E-02
SLC44A5	-6,15E-01	3,26E-02		MICB	-7,71E-01	4,01E-02
CYP1B1	-2,21E+00	2,18E-02		RET	-9,22E-01	8,86E-03
PVALB	-1,98E+00	1,22E-04		**GFRA1**	-1,14E+00	8,91E-03
HOXA6	-1,69E+00	1,28E-04		TMEM200C	-1,58E+00	1,02E-02
DKK3	-1,38E+00	1,59E-04		DDAH2	-7,29E-01	1,78E-02
FRAS1	-6,65E-01	1,50E-02		**HOXA3**	-9,18E-01	9,12E-03
SLC38A4	-1,64E+00	1,12E-02		PRKCH	-7,96E-01	9,13E-03
IFI27L2	-9,44E-01	1,59E-04		TP73	-6,94E-01	9,41E-03
SNAP23	-8,66E-01	1,59E-04		KIAA0913	-5,64E-01	4,75E-02
FAM105A	-8,49E-01	2,48E-04		RP11-428C6.1	-9,18E-01	2,47E-02
OTX2	-1,28E+00	2,58E-04		**KCNT2**	-2,07E+00	9,69E-03
CACNA2D3	-1,04E+00	2,63E-04		ATXN1L	-5,93E-01	2,39E-02
FREM2	-9,02E-01	2,78E-04		EPPK1	-2,12E+00	3,39E-02
IQGAP1	-6,55E-01	1,39E-02		PCDHGC4	-1,51E+00	2,24E-02
SECTM1	-1,68E+00	1,11E-02		**PRR16**	-1,11E+00	9,98E-03
FAM71E1	-1,13E+00	1,24E-02				

Table S 5: List of significantly (p<0.05) up-regulated transcripts in HEK-miR-155 TL compared to the TL of HEK-vector (n= 121).

Gene	Log2-FC	P-value		Gene	Log2-FC	P-value
FAM78A	2,13E+00	1,38E-23		PALM2	1,01E+00	1,02E-02
TNFRSF11B	5,53E+00	1,36E-19		GABRD	9,54E-01	1,10E-02
DPYSL3	1,98E+00	1,94E-19		FAM91A1	6,37E-01	1,16E-02
CCND1	4,19E+00	1,96E-12		EFR3A	6,42E-01	1,17E-02
ZNF813	2,02E+00	4,35E-12		CAMKV	7,14E-01	1,26E-02
KCNQ2	1,32E+00	1,88E-10		WDR67	6,47E-01	1,30E-02
ALDH1A2	1,24E+00	1,71E-09		UTP23	6,45E-01	1,33E-02
FAM84B	1,09E+00	1,04E-07		ZNF44	8,38E-01	1,38E-02
CA12	1,14E+00	6,92E-07		TEX15	6,45E-01	1,54E-02
NDRG1	1,19E+00	1,95E-06		SEH1L	6,25E-01	1,56E-02
ZNF85	2,18E+00	3,35E-06		PCDH19	8,58E-01	1,62E-02
PROCR	1,04E+00	1,09E-05		PPID	6,26E-01	1,74E-02
EDA2R	3,78E+00	1,46E-05		CACYBP	6,22E-01	1,78E-02
ADCYAP1R1	9,74E-01	1,62E-05		TNFRSF10D	6,87E-01	1,87E-02
POLR3G	1,14E+00	2,24E-05		C4orf43	6,09E-01	1,96E-02
BMP2	1,83E+00	2,51E-05		ADA	6,85E-01	2,00E-02
C19orf51	9,74E-01	4,40E-05		ZNF586	8,54E-01	2,00E-02
ATP1A3	9,36E-01	5,23E-05		DSCC1	5,93E-01	2,00E-02
HMOX1	1,05E+00	6,45E-05		MT1X	7,22E-01	2,04E-02
LY6E	8,72E-01	9,48E-05		TRIB1	1,20E+00	2,04E-02
BEND4	9,23E-01	1,10E-04		CYC1	7,01E-01	2,14E-02
BOP1	9,07E-01	1,38E-04		EGLN3	6,74E-01	2,24E-02
TRMT12	8,56E-01	3,61E-04		TAP2	6,40E-01	2,32E-02
COTL1	8,24E-01	5,14E-04		CHRAC1	6,24E-01	2,32E-02
ZNF256	1,25E+00	5,54E-04		MMP2	9,21E-01	2,35E-02
MRPL13	8,04E-01	6,32E-04		CHRNA4	1,34E+00	2,35E-02
EXT1	8,09E-01	7,92E-04		C3orf14	6,10E-01	2,43E-02
SPRY1	8,28E-01	8,33E-04		BCL6B	6,20E-01	2,85E-02
KLRG2	8,24E-01	1,22E-03		NRG2	9,31E-01	2,95E-02
ETV1	1,25E+00	1,57E-03		WT1	6,78E-01	2,97E-02
DHRS2	1,13E+00	1,61E-03		NIP7	5,97E-01	2,99E-02
C8orf33	7,39E-01	2,20E-03		NEIL2	6,46E-01	2,99E-02
ALPL	8,46E-01	2,88E-03		TRIM71	7,61E-01	2,99E-02
ARSJ	9,01E-01	3,05E-03		IL12RB2	8,68E-01	3,08E-02
ELOVL6	7,35E-01	3,53E-03		TESC	7,78E-01	3,09E-02
ABCE1	6,83E-01	3,58E-03		SQLE	5,86E-01	3,15E-02
C12orf35	7,26E-01	3,62E-03		SLC24A4	8,73E-01	3,23E-02
FAM150A	1,93E+00	3,67E-03		LYAR	5,91E-01	3,23E-02
COL14A1	1,28E+00	3,80E-03		HRSP12	6,01E-01	3,24E-02
DNMT3B	7,34E-01	3,93E-03		FBXO41	6,51E-01	3,24E-02
SULT1A1	1,04E+00	3,93E-03		TOP1MT	5,97E-01	3,24E-02
TATDN1	7,31E-01	4,06E-03		TRPS1	5,95E-01	3,27E-02
GPATCH4	7,12E-01	4,29E-03		CCT6A	5,69E-01	3,39E-02
SPRED2	7,40E-01	4,96E-03		ZNF528	1,63E+00	3,52E-02
TERT	1,30E+00	4,98E-03		NFASC	8,08E-01	3,55E-02
RNF125	7,19E-01	5,25E-03		ZC3H15	5,74E-01	3,55E-02
GPRIN3	7,53E-01	5,34E-03		PRPS2	5,66E-01	3,69E-02
PYCRL	7,81E-01	5,43E-03		NCS1	5,89E-01	3,74E-02
RASGEF1A	7,31E-01	5,83E-03		PLCD3	5,85E-01	3,94E-02
THEM4	6,95E-01	6,45E-03		PRR5L	8,79E-01	4,07E-02
FBXO32	7,56E-01	6,97E-03		ANKRD34A	6,69E-01	4,20E-02
PDZRN3	7,76E-01	7,48E-03		ASAP1	5,68E-01	4,23E-02
RAB39	9,65E-01	7,58E-03		ADAT2	5,88E-01	4,28E-02
POP1	6,83E-01	7,91E-03		ZNF121	6,05E-01	4,48E-02
KHDRBS3	7,12E-01	8,54E-03		GCLM	5,55E-01	4,50E-02
SLC11A1	1,49E+00	8,66E-03		RBFOX3	1,16E+00	4,50E-02

Gene	Log2-FC	P-value		Gene	Log2-FC	P-value
ETV5	1,85E+00	8,71E-03		OR2V2	4,11E+00	4,77E-02
HSPE1	6,82E-01	8,99E-03		FAM196A	1,31E+00	4,78E-02
ETV4	2,16E+00	9,60E-03		C1QBP	5,48E-01	4,86E-02
FAM49B	6,55E-01	9,91E-03		EPHA8	1,00E+00	5,00E-02
TMEM145	8,37E-01	1,02E-02				

Table S 6: Summary of mapped and quantified Sequencing reads per sample and replicate

Cell line	Fraction	Replicate	Total count	Usable count	% of total count
JEKO-1	IP AGO2	1	27019022	19411847	71.85
JEKO-1	IP AGO2	3	27083054	19320009	71.34
JEKO-1	IP IgG1	1	22964967	15850150	69.02
JEKO-1	IP IgG1	3	24249235	16848261	69.48
JEKO-1	TL	1	36589431	26452402	72.30
JEKO-1	TL	3	47718747	34900024	73.14
MEC-1	IP AGO2	1	35201658	25259905	71.76
MEC-1	IP AGO2	2	28727071	20896781	72.74
MEC-1	IP AGO2	3	36410713	26467541	72.69
MEC-1	IP IgG1	1	36612969	25650654	70.06
MEC-1	IP IgG1	2	32981148	23281289	70.59
MEC-1	IP IgG1	3	31578804	21761586	68.91
MEC-1	TL	1	48052168	35624017	74.14
MEC-1	TL	2	59188878	44297512	74.84

Danksagung

Ich bedanke mich bei Peter Lichter, dass er mir die Möglichkeit gegeben hat in seinem Labor zu arbeiten. Ich danke ihm für eine immer faire, verantwortungsvolle und freundliche Betreuung. Die Entwicklung und Verfolgung neuer Ideen wurden immer unterstützt und Fehler großzügig toleriert.

Ich danke Martina Seiffert, dass sie mich, nachdem mein erster Betreuer das DKFZ verlassen hat, als ihren Doktoranden „adoptiert“ und sich in das für sie neue Themengebiet meiner Doktorarbeit eingearbeitet hat. Ich danke ihr für die sehr inspirierenden Besprechungen der neuesten Versuchsergebnisse und die Unterstützung neuer Ideen. Die stets optimistische Einschätzung der Daten hat mir häufig neue Energie und Motivation gegeben.

Ich Danke Armin Pscherer, dass er bei mir das Interesse für die MikroRNAs geweckt und gefördert hat. Ich danke ihm dafür, dass er mich zunächst als Diplomanden und darauf folgend als Doktoranden unterstützt hat. Auch nach seinem Berufswechsel erhielt ich noch gelegentlich wertvolle Ratschläge für meine Arbeit und persönliche Entwicklung.

Ich danke meinem Thesis Advisory Committee (TAC), bestehend aus Stefan Wiemann, Peter Lichter und Gerhard Schratt, für sehr wertvolle Diskussionen zum Fortschritt meiner Doktorarbeit.

Ich danke Peter Lichter und Stefan Wiemann für die Begutachtung dieser Arbeit.

Ich danke Volker Hovestadt und Marc Zapatka für die wichtige Unterstützung bei der Auswertung der RIP-Seq Datensätze. Die Gespräche mit Volker und Marc, sowie Thorsten Kolb, Verena Thewes, Jan Gronych und Daniel Haag waren für die Entwicklung und den Erfolg der hier etablierten RIP-Seq Methode mit entscheidend.

Ich danke André Leischwitz und Stephan Wolf für die exzellente Unterstützung bei der Sequenzierung meiner Proben. Es war mir eine Freude als Gast in der DKFZ Sequencing Core Facility zu arbeiten.

Bei Martina Schnölzer, Christopher Lößner, Tore Kempf und Uwe Warnken bedanke ich mich für die freundliche Unterstützung bei den massenspektrometrischen Analysen und der erfolgreichen Zusammenarbeit beim SILAC-Projekt.

Ich danke allen Kooperationspartnern für die erfolgreiche Zusammenarbeit.

Ich danke allen Kollegen aus meinem Labor und Büro für eine Menge Spaß am Arbeitsplatz. Die gemeinsamen Unternehmungen mit Kollegen in meiner Freizeit, haben ebenfalls maßgeblich zu dieser Arbeit beigetragen. Die musikalischen Aktivitäten mit Angela Schulz und Daniel Haag in der Band „2Hybrid“ und die Mountainbike- oder Cyclocrosstouren mit Sebastian Barbus, Martje Tönjes, Marc Zapatka und Michael Bocker haben einen wichtigen Ausgleich zum Arbeitsalltag geboten.

Ich danke den Mitgliedern des DKFZ „Welcome Teams“, „Pizza & Talk Teams“ und dem PhD Council für die stets erfreuliche Zusammenarbeit. Die Arbeit in diesen Teams war für mich eine wertvolle Quelle neuer Erfahrungen und neuer Freundschaften.

Ich danke meiner Familie für die liebvolle und grenzenlose Unterstützung in allen Lebenslagen, ohne die meine persönliche und berufliche Entwicklung nicht möglich gewesen wäre.